Photophysics and Photochemistry of Iron Carbene Complexes

Lindh, Linnea

2023

Document Version:
Publisher's PDF, also known as Version of record

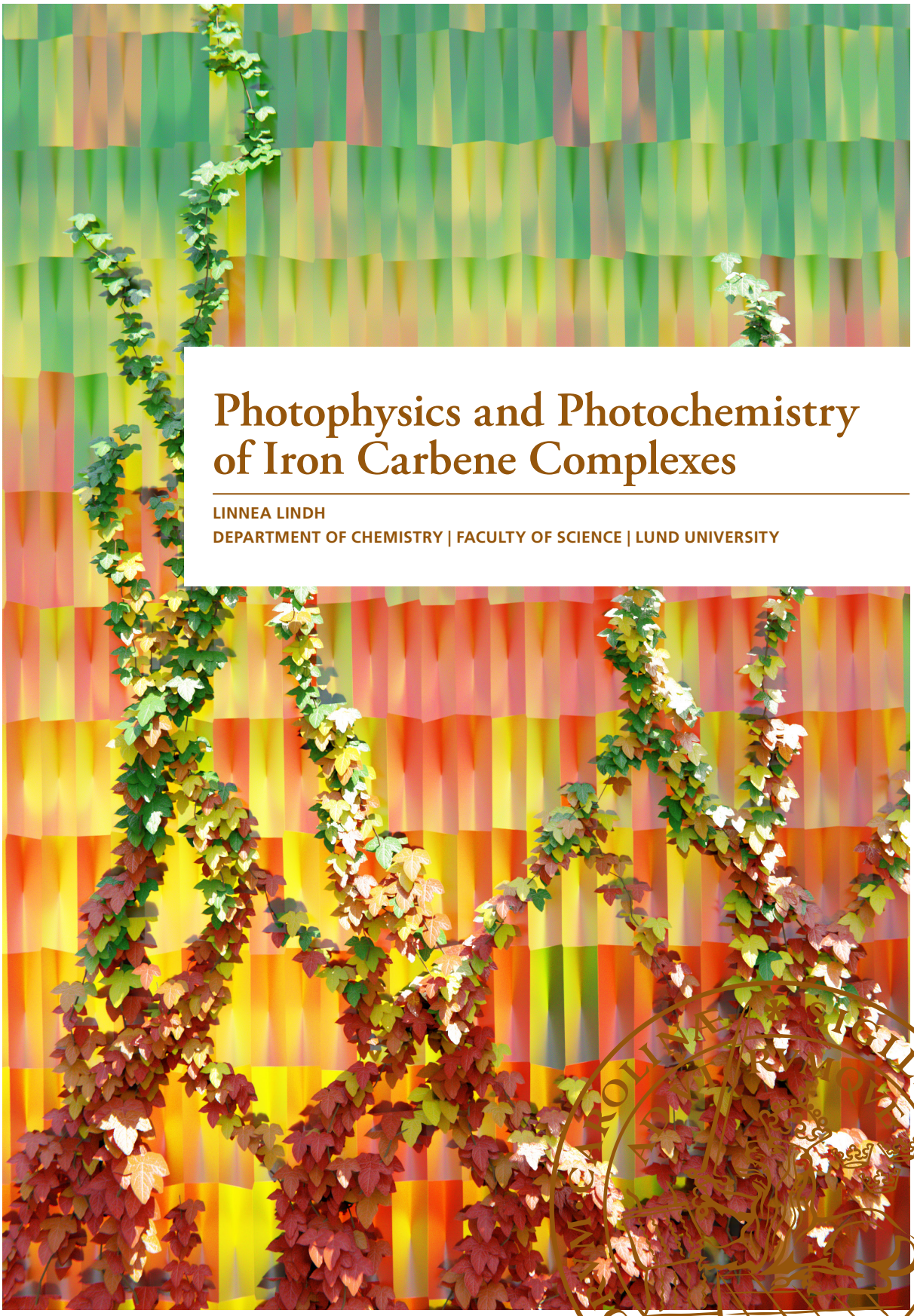

Photophysics and Photochemistry of Iron Carbene Complexes

LINNEA LINDH
DEPARTMENT OF CHEMISTRY | FACULTY OF SCIENCE | LUND UNIVERSITY

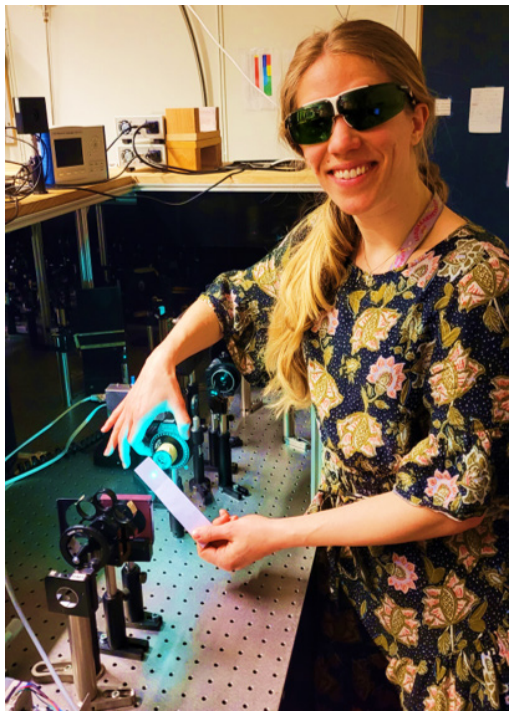

The author working in her favourite lab, Millenia, at Chemical Physics Lund University.

Printed by Media-Tryck, Lund 2023 NORDIC SWAN ECOLABEL 3041 0903

LUND UNIVERSITY

Faculty of Science
Department of Chemistry
Division Chemical Physics

ISBN 978-91-7422-976-9

Photophysics and Photochemistry of Iron Carbene Complexes

Photophysics and Photochemistry of Iron Carbene Complexes

by Linnea Lindh

LUND
UNIVERSITY

Thesis for the degree of Doctor of Technology
Thesis advisors: Prof. Petter Persson, Prof. Arkady Yartsev, Dr. Pavel Chábera
Faculty opponent: Prof. Gerald J. Meyer

To be presented, with the permission of the Faculty of Science of Lund University, for public criticism at KC:A (Kemicentrum) on Friday, the 6th of October 2023 at 9:00.

Organization	Document name
LUND UNIVERSITY Department of Chemistry Box 124 SE–221 00 LUND Sweden	**PHD THESIS**
	Date of disputation 2023-10-06
	Sponsoring organization
Author(s) Linnea Lindh	

Title and subtitle

Photophysics and Photochemistry of Iron Carbene Complexes

Abstract

Nature captures sunlight via light-absorbing molecules. Similarly, photosensitisers are used in applications of solar cells and artificial photosynthesis to absorb sunlight, and transfer the excited electron. Successful photosensitisers have in the past been based on a Ru polipyridyl scaffold, despite Ru being one of the scarcest elements in Earth's crust. This thesis work aims to replace Ru polipyridyl complexes by Fe carbene complexes, that by clever ligand design have approached suitable photosensitiser properties.

One crucial property that is not yet competitive for Fe carbene photosensitisers is how long they stay in the excited state, i.e. their lifetime. This is controlled by the deactivation pathways of the molecule, dictated by the excited state landscape. Several Fe carbene photosensitisers were in this thesis investigated by spectroscopic and computational methods, to understand their deactivation pathways. For the Fe(II) carbene complexes investigated, small changes in the ligand structure influenced both what excited state (charge-transfer or metal-centred) that was mainly populated and the lifetime of the state. For the Fe(III) carbene complexes investigated, there was instead one dominating charge-transfer excited state that was rather unaffected by changes to the ligand. Furthermore, for the Fe(II) complexes metal-centred states played a large role in the deactivation pathway but for the Fe(III) complexes this was not the case. Also, one Co(III) carbene complex was investigated which displays remarkable long lifetime and emission from a metal-centred state.

As a first step towards application, the electron-transfer properties of some of the photosensitisers were investigated. Fe(II) complexes with a push-pull design were able to transfer electrons to TiO_2 in a solar cell configuration. The solar cell performance was however limited by an ultrafast recombination reaction, that brought a majority of the transferred electrons back to the photosensitiser. The Fe(III) complexes investigated had long enough lifetime to participate in electron transfer with other molecules in solution, if the concentration was high. Furthermore, at very high concentrations of the photosensitiser a light-induced charge-disproportionation reaction outcompeted all other deactivation pathways. In a heterogeneous catalysis configuration, this reaction could generate long-lived Fe(IV) species with the correct additives. The thesis work thus provide fundamental insights to the early implementations of Fe carbene photosensitisers in applications, by resolving key electron-transfer processes on the ultrafast timescale.

Key words

time-resolved spectroscopy, density functional theory, earth-abundant, iron-complex, photosensitiser, dye-sensitised solar cell, photocatalysis, electron transfer

Classification system and/or index terms (if any)

Supplementary bibliographical information	Language English
ISSN and key title	ISBN 978-91-7422-976-9 (print) 978-91-7422-977-6 (pdf)
Recipient's notes	Number of pages 288 / Price
	Security classification

Signature _____ Date 2023-08-21

Photophysics and Photochemistry of Iron Carbene Complexes

by Linnea Lindh

LUND
UNIVERSITY

A doctoral thesis at a university in Sweden takes either the form of a single, cohesive research study (monograph) or a summary of research papers (compilation thesis), which the PhD student has written alone or together with one or several other author(s).

In the latter case the thesis consists of two parts. An introductory text puts the research work into context and summarizes the main points of the papers. Then, the research publications themselves are reproduced, together with a description of the individual contributions of the authors. The research papers may either have been already published or are manuscripts at various stages (in press, submitted, or in draft).

Cover illustration front: Illustration by Martin Aurell.

Cover illustration back: Image by Pavel Chábera.

Funding information: The thesis work was financially supported by the Swedish Foundation for Strategic Research (SSF), the Knut and Alice Wallenberg Foundation (KAW) and the Swedish Research Council (VR).

Faculty of Science, Department of Chemistry

isbn: 978-91-7422-976-9 (print)
isbn: 978-91-7422-977-6 (pdf)

Printed in Sweden by Media-Tryck, Lund University, Lund 2023

Media-Tryck is a Nordic Swan Ecolabel certified provider of printed material. Read more about our environmental work at www.mediatryck.lu.se

MADE IN SWEDEN

Dedicated to all
inspiring teachers
who light a spark
in their students.

Contents

List of Publications . . . iii
Acknowledgements . . . vi
Abbreviations . . . viii
Popular Scientific Summary in English . . . ix
Populärvetenskaplig sammanfattning på svenska . . . xi

Photophysics and Photochemistry of Iron Carbene Complexes **1**

1 Harvesting Solar Energy **3**
1.1 Global Energy Demand . . . 3
1.2 Solar Fuels using Photosensitisers . . . 5
1.3 Solar Cells using Photosensitisers . . . 8

2 Exploring Molecular Photosensitisers **11**
2.1 The Ideal Photosensitiser . . . 11
2.2 Electronic Structure . . . 13
2.3 Steady-State Spectroscopy . . . 16
2.4 Time-Resolved Spectroscopy . . . 19
2.5 Quantum Chemical Calculations . . . 23
2.6 Earth-Abundant Photosensitisers . . . 26

3 Photophysics of Iron Carbene Complexes **27**
3.1 d^6 Fe Carbene Complexes . . . 27
3.1.1 Strategy: Destabilising MC States . . . 29
3.1.2 Strategy: Stabilising MLCT States . . . 32
3.1.3 Strategy: Increasing Charge Separation . . . 33
3.1.4 Revising d^6 Fe Carbene Photophysics . . . 38
3.1.5 CoChamp - a Photofunctional ^{3}MC State . . . 42
3.2 d^5 Fe Carbene Complexes . . . 45
3.2.1 Introducing the ^{2}LMCT State . . . 46
3.2.2 Deactivation of the ^{2}LMCT state . . . 48
3.2.3 The robust ^{2}LMCT state . . . 52
3.3 Conclusions . . . 54

4 Photochemistry of Iron Carbene Complexes **57**

4.1 Intermolecular Charge-Transfer 57
4.1.1 Marcus Electron-Transfer Theory 58
4.1.2 Bimolecular Charge-Transfer 60
4.1.3 Light-Induced Charge-Disproportionation 62
4.1.4 First Demonstrations of Photocatalysis 65
4.2 Interfacial Charge-Transfer 66
4.2.1 Interfacial Charge-Transfer Theory 67
4.2.2 The Fe-Based Solar Cell: Current Limitations 70
4.2.3 Towards Heterogeneous Catalysis 73
4.2.4 Ideas to Improve the Solar Cell Performance 77

5 Reflections and Outlook **81**

References **85**

Scientific publications **105**
Paper I: Tailoring the Photophysical Properties of a Homoleptic Iron(II) Tetra N-Heterocyclic Carbene Complex by Attaching an Imidazolium Group to the (C^N^C) Pincer Ligand – A Comparative Study . . . 107
Paper II: Dye-Sensitized Solar Cells Based on Fe N-Heterocyclic Carbene Photosensitizers with Improved Rod-Like Push-Pull Functionality . . 137
Paper III: Interplay of MLCT and MC Relaxation Pathways as a Function of Side-Group Variation on the Iron(II) Carbene Scaffold 159
Paper IV: Multifaceted Deactivation Dynamics of Fe(II) N-Heterocyclic Carbene Photosensitizers 181
Paper V: Microsecond Photoluminescence and Photoreactivity of a Metal-Centered Excited State in a Hexacarbene-Co(III) Complex 207
Paper VI: Luminescence and Reactivity of a Charge-Transfer Excited Iron Complex with Nanosecond Lifetime 215
Paper VII: Competing Dynamics of Intramolecular Deactivation and Bimolecular Charge Transfer Processes in Luminescent Fe(III) N-Heterocyclic Carbene Complexes 223
Paper VIII: Photophysical Integrity of the Iron(III) Scorpionate Framework in Iron(III)-NHC Complexes with Long-Lived ^{2}LMCT Excited States 237
Paper IX: Light-Induced Dynamics of an Fe(III) Carbene Photosensitizer with ^{2}LMCT State in a Heterogeneous System 251

List of Publications

This thesis is based on the following publications, referred to by their Roman numerals:

I **Tailoring the Photophysical Properties of a Homoleptic Iron(II) Tetra N-Heterocyclic Carbene Complex by Attaching an Imidazolium Group to the (C^N^C) Pincer Ligand – A Comparative Study**
O. Prakash, **L. Lindh**, A. Kumar Gupta, Y. Hoang Hai Tran, N. Kaul, P. Chábera, F. Lindgren, T. Ericsson, L. Häggström, D. Strand, A. Yartsev, R. Lomoth, P. Persson, K. Wärnmark
Submitted Manuscript

I performed calculations and spectroscopic measurements, as well as contributed to writing the paper.

II **Dye-Sensitized Solar Cells Based on Fe N-Heterocyclic Carbene Photosensitizers with Improved Rod-Like Push-Pull Functionality**
L. Lindh, O. Gordivska, S. Persson, H. Michaels, H. Fan, P. Chábera, N.W. Rosemann, A. Kumar Gupta, I. Benesperi, J. Uhlig, O. Prakash, E. Sheibani, K.S. Kjaer, G. Boschloo, A. Yartsev, M. Freitag, R. Lomoth, P. Persson, K. Wärnmark
Chemical Science, 2021, 12, 48, pp. 16035-16053

I contributed to acquiring experimental data, performing calculations, analysing the data and coordination of the paper writing.

III **Interplay of MLCT and MC Relaxation Pathways as a Function of Side-Group Variation on the Iron(II) Carbene Scaffold**
L. Lindh, N.W Rosemann, I. Bolaño Losada, S. Persson, Y. Goriya, H. Fan, K. Wärnmark, J. Uhlig, P. Chábera, A. Yartsev, P. Persson
Manuscript

I coordinated the project, acquired experimental data, performed calculations, analysed the data and wrote the paper.

IV **Multifaceted Deactivation Dynamics of Fe(II) N-Heterocyclic Carbene Photosensitizers**
L. Lindh, T. Pascher, S. Persson, Y. Goriya, K. Wärnmark, J. Uhlig, P. Chábera, P. Persson, A. Yartsev
Submitted Manuscript

I coordinated the project, acquired experimental data, analysed the data and wrote the paper.

V **Microsecond Photoluminescence and Photoreactivity of a Metal-Centered Excited State in a Hexacarbene-Co(III) Complex**
S. Kaufhold, N.W. Rosemann, P. Chábera, **L. Lindh**, I. Bolaño Losada, J. Uhlig, T. Pascher, D. Strand, K. Wärnmark, A. Yartsev, P. Persson
Journal of the American Chemical Society, 2021, 143, 3, pp. 1307-1312

I contributed to acquiring experimental data and writing the paper.

VI **Luminescence and Reactivity of a Charge-Transfer Excited Iron Complex with Nanosecond Lifetime**
K.S Kjaer, N. Kaul, O. Prakash, P. Chábera, N.W. Rosemann, A. Honafar, O. Gordivska, L.A. Fredin, K-E. Bergquist, L. Häggström, T. Ericsson, **L. Lindh**, A. Yartsev, S. Styring, P. Huang, J. Uhlig, J. Bendix, D. Strand, V. Sundström, P. Persson, R. Lomoth, K. Wärnmark
Science, 2019, 363, 6424, pp. 249-253

I contributed to the initial temperature-dependent measurements followed-up in paper VII.

VII **Competing Dynamics of Intramolecular Deactivation and Bimolecular Charge Transfer Processes in Luminescent Fe(III) N-Heterocyclic Carbene Complexes**
N.W. Rosemann, **L. Lindh**, I. Bolaño Losada, S. Kaufhold, O. Prakash, A. Ilic, J. Schwarz, K. Wärnmark, P. Chábera, A. Yartsev, P. Persson
Chemical Science, 2023, 14, 13, pp. 3569-3579

I contributed to acquiring and analysing experimental data, as well as writing the paper.

VIII **Photophysical Integrity of the Iron(III) Scorpionate Framework in Iron(III)-NHC Complexes with Long-Lived ^{2}LMCT Excited States**
O. Prakash, **L. Lindh**, N. Kaul, N.W. Rosemann, I. Bolaño Losada, C. Johnson, P. Chábera, A. Ilic, J. Schwarz, A. Kumar Gupta, J. Uhlig, T. Ericsson, L. Häggström, P. Huang, J. Bendix, D. Strand, A. Yartsev, R. Lomoth, P. Persson, K. Wärnmark
Inorganic Chemistry, 2022, 61, 44, pp. 17515-17526

I contributed to acquiring and analysing experimental data, as well as writing the paper.

IX **Light-Induced Dynamics of an Fe(III) Carbene Photosensitizer with ^{2}LMCT State in a Heterogeneous System**
L. Lindh, P. Chábera, N.W. Rosemann, O. Prakash, A. Ilic, J. Schwarz, K. Wärnmark, P. Persson, A. Yartsev
Manuscript

I coordinated the project, acquired experimental data, analysed the data and wrote the paper.

All papers are reproduced with permission of their respective publishers.

Publications not included in this thesis:

X **Photophysics and Photochemistry of Iron Carbene Complexes for Solar Energy Conversion and Photocatalysis**
L. Lindh, P. Chábera, N.W. Rosemann, J. Uhlig, K. Wärnmark, A. Yartsev, V. Sundström, P. Persson
Catalysts, 2020, 10, 3, pp. 315

XI **Photofunctionality of Iron(III) N-Heterocyclic Carbenes and Related d5 Transition Metal Complexes**
P. Chábera, **L. Lindh**, N.W. Rosemann, O. Prakash, J. Uhlig, A. Yartsev, K. Wärnmark, V. Sundström, P. Persson
Coordination Chemistry Reviews, 2021, 426, pp. 213517

XII **Viking Spectrophotometer: A Home-Built, Simple, and Cost-Efficient Absorption and Fluorescence Spectrophotometer for Education in Chemistry**
P.V. Kolesnichenko, A. Eriksson, **L. Lindh**, D. Zigmantas, J. Uhlig
Journal of Chemical Education, 2023, 100, 3, pp. 1128–1137

Acknowledgements

I have conducted my PhD split between the divisions of Chemical Physics and Theoretical (Computational) Chemistry at Lund University, as a part of the iron-carbene-project. Thank you for welcoming me and giving me the opportunity to pursue PhD studies, which was since long one of my goals in life. I have very much enjoyed teaching during my PhD, and therefore thank the undergraduate teaching-team at Kemicentrum (Saywan, Lovisa, Sophie), and the professors who helped me get into the teaching activities. I also enjoyed going to Uppsala to make solar cells, thank you Dr. Hannes Michaels, and professors Marina Freitag and Gerrit Boschloo for this opportunity. Thanks to the many admin and support personnel at Kemicentrum, especially Maria Lövgren, who make things go round. Thank you for fruitful collaborations professors Kenneth Wärnmark and Reiner Lomoth.

Supervisors can be official or unofficial, and in general many colleagues have been generous with advice and support. My two main supervisors, Arkady and Petter, however more than all others. I can hardly comprehend how much time you have spent on my education, I am really lucky to have gotten supervisors who were always there for me. One of the things I have enjoyed absolutely the most is our scientific discussions, even though you go on way too long with too little fika. Pavel, my co-supervisor and friend, had further patience to teach me how to operate and build a pump-probe setup. Thank you Pavel for all your support, and for initially taking me on as a master student. Thank you Nils, who initially taught me a great deal of photophysics and set me off on the right track. Thank you Jens, my data analysis guru, who has supported me along the way. And thank you Torbjörn, who together with Pavel make the Millenia lab run and who is always eager to help.

Thank you all colleagues, at both my divisions, for providing a friendly work environment for me to thrive in. In particular, it has been fun to share office with Samuel and Oliver, and to sit in the "tofu-box office" with Edoardo, Weihua and Albin. I would like to thank the PhD and postdoc members of the "FeCAB-dynamics" team for fruitful discussions and fun activities; Iria, Yen, Simon, Zehan, Edoardo, Mani, Christina, Nils. Furthermore, I am grateful for the tiny female support network at Chemical Physics consisting of Egle, Klara and Christina. Finally, I would like to send special appreciation to my fellow PhD student Nidhi at Uppsala University and the "FeCAB-juniors" at CAS in Lund; Olga, Samuel, Jesper, Lisa, Valtýr, Aleksandra, Simon, Hao, Om, Arvind, Alpesh, Yogesh. I have learned many things from you, and wished we could have had a closer collaboration.

I have learned that pursuing a PhD is a challenging experience without exceptions, and that Murphy's law is constantly proven correct. In my case, Covid-19 and a demanding research collaboration posed complications. Many mentors, or especially caring colleagues, have in these times helped me to carry on; Charlotta, Knut, Pavel, Christina, Jens, Marie. I am forever grateful.

I came to Lund 10 years ago, to start the engineering nanoscience program. Now my Lund-adventure has come to an end, hopefully with a PhD degree in chemical physics. The journey has resulted in major personal growth, invaluable experiences and friends for life. A PhD degree in my case could not have been obtained without all fun side-projects, creative groups, and leadership teams that I am very grateful I got the opportunity to participate in. A special shoutout to the INASCON team, who together with me arranged an international nanoscience conference. I am also lucky to have a big network of friends, who are even too many to be mentioned here. Furthermore, I have a big supporting family who believes in me and I would especially like to mention my mother, father, brother and grandmother. Finally, I would like to thank Robin, who is best described as the rock on which this tree is rooted in all kinds of weathers. All things I would like to share with you, and in the end we have even supported each other's PhD journeys from getting a position to writing the thesis.

Abbreviations

Abbreviation	Explanation
A	electron acceptor
CB	conduction band
CR	charge recombination
CS	charge separation
D	electron donor
DAS	decay associated spectrum
DFT	density functional theory
DSPEC	dye-sensitised photoelectrochemical cell
DSSC	dye-sensitised solar cell
ESA	excited state absorption
GS	ground state
GSB	ground state bleach
HOMO	highest occupied molecular orbital
LC	ligand-centred
LF	ligand field
LICD	light-induced charge-disproportionation
LMCT	ligand-to-metal charge-transfer
LUMO	lowest unoccupied molecular orbital
MC	metal-centred
MLCT	metal-to-ligand charge-transfer
MPCT	metal-to-particle charge-transfer
MV^{2+}	methyl viologen di-cation
NIR	near-infrared
NTO	natural transition orbital
OPA	optical parametric amplifier
PA	product absorption
PPES	projected potential energy surfaces
PS	photosensitiser
Q	quencher
SE	stimulated emission
TA	transient absorption
TCSPC	time-correlated single photon counting
TD-DFT	time-dependent density functional theory
TEA	triethylamine
UV	ultraviolet

Popular Scientific Summary in English

We are living during an ongoing climate crisis, where a transition from fossil to renewable energy sources needs to take place as soon as possible. At the same time the population on Earth is growing, and people gain higher living standards, which leads to a growing global energy demand. To meet the massive demand of renewable energy that already exists and that is expected to grow during my entire life, currently available technology might just not be enough. Research must therefore strive to find solutions that will be more efficient in the long run, more specialised, or that can be applied in new systems. The renewable energy source that according to many have the largest potential is solar energy, since the energy content reaching Earth from the sun is more than enough to cover the global energy consumption. Apart from solar cells, researchers also try to develop solar fuels, a technology that can convert a simple starting material (e.g. water) into a fuel (e.g. hydrogen) by the energy from sunlight directly. Solar fuels are likely better suited compared to electricity and batteries for applications of long-distance transport by container ships or aircraft, due to the ease of storing and fuelling.

In my research, I study molecules that have potential for application in solar cells and solar fuel devices. The molecules are called photosensitisers, since they can absorb sunlight and create a charge separation. The photosensitisers are designed to mimic the chlorophyll molecules of photosynthesis, that perform the same processes which enable light harvesting in plants. The energy content of the separated charge carriers can be utilised either via direct extraction, which would be a solar cell, or to drive chemical reactions that build a solar fuel. To understand how these important molecules can absorb sunlight and utilise the separated charge carriers, I study them via laser spectroscopy. With laser spectroscopy we can excite the molecules, i.e. put them in a state of higher energy by absorbing light. We then measure how long they stay in various excited states - something that is crucial to what type of reactivity that has time to take place for an application purpose. For example, we can follow how charge carriers are transferred from molecule to semiconductor (which happens in the solar cells) or to another molecule (which is the first step to chemically build solar fuels).

Within the research field of solar cells and fuels, there are currently many materials competing for attention. In my case we study molecules, which have certain advantages. The molecules can be adapted ad infinitum, and our colleges at Lund University who make the molecules can relatively easily change their structure. This means for example that the colour of the light absorbed by the molecule can be adapted, which results in that beautiful solar cells of different colours (see Figure 1) can be fabricated or tandem solar cells that absorb a broad range of the light spectrum. This type of

solar cells (called dye-sensitised solar cells) currently have lower efficiency than the conventional silicon solar cell, but have the advantage of being printable. This means that they can be printed on a conductive plastic material resulting in flexible solar cells to be rolled out when needed, or to be incorporated in bags and headphones (something a Swedish company is working on).

Figure 1: Solar cells at the EPFL SwissTech convension centre in Lausanne.

The research field of solar fuels is not close to commercialisation yet. However, photosensitisers play an important part in many fundamental systems to absorb light and transfer charge carriers to catalysts that then convert raw material to solar fuel. What both applications have in common is that when photosensitisers are used, they are often based on coordination complexes with the noble metal ruthenium. Ruthenium is approximately as abundant as gold in Earth's crust, which results in a high price. It is not sustainable to base technology we need access to in large quantities on noble metals that are scarce. Many researchers in the field therefore advocate a change to using abundant elements, often from the first row transition metals, which has sparked a lot of initiatives within photosensitiser research.

The research group where I am a part, together with our collaborators, have since the first publication in 2013 run a successful project with the goal of replacing ruthenium with iron. Iron is one of the most abundant elements in Earth's crust, cheap, non-toxic and therefore suitable for sustainable technology. At a first glance researchers thought it would be an easy task to replace ruthenium with iron since they are from the same group in the periodic system, but this task turned out to take years of optimisation of the molecular structure. Today, the project has managed to prolong the important time the iron-based photosensitisers spend in the exited state from <100 fs to 2 ns. This 10 000-fold improvement has made large impact in the research field, and many more researchers are now working with iron-based photosensitisers. The photosensitisers have since been used in solar cells, in OLEDs and for hydrogen production. In this thesis work, I characterise the light absorbing properties of new iron-based photosensitisers, and investigate how they work when incorporated into solar cells or schemes for solar fuel production.

Populärvetenskaplig sammanfattning på svenska

Vi lever under en pågående klimatkris, där omställningen från fossila till förnyelsebara energikällor måste ske med omedelbar verkan. Samtidigt blir antalet människor på jorden fler, och trenden visar att vi får det allt bättre, vilket leder till att energiförbrukningen ökar. För att kunna möta det massiva behov av förnyelsebar energi som redan finns och som förväntas öka under hela min livstid, så räcker troligtvis inte befintliga utvinningstekniker till. Vi forskare måste sträva efter att i det långa loppet hitta nya tekniker som är effektivare, mer specialiserade eller som kan appliceras i nya system. Den förnyelsebara energikälla som många menar har störst potential är solenergi, då energiinstrålningen som når jorden från solen är mycket större än den mängd energi mänskligheten förbrukar. Utöver solenergi så jobbar forskare även på att utveckla solbränslen, en teknologi som direkt kan omvandla en enkel råvara (exempelvis vatten) till ett bränsle (exempelvis vätgas) med hjälp av energin i solljuset. Solbränslen skulle potentiellt vara bättre än el och batterier i tillämpningar för långväga transport med tunga fartyg eller flygplan, då de går att tanka och förvara på enkelt sätt.

I min forskning studerar jag molekyler vilka potentiellt kan användas i solceller och för att skapa solbränslen. Dessa molekyler kallas färgämnen, då de kan absorbera solljus och skapa laddningsseparation. Färgämnen imiterar fotosyntesens klorofyll-molekyler som utför ett identiskt steg vilket därmed möjliggör för växter att utnyttja energin i solljuset. Den energi som finns i de separerade laddningsbärarna kan utnyttjas antingen för direkt extraktion (vilket ger en solcell) eller för att driva kemiska reaktioner som skapar ett solbränsle. För att förstå hur dessa viktiga molekyler kan absorbera ljus och utnyttja de separerade laddningsbärarna så studerar jag dem med hjälp av laserspektroskopi. Med laserspektroskopi kan vi excitera molekylerna, d.v.s. försätta dem i ett tillstånd av högre energi genom absorption av ljus. Vi kan sedan mäta hur länge de befinner sig i olika exciterade tillstånd – något som är strikt avgörande för vilken typ av reaktioner som kan hinna ske i den senare applikationen. Vi kan också följa hur laddningsbärare förs över från molekyl till halvledare (vilket är vad som sker i solcellerna) eller till en annan molekyl (vilket är första steget för att på kemisk väg bygga solbränslen).

Inom forskningsfältet solceller och solbränslen finns det idag många olika material som konkurrerar om uppmärksamheten. I mitt fall studerar vi specifikt molekyler vilket har sina fördelar. Molekyler kan varieras in i det oändliga, och våra kollegor på Lunds universitet som tillverkar dessa kan relativt enkelt variera deras struktur. Detta medför exempelvis att man kan ändra vilken färg på ljuset som ska absorberas och kan alltså göra vackra solceller i flera olika färger (se Figur 2) alternativt tandemsolceller där olika molekyler hjälps åt att absorberar ett brett spektrum av solljus. När det kommer till färgämnesbaserade solceller (eller Grätzelsolceller) så har de idag lägre effektivitet

än de vanliga kiselsolcellerna, en fördel är dock att de kan tillverkas på ett enkelt sätt genom tryckning. Solcellerna kan t.o.m. tryckas på ledande plast vilket ger en flexibel solcell som kan rullas ut vid behov, eller som kan inkorporeras i väskor och hörlurar (vilket ett svenskt företag jobbar på).

Figur 2: Solceller på EPFL SwissTech konferenscenter i Lausanne.

När vi talar om solbränsle så har forskningsfältet ännu inte genererat kommerciella produkter. Färgämnen spelar dock en roll i många fundamentalt viktiga system där de absorberar ljus och skickar laddningsbärare vidare till en katalysator som sedan omvandlar råmaterial till solbränsle. Vad som är gemensamt för båda applikationer är att när färgämnesmolekyler används, är de till mycket hög grad baserade på koordinationskomplex av ädelmetallen rutenium. Rutenium är ungefär lika vanligt förekommande som guld i jordskorpan, vilket medför ett högt pris. Det är inte hållbart att basera teknologi vi behöver tillgång till i stor skala på ädelmetaller som är svåra att tillgå. Många forskare i fältet anser därför att det måste ske ett skifte till mer vanligt förekommande ämnen, ofta första radens övergångsmetaller, vilket har skapat många initiativ inom färgämnesforskningen.

Den forskargrupp jag tillhör, har tillsammans med våra forskarpartners, sedan första publikationen 2013 drivit ett framgångsrikt projekt med att ersätta ruteniumet i färgämnena med järn. Järn är ett av de vanligaste grundämnena i jordskorpan, billigt, inte giftigt och lämpar sig därför utmärkt för hållbar teknologi. Från början trodde forskare att det skulle vara enkelt att ersätta rutenium med järn då de är i samma grupp i det periodiska systemet, men denna uppgift visade sig kräva år av optimering av molekylstrukturen. Idag har projektet lyckats förlänga den viktiga livstiden som de järnbaserade färgämnena spenderar i exciterat tillstånd från <100 fs till 2 ns. Denna 10 000-faldiga ökning har gjort ett stort avtryck i forskningsfältet, och flera forskare har hoppat på trenden med att skapa järnbaserade färgämnen. Dessa färgämnen har sedan dess använts i solceller, i OLEDs, samt för vätgasproduktion. I mitt doktorandarbete karaktäriserar jag nya färgämnens ljusabsorberande egenskaper, samt hur färgämnena fungerar när de inkorporeras i solceller eller i system för att generera solbränsle.

Photophysics and Photochemistry of Iron Carbene Complexes

Chapter 1

Harvesting Solar Energy

I'd put my money on the sun and solar energy.
What a source of power!
I hope we don't have to wait until oil
and coal run out to before we tackle that.[1]

1.1 Global Energy Demand

Humanity faces a growing global energy demand, where both the number of people on Earth and the average energy consumption are increasing. On top of that, a related challenge is the global warming caused by burning of fossil fuels for energy consumption.[1, 2] At present time, the United Nations has agreed to treaties such as the Paris Agreement, that if met will lead to the end of using fossil fuels.[3] This means that humanity at the same time as expanding the energy usage, needs to cut the energy resource today making up >75% of the world's energy supply.[4] One of the needed solutions, that relates to this thesis work, is a decentralised energy supply not based on fossil fuels. The concept means that many smaller energy harvesting facilities are placed close to the users, in contrast to few, big facilities e.g. extracting raw oil which is then exported around the globe.[5]

We have built our society around the "energy currencies" electricity and fuel, that are for us easy to utilise and transport. The source of these energy currencies does, however, not have to be fossil fuels. In Figure 1.1 the energy potential of different energy sources, both renewable and finite (including fossil), are compared.[6] Sys-

[1] Thomas Edison

tems for harvesting solar energy are investigated in this thesis work, and it is easy to understand why when looking at Figure 1.1. The amount of energy supplied by the sun as light annually exceeds by far all other renewable energy sources, as well as the total remaining reserves of non-renewable energy sources.[6] Sunlight is also freely accessible at all places on Earth, which fits the decentralised energy concept. It is therefore a promising direction of development, to invest in the installation of existing solar harvesting technologies, and to put research effort into future generations of the technology.

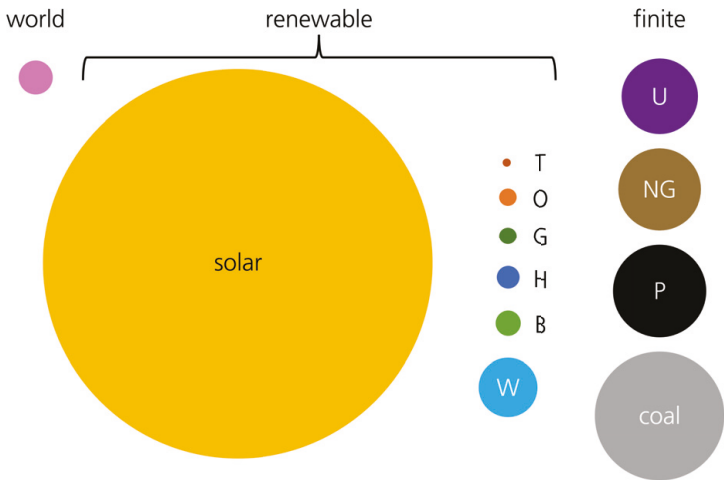

Figure 1.1: The energy potential of different energy sources compared by the area of their circles. Note that renewable energy sources are compared per year, whereas non-renewable sources are compared by their total remaining amount. The annual world energy usage from 2021 is also shown to scale.[4] Adapted from Perez et al..[6] U - uranium, NG - natural gas, P - petroleum, T - tidal, O - ocean thermal, G - geothermal, H - hydro, B - biomass, W - wind and waves.

Also nature uses sunlight as the one form of renewable energy supply at the heart of all living systems. Furthermore, the energy currencies in nature are circular, stored in chemical bonds in various carbon-based molecules. In the initial steps of photosynthesis, where light is harvested, the quantum efficiency of turning an absorbed photon into a reactive intermediate is near unity.[2][7, 10, 11] Light harvesting in natural photosynthesis therefore serves as an inspiration when developing solar energy conversion technology. To understand how nature so efficiently harvests sunlight, the first steps of photosynthesis are depicted in Figure 1.2. The photosystems in a plant contain a large number of molecules that can absorb visible light, together contributing to give the plant its colour. These molecules are called pigments, and some of them consist of transition metal complexes.

[2]The light to glucose efficiency is however often $<1\%$ since nature has optimised plants for performing not only photosynthesis but also metabolism and reproduction.[7–9]

The excited pigments, i.e. after light is absorbed, also perform the next fundamental step of photosynthesis which is charge separation. This is accomplished by transferring an electron to a nearby molecule in a reaction becoming thermodynamically possible only when the pigment is excited. The efficiency of the charge separation in this step is near unity since the charge separation occurs much faster than the deexcitation of the pigment. The excited electron is further transferred through a cascade of units with decreasing redox potential, making it virtually impossible for the electron to recombine (i.e. travel in the "wrong" direction, back to the initial pigment). Light harvesting in photosynthesis is thus enabled by a clever photosystem design, but also by the special properties of the pigment molecules.[7, 8, 12] Inspired by the natural pigments, artificial pigments for application in solar energy conversion technology are discussed in this thesis. Such artificial pigments are called molecular photosensitisers, which means that they are molecules that make a system sensitive to light.[13–16]

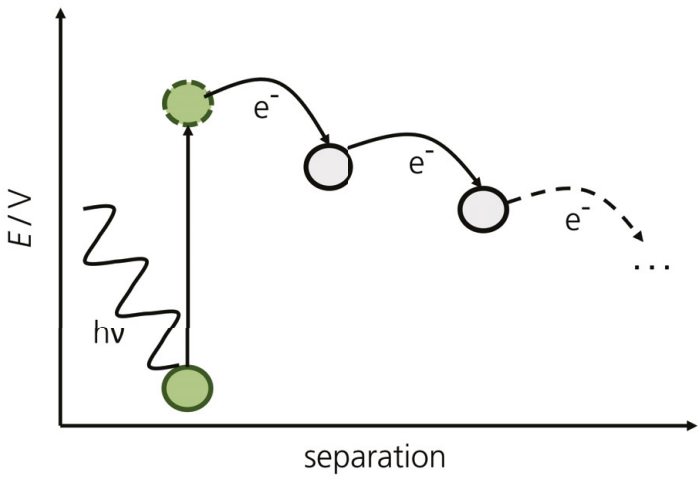

Figure 1.2: A simplified illustration of the initial steps involved in the photosynthetic "light reaction" in plants. The vertical axis represents the redox potential of the system, whereas the horizontal axis instead represents separation in space. The pigment (green) is excited by light ($h\nu$), and consequently creates a charge separation by transferring an electron to a neighbouring molecule (grey). This starts a cascade of electron transfer events that increases the charge separation.

1.2 Solar Fuels using Photosensitisers

The technological strategy that is most similar to photosynthesis is artificial photosynthesis, where a "solar fuel" is created from a device that absorbs sunlight.[3] Instead of letting nature build biomass for us, artificial photosynthesis offers a direct way of

[3]Artificial photosynthesis as a concept also includes strategies that do not convert sunlight directly, such as synthetic biology and electrolysis approaches, but these will not be considered here.

optimising the yield of fuel production.[1, 7, 8, 17, 18] The solar fuel device could also operate at places not suitable for growing crops, and thus not be in competition with food production. Solar fuel candidates include syngas (mixture of CO and H_2), methanol and maybe most well-known hydrogen.[2] These high energy content chemicals can in principle be produced by utilising solar harvesting photosensitisers together with catalysts, in a photocatalysis reaction scheme.[13–17]

The fundamental steps in the photocatalysis reaction scheme are similar to the first steps of natural photosynthesis. First, the photosensitiser absorbs light, which is followed by an electron-transfer reaction between the excited photosensitiser and a reactant. Consecutive absorption and electron-transfer events accumulate positive and negative charges at two different catalyst sites respectively. The catalysts then convert a raw material into solar fuel when enough charges are accumulated. Taking hydrogen evolution as an example, the photocatalysis system would use the same raw material as nature, H_2O, and oxidise it generating oxygen, protons and electrons. This means that one of the catalysts is an oxygen evolution catalyst, which after transferring four electrons to the photosensitiser (i.e. accumulating four positive charges) performs the reaction.

$$2H_2O \rightarrow 4H^+ + 4e^- + O_2$$

At the other catalyst site, two protons are reduced by a hydrogen evolution catalyst after receiving two electrons from the photosensitiser.

$$2H^+ + 2e^- \rightarrow H_2$$

Alternatively, CO_2 can be added as a secondary raw material to be reduced to hydrocarbons of higher energy content than hydrogen (e.g. methanol). Which fuel the system produces, depends on the selected reduction catalyst. Producing larger fuel molecules than H_2, however, comes at the expense of a more complex reduction reactions, where more than two electrons are involved.[1, 7, 14, 17, 19]

Two design strategies for solar fuel devices that utilise molecular photosensitisers are depicted in Figure 1.3. Figure 1.3a shows an example of homogeneous catalysis, that entails one molecule that performs all reactivity. In this supramolecular system, different parts of the molecule perform the tasks of light harvesting and catalysing reactions, but the parts are held together by covalent or strong intermolecular bonds.[7] In this way, electronic communication between the parts and closeness in space are realised, which are important prerequisites for the system to work.[15, 17] In homogeneous catalysis both the produced fuel and side-product (e.g. hydrogen and oxygen) will be mixed, which can make them difficult to separate and potentially lead to side-reactions.[20] Therefore, there are also heterogeneous catalysis approaches, and as an example a dye-sensitised photoelectrochemical cell (DSPEC) is shown in Figure 1.3b.[21] The photosensitiser is in this device combined with a semiconductor, which

it can bind to if certain anchor groups are incorporated in the molecular structure. The semiconductor (commonly TiO_2) does not by itself absorb in the visible spectral range, but has the ability to extract and accumulate charges from the photosensitiser. After excitation, the photosensitiser thus transfers an electron to the semiconductor. The oxygen evolution catalyst then transfers an electron to the oxidised photosensitiser, and after four such events the water splitting reaction takes place. With the help of a small applied bias, the electrons are transferred from the semiconductor to the counter-electrode where hydrogen evolution is performed by the hydrogen evolution catalyst. In this arrangement, the solar fuel and the side-product are produced in separate compartments.[2, 7, 16, 22, 23]

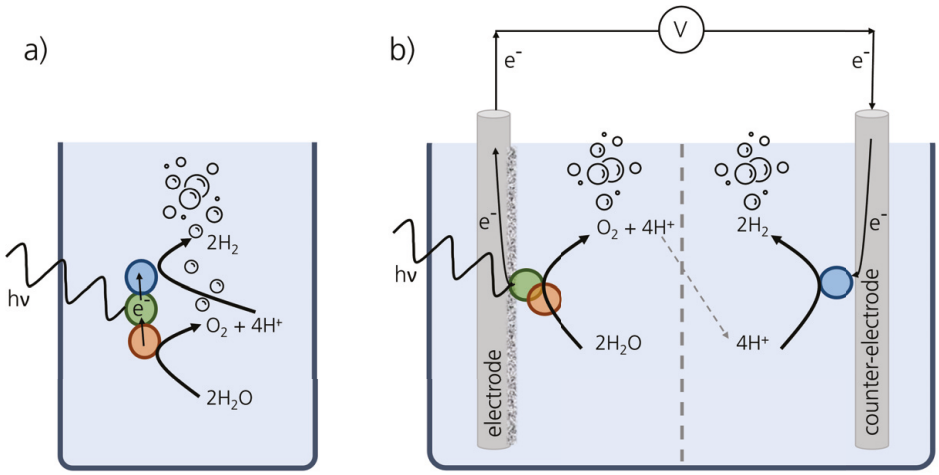

Figure 1.3: a) Homogeneous catalysis exemplified by a supramolecular system. b) Heterogeneous catalysis exemplified by a DSPEC. The example reactions are water splitting and hydrogen evolution. Green - photosensitiser, orange - oxygen evolution catalyst, blue - hydrogen evolution catalyst, $h\nu$ - light excitation.

The research field of solar fuels entails many different approaches, schemes and materials. Only some suggestions utilising photosensitisers have been presented in this section, according to the scope of the thesis work. The major challenges for solar fuel systems are still to increase the efficiency and stability, in order to make the technology commercially viable. Unfortunately, many materials (including molecules) tend to corrode or break in the presence of water under oxidative/reductive conditions. Here, molecular based solutions have an advantage of being much easier to adapt with methods from chemical synthesis.[20, 24]

1.3 Solar Cells using Photosensitisers

By slightly altering the device design of the DSPEC, electricity can be extracted from the harvested light instead of fuel. Such a device is called a dye-sensitised solar cell (DSSC), and is schematically shown in Figure 1.4.[25] The working principle of an n-type DSSC[4] is outlined in Figure 1.4 by the steps A-D. First, the photosensitiser (PS) absorbs sunlight (A) and reaches an excited state of higher redox potential than the conduction band (CB) edge of the semiconductor. An electron is then injected (B) from the excited photosensitiser into the CB. Electrons in the CB are continuously extracted (C) and travel to the counter-electrode due to the difference in redox potential between the electrodes. At the counter-electrode, the circuit is completed by a redox mediator (M) that has a driving force to be reduced at the counter-electrode, and then reduce the oxidised photosensitiser (D). During the DSSC operation, a current flows between the electrodes and a voltage is generated by the difference in redox potential between the CB edge and the redox mediator.[7, 23, 26–28]

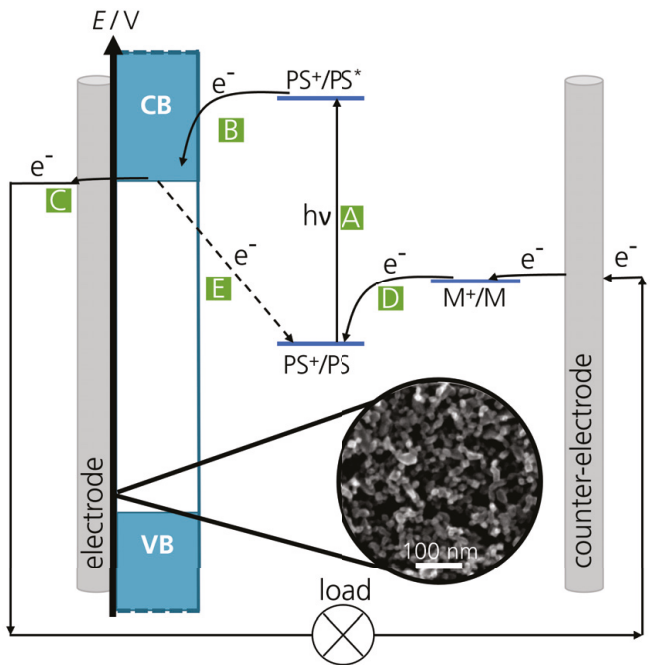

Figure 1.4: Schematic of a DSSC, also indicating the key processes involved in its operation: A - absorption, B - injection, C - extraction, D - regeneration, E - recombination. CB - conduction band, VB - valence band, PS - photosensitiser, M - redox mediator, hν - light excitation. Scanning electron microscopy image of the TiO_2 nanoparticle layer by Linnéa Jönsson.

[4]A p-type DSSC works by the same principle but with a reverse flow of charges, meaning that the semiconductor transfers electrons to the photosensitiser.[23]

The record power-conversion efficiency is to date 13% for the DSSC (see Figure 1.5),[29] and crucial for this performance is to prepare the semiconductor as nanoparticles and not as a thin layer (see Figure 1.4).[25] This increases the surface area tremendously, which enables many more photosensitisers to be incorporated and thus more light to be absorbed. The efficiency is still lower than the dominant solar cell technology using silicon (and not photosensitisers) that today has ∼26% power-conversion efficiency (see Figure 1.5).[29] Common limiting factors for the DSSC are the specific absorption spectrum of the photosensitiser, recombination processes (e.g. process E in Figure 1.4) which returns the electron to the photosensitiser before it is extracted, and voltage losses to create a driving force for the redox reactions (e.g. process B and D in Figure 1.4). The DSSC technology, however, has the advantages of being easy to fabricate via screen printing, the possibility to make solar cells of different colours and patterns, and the possibility to make flexible solar cells.[23] DSSCs are also more competitive to silicon solar cells for indoor applications, and should be seen as a complementary technology to other types of solar cells.[30] Moreover, with the DSSC as the role model, many new solar cell technologies have developed based on the same fundamental principle (see Figure 1.5, "Emerging PV").[29]

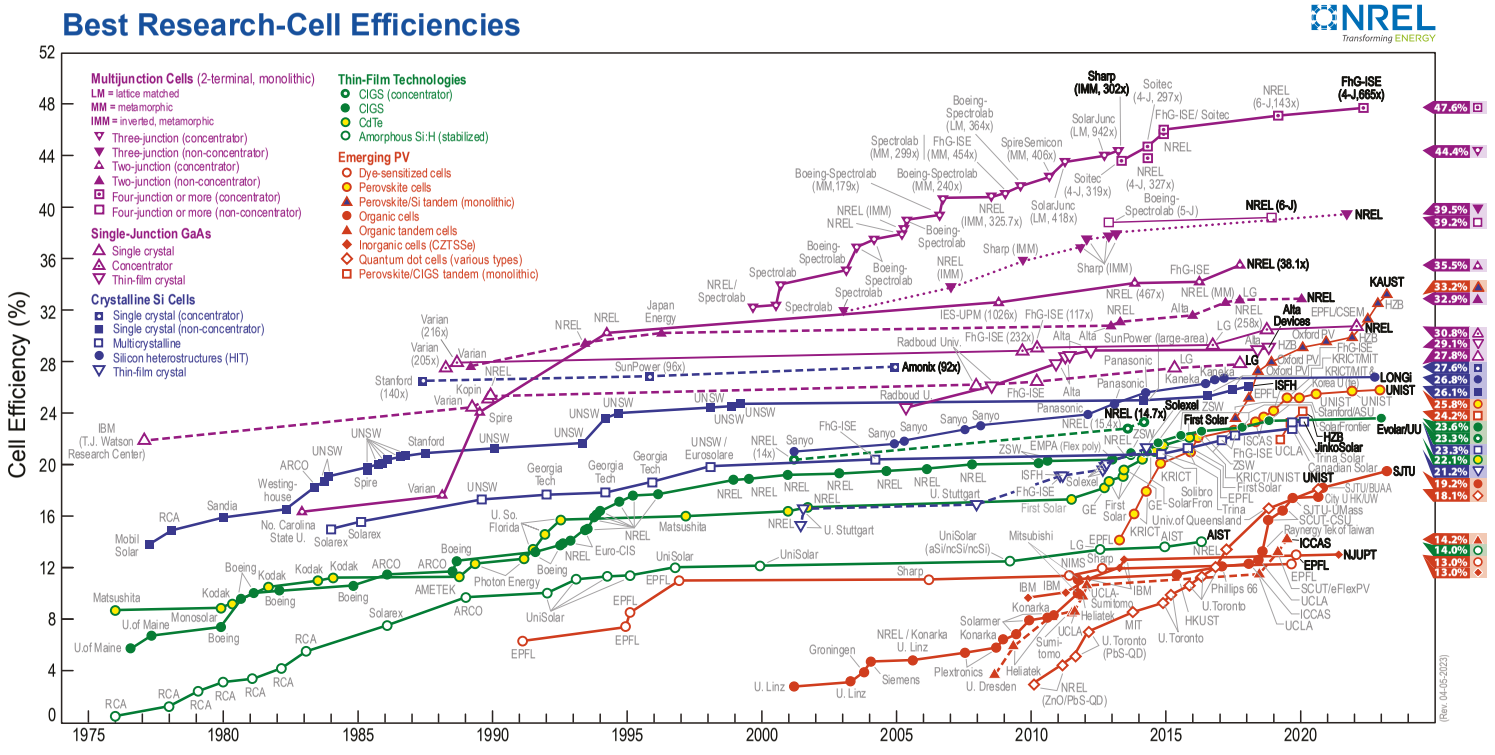

Figure 1.5: The well-known solar cell efficiency chart from National Renewable Energy Laboratory (NREL). All known solar cell technologies are compared by their certified power-conversion efficiency.[29] This plot is courtesy of the National Renewable Energy Laboratory, Golden, CO.

Chapter 2

Exploring Molecular Photosensitisers

Show me the data,
and then we can talk.[1]

2.1 The Ideal Photosensitiser

The work in this thesis is centred around the development and characterisation of novel photosensitisers, and their application towards solar energy conversion. The most fundamental property of a photosensitiser is to absorb visible light, but to make a good photosensitiser more is required. A set of criteria for the ideal photosensitiser[31, 32] is summarised here:

- strong visible absorption
- stability in all involved states
- high excited state redox potential
- long-lived excited state
- charge-separated excited state

[1]Modus operandi at Chemical Physics, Lund University.

Many of these properties concern the excited state, which is the state responsible for transferring charges to other compounds both in photocatalysis and solar cells. During the charge-transfer reaction, the oxidised or reduced form of the photosensitiser is generated. For the desired reactivity to take place, and to have a chance of regenerating the ground state of the photosensitiser, it is therefore important that all involved states (including oxidation states) of the photosensitiser are stable.[31, 32]

The reactivity of the excited state is determined by its redox potential as well as its lifetime. The redox potential dictates what reactions are thermodynamically possible, whereas the lifetime controls what reactions have time to take place (i.e. kinetically possible).[31] The excited state lifetime τ describes how long the photosensitiser stays in the excited state before deexcitation, and is defined as the inverse of the deexcitation rate k shown in Equation 2.1.

$$\frac{d[PS]}{dt} = -k[PS] = -\frac{1}{\tau}[PS] \tag{2.1}$$

In Equation 2.1, $[PS]$ is the concentration of the excited photosensitiser and t is the time.[7]

The final point, a charge-separated excited state, means that electron and hole density are separated to different parts of the molecule in the excitation process. This often results in reactive frontier orbitals on auxiliary, less hindered parts of the photosensitiser, which facilitates participation in charge-transfer reactions.[32–34]

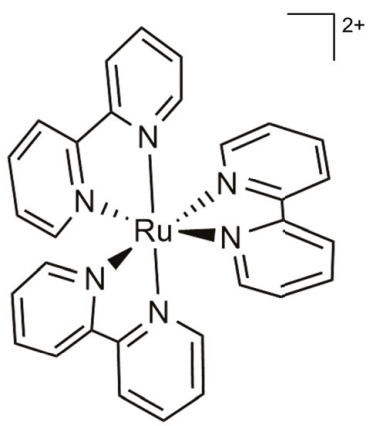

Figure 2.1: The molecular structure of the photosensitiser $Ru(bpy)_3^{2+}$.

The Ru polypyridyl complexes, a type of transition metal complexes featuring a Ru(II) ion coordinating organic ligands, fulfil all criteria for the ideal photosensitiser. This class of complexes are therefore commonly used in fundamental research and well as in applications. The "parent complex" in this class is $Ru(bpy)_3^{2+}$, that is depicted in

Figure 2.1.[16, 31, 35–37] $Ru(bpy)_3^{2+}$ will in the rest of this chapter be used as an illustrative example for explaining the underlying electronic structure resulting in the excellent properties, as well as how these properties are measured.

2.2 Electronic Structure

$Ru(bpy)_3^{2+}$ is a homoleptic complex, which means it has three identical ligands. Each ligand binds with two coordination sites to Ru(II), since they are bidentate (see Figure 2.1). The nitrogen atoms in the ligand interact both with σ- and π-type orbitals to bind with the $4d$-orbitals of Ru(II).[31, 37] To understand the bonding interaction between Ru(II) and the ligands, and realise what electronic states this bonding gives rise to, ligand field (LF) theory is briefly introduced.[38]

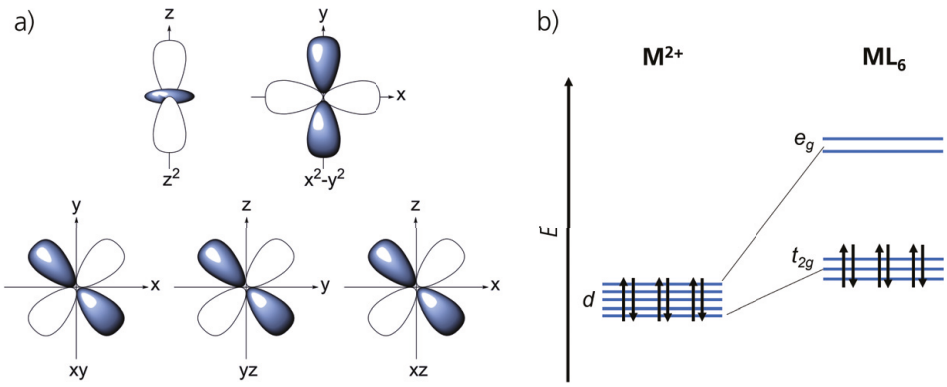

Figure 2.2: a) The five d-orbitals that are the frontier orbitals of transition metals. The lobes represent the electron probability distribution, and the colour represent the phase of the wave function. b) Illustration of the d-orbital splitting caused by the ligand field strength when ligands (L) are coordinated to the metal (M). Here populated by six electrons (d^6 electronic configuration).

Ligand-field theory describes the bonding interaction between transition metals and ligands, such as the case of $Ru(bpy)_3^{2+}$. As already indicated, the frontier orbitals in Ru(II) involved in the bonding are the five $4d$-orbitals shown in Figure 2.2a. The orbitals are degenerate in an environment without ligands, and since Ru(II) has a d^6 electronic configuration these orbitals hold six electrons (see Figure 2.2b).[38] For simplicity, it is assumed that the three ligands coordinate to Ru(II) at six sites in an octahedral arrangement.[2] The directions of the Ru(II)-ligand interactions are then along the x, y and z-axes in the coordinate system of Figure 2.2a. Due to the symmetry of the $4d$-orbitals, two of them feature lobes pointing in the direction of the axes, whereas the other three have lobes in between axes. The orbitals d_{z^2} and $d_{x^2-y^2}$,

[2] $Ru(bpy)_3^{2+}$ is in reality not a perfectly octahedral molecule (it has D3 symmetry), but it is a commonly used simplification.[7, 28]

with lobes pointing towards the ligands, are strongly destabilised since electron rich domains are placed close. The orbitals d_{xy}, d_{yz} and d_{xz} are not as strongly destabilised, which results in a lower energy compared to d_{z^2} and $d_{x^2-y^2}$. The orbitals are thus divided in two groups named e_g and t_{2g} based on their symmetry (see Figure 2.2b). The ligand field strength, i.e. the electrostatic field from the ligands, determine the splitting between the e_g- and t_{2g}-orbitals.[38] In $Ru(bpy)_3^{2+}$, the ligands have a rather high ligand field strength which results in a significant splitting. The most favourable way to position six electrons is to fill the t_{2g}-orbitals, which yields a low-spin complex with multiplicity 1 in the ground state.[31, 37]

A simplified molecular orbital structure diagram of $Ru(bpy)_3^{2+}$ is shown in Figure 2.3a, including bonding electrons both from Ru(II) and the ligands. The electronic structure can also be described within the state formalism, where the specific arrangement of all electrons over the available set of orbitals is described as one state. The arrangement shown in Figure 2.3a is the ground state (GS) of $Ru(bpy)_3^{2+}$. Upon excitation by light, an electron is promoted from the t_{2g}-orbitals to empty orbitals on either the ligands or the metal which results in another electronic state being populated. The transition can be of metal-to-ligand charge-transfer (MLCT) character or metal-centred (MC) character which is indicated in Figure 2.3a. The electronic states are named after the electronic transitions, and can have multiplicity 1, 3 or 5. Figure 2.3b shows the relevant electronic states of $Ru(bpy)_3^{2+}$, and how their energy depend on a reaction coordinate r (which commonly is the metal-ligand bond distance).[31, 37, 39]

In a simplified picture, the ^{1}MLCT state is populated when $Ru(bpy)_3^{2+}$ absorbs sunlight.[31, 32, 40] The deexcitation of the ^{1}MLCT state entails multiple deactivation pathways that together contribute to return the complex to ^{1}GS, indicated in Figure 2.3b. The first set of competing processes are fluorescence (fl), which returns the complex to ^{1}GS by emitting a photon, and intersystem crossing (ISC), which changes the excited state to ^{3}MLCT. Since ruthenium is a heavy atom, the spin-orbit coupling is large which favours the ISC process.[7] Therefore, the rate of ISC is faster ($k_{ISC} > k_{fl}$) and fluorescence is rarely observed. The ^{3}MLCT state is long-lived, meaning for $Ru(bpy)_3^{2+}$ an excited state lifetime of 930 ns[3] (for Ru polypyridyl complexes in general from 10 ns - 1 μs).[31] The lifetime is long since the return to ^{1}GS is spin-forbidden, as well as there is a substantial energy gap between the ^{3}MLCT state and ^{1}GS. The latter is called the energy-gap law, which describes how a large energy difference between two states results in a small overlap between vibrational sublevels, which hinders non-radiative transitions.[7] The deactivation of the ^{3}MLCT state can

[3]The lifetime can range between 500–1000 ns, depending on parameters such as the solvent, the oxygen concentration in the sample, the temperature, etc. 930 ns corresponds to a measurement in deoxygenated acetonitrile at room temperature.[39]

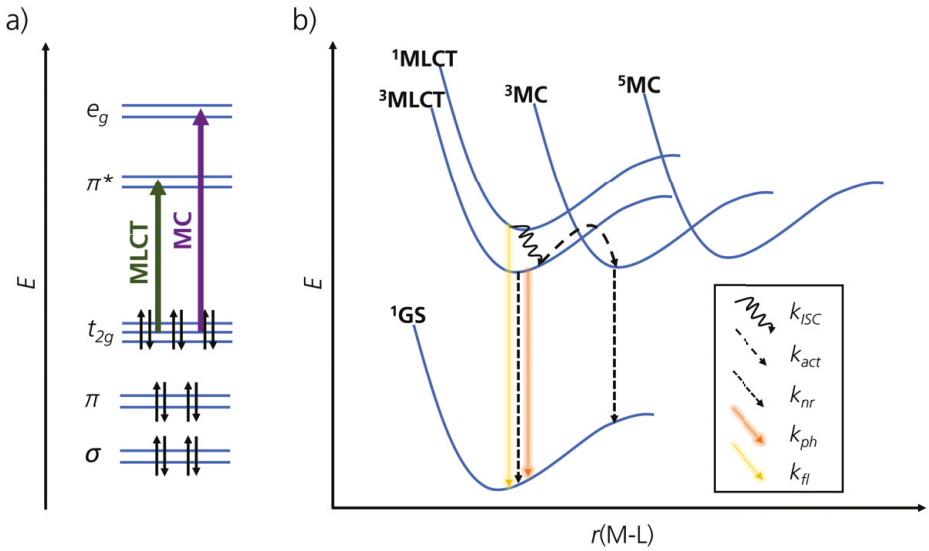

Figure 2.3: a) Molecular orbital structure diagram of $Ru(bpy)_3^{2+}$, with MLCT and MC transitions indicated. b) Schematic of the excited state landscape in $Ru(bpy)_3^{2+}$, together with the relevant deactivation rates. ISC - intersystem crossing, act - activation, nr - non-radiative, ph - phosphorescence, fl - fluorescence. On the horizontal axis, the average metal-ligand (M-L) bond length is plotted.

occur via emitting a photon i.e. phosphorescence (rate k_{ph}), non-radiative direct decay (rate k_{nr}) and via the ^{3}MC state (rate k_{act}), see Figure 2.3b). A change of excited state to ^{3}MC or ^{5}MC is associated with an activation energy, but at room temperature this barrier can be overcome for the ^{3}MC state. The ^{3}MC state does not show phosphorescence as it is very short-lived, and efficiently returns the complex to ^{1}GS via non-radiative decay (rate $k_{nr'}$). $k_{nr'}$ is high since the ^{3}MC state has a small barrier towards the ^{1}GS in some reaction coordinate (not shown in Figure 2.3b). The small barrier is a result of the geometrical distortion of the MC states compared to the ^{1}GS and MLCT states.[31, 32, 40]

As a consequence of the excited state landscape, $Ru(bpy)_3^{2+}$ has all the desired properties of a good photosensitiser. The absorption in the visible spectral region is strong, due to the nature of the MLCT transition. There are no dissociative states that make the complex unstable. The excited state involved in charge-transfer processes is the ^{3}MLCT state which has both high redox potential and long lifetime. The ^{3}MLCT state even has some degree of charge separation, with the electron located on the ligands and the hole on the metal. The ^{3}MLCT state is therefore called the photofunctional state of $Ru(bpy)_3^{2+}$, where photofunctionality in this thesis is defined as participating in either electron- or energy transfer reactions, alternatively displaying emission. $Ru(bpy)_3^{2+}$ also shows both reversible oxidation and reduction, which makes it more robust than natural pigments.[16, 31, 32, 39] The excited state landscape

and associated properties have been discovered by scientist performing measurements and calculations on $Ru(bpy)_3^{2+}$. In the following sections (2.3-2.5), typical methods needed to investigate a photosensitiser will be outlined, with $Ru(bpy)_3^{2+}$ as the illustrative example.

2.3 Steady-State Spectroscopy

Steady-state spectroscopy can determine what excited states in $Ru(bpy)_3^{2+}$ that interacts with light, and which is the lowest excited state. The focus of this discussion is electronic transitions, i.e. transitions between the states outlined in Figure 2.3b. Absorption spectroscopy probes what electronic transitions can take place from the ground state of $Ru(bpy)_3^{2+}$. Emission spectroscopy, on the other hand, probes the lowest excited state via its radiative transitions to the ground state. That only the lowest excited state will emit light is an assumption that is called Kasha's rule.[7, 41]

In Figure 2.4a, the absorption spectrum of $Ru(bpy)_3^{2+}$ is shown in the visible to ultraviolet (UV) wavelength range.[16] The vertical axis is plotted in an absolute scale called the extinction coefficient (ϵ), which is a material property representing the strength of the transition. The extinction coefficient varies depending on if the transition is spin- and/or Laporte-allowed, see Table 2.1.[7, 42] In Figure 2.4a the absorption bands are assigned to MLCT, MC and (ligand-centred) LC transitions based on the extinction coefficient (see Table 2.1).[16, 31, 35–37] The assignments can be cross-checked with complementary methods (such as quantum chemical calculations, see Section 2.5).[43] To summarise, the absorption measurement gives insight into what states are involved in the excited state landscape of $Ru(bpy)_3^{2+}$, their energy (relative to the ground state) and how well the photosensitiser absorbs sunlight. The absorption measurement can also be used to probe the stability of $Ru(bpy)_3^{2+}$ over time, by monitoring how the absorption spectrum changes on a timescale of hours or days.[7] This also applies to the oxidised and reduced species of $Ru(bpy)_3^{2+}$, that can be generated by applying a potential to the sample. By this technique, often referred to as spectroelectrochemistry, the absorption spectrum of other oxidation-states of $Ru(bpy)_3^{2+}$ can be measured.[44]

In Figure 2.4b, the emission spectrum of $Ru(bpy)_3^{2+}$ at room temperature is shown (298 K).[16] To identify the nature of the lowest excited state in $Ru(bpy)_3^{2+}$, the emission spectrum is compared to the absorption spectrum. The emission from an excited state is always red-shifted compared to the absorption to that excited state.[4]

[4]This is sometimes referred to as the Stokes shift. The definition of the Stokes shift however varies depending on the source, and becomes nontrivial when the emission is not coming from the same state as the absorbing state.

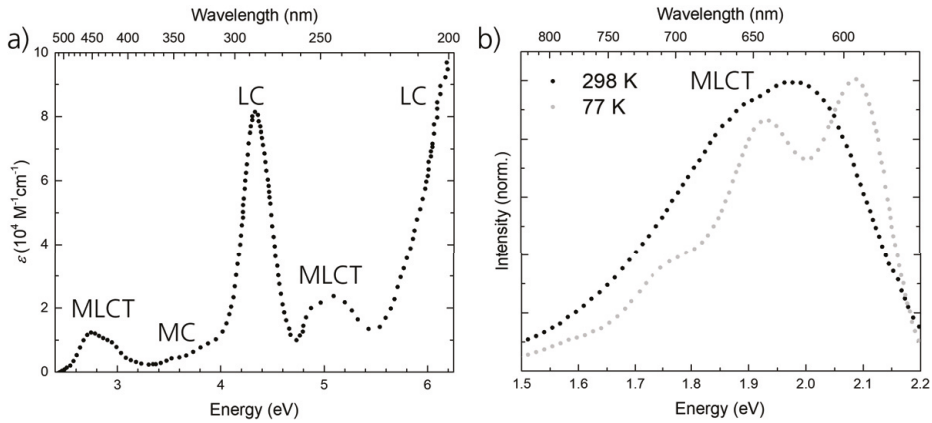

Figure 2.4: a) Extinction coefficient of Ru(bpy)$_3^{2+}$ with indicated transition assignments. b) Emission spectra of Ru(bpy)$_3^{2+}$ at two different temperatures compared (normalised intensity scale), the emission is associated with a MLCT transition. Adapted from Thompson et al..[16]

Table 2.1: Table with typical extinction coefficient (ϵ) values for different types of transitions. MC - metal-centred, MLCT - metal-to-ligand charge-transfer, LMCT - ligand-to-metal charge-transfer, LC - ligand-centred.[7, 42]

Type of Transition	**Typical ϵ ($M^{-1}cm^{-1}$)**	**Comment**
Spin-forbidden MC	<1	Spin- and Laporte-forbidden
Spin-allowed MC	1-1000	Laporte-forbidden Depends on symmetry
MLCT, LMCT	1000-50000	Allowed
LC	>10000	Allowed

This is due to changes in the solvent environment and the structural relaxation of the molecule after excitation. Furthermore, an emission excitation spectrum should match the absorption feature of the state giving rise to the emission signal.[7, 41] This is because the excitation spectrum maps the emission intensity as a function of excitation wavelength, and the absorption spectrum describes how much of the excitation wavelength that is absorbed. In Ru(bpy)$_3^{2+}$, the emission in Figure 2.4b has been assigned to the lowest ^{3}MLCT state.[16, 31, 35–37]

The emission energy provides a way to determine the energy of the relaxed ^{3}MLCT state, and not just the energy at ground state geometry (which is what the absorption measurement provides). The energy difference between the ^{1}GS and ^{3}MLCT minima (see Figure 2.3b) is often approximated by the intersection between the absorption and emission spectra (called the E_{00} energy). Furthermore, how prominent the non-radiative decay pathways are can be estimated from the emission quantum yield. The emission quantum yield (Φ) is generally defined as the ratio between the rate of the radiative transition (k_r) and the sum of all deactivation rates (k_i) from that state, see

Equation 2.2.[7, 41]

$$\Phi = \frac{k_r}{\sum_i k_i} = \frac{k_{ph}}{k_{ph} + k_{nr} + k_{act}} \tag{2.2}$$

For the specific case of the ^{3}MLCT state phosphorescence in Ru(bpy)$_3^{2+}$, Φ is described by the last expression in Equation 2.2 based on the processes in Figure 2.3b (k_{ph} - phosphorescence rate, k_{nr} - non-radiative rate and k_{act} - activated decay rate). The phosphorescence quantum yield of Ru(bpy)$_3^{2+}$ is 9.5% at room temperature.[5][39] If the system is cooled down, the quantum yield increases since some of the non-radiative deactivation processes are slowed down (especially k_{act} that has an activation energy). The emission spectrum at 77 K in Figure 2.4b also displays more features than the spectrum at 298 K. These are the vibrational sublevels of the electronic state, corresponding to vibrational modes involved in the deactivation of the ^{3}MLCT state.[7, 16]

Absorption and emission spectra are measured by probing light intensity as a function of wavelength, see Figure 2.5. The absorbance is given on a logarithmic scale, and is defined Equation 2.3 by the light intensity sent on the sample (I_0) compared to the light intensity transmitted through the sample (I_t).

$$A = -\log(\frac{I_t}{I_0}) = \epsilon c l \tag{2.3}$$

The absorbance is linearly dependent on the extinction coefficient (ϵ), the concentration of the photosensitiser (c) and the path length of the sample (l). Equation 2.3 is called the Beer-Lambert law.[7] The emission can be probed at any geometry since light is emitted isotropically in space after exciting the sample. To estimate the emission quantum yield, the sample is either placed in an integrating sphere to capture the emission in all directions, or measured comparative to a reference sample of know quantum yield.[7, 41]

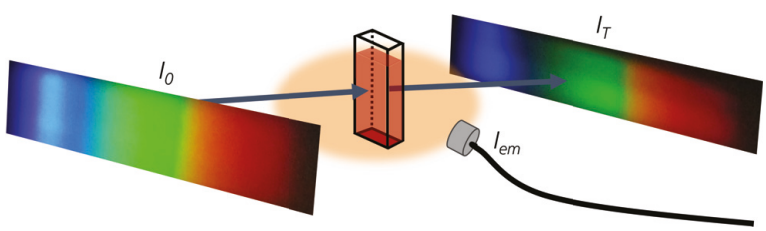

Figure 2.5: Sketch indicating the principle of how steady-state absorption and emission signals are measured. I_0 - incoming light intensity, I_T - transmitted light intensity, I_{em} - emitted light intensity.

[5] 9.5% corresponds to a measurement in deoxygenated acetonitrile.[39]

2.4 Time-Resolved Spectroscopy

Since the lowest excited state in $Ru(bpy)_3^{2+}$ (^{3}MLCT) is emissive, the easiest approach to measure the lifetime is to use a time-resolved emission spectroscopy technique. One such technique is time-correlated single photon counting (TCSPC), which measures the delay time between sample excitation and detection of a singly emitted photon. Many excitation-detection events are measured in succession by the setup that counts the number of times each delay time was measured. The distribution of the different counted delay times is representative of the excited state lifetime if the counting rate is low, i.e. the excitation density is adapted so only one molecule has the chance to emit in $\leq$2% of the measurements. The low counting rate ensures that the probability of emission from more than one molecule (which would distort the statistics) is very low.[7, 11] The number of counted emission events (N) at each delay time decreases exponentially with time (t) according to Equation 2.4.

$$N(t) = N_0 e^{\frac{-t}{\tau}} \tag{2.4}$$

In Equation 2.4, N_0 is the count of photons detected simultaneously as the excitation (delay time is zero) and τ is the excited state lifetime. By fitting this function to the obtained data, the ^{3}MLCT state lifetime of $Ru(bpy)_3^{2+}$ is extracted.[7]

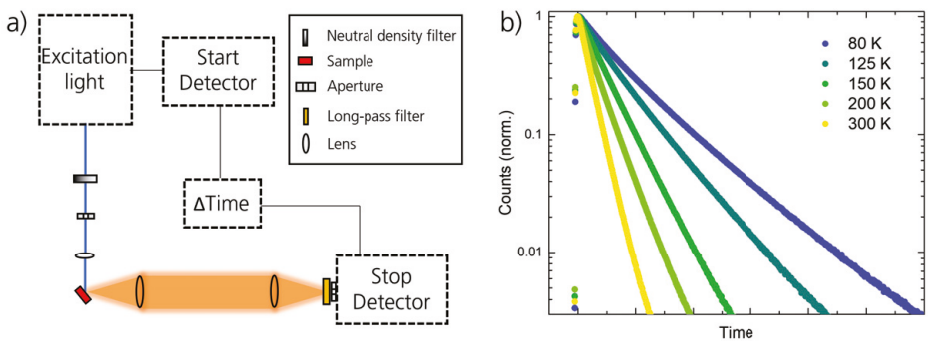

Figure 2.6: a) A simplified TCSPC setup. b) Typical emission transients obtained from TCSPC, measured at different temperatures.

In Figure 2.6a, a simple TCSPC setup is shown. The sample is excited by a focused laser beam tuned to a wavelength that the sample absorbs, and a low enough excitation density. The laser is pulsed and has high repetition rate, in order to measure many excitation-detection events in reasonable time. The excitation light is also sent to the start-detector, that triggers the delay time measurement. The emitted photon is focused by lenses to the stop-detector, that stops the delay time measurement. A long-pass filter is used to filter out the excitation laser intensity, which naturally has shorter wavelength than the emission from the sample.[7] Typical emission transients

measured at different temperatures are shown in Figure 2.6b, illustrating that the lifetime is dependent on temperature. The phosphorescence rate (k_{ph}) is temperature independent, but the ^{3}MLCT lifetime (τ) in Ru(bpy)$_3^{2+}$ also depends on two non-radiative processes (k_{nr} and k_{act}) according to Equation 2.5 (see Figure 2.3b).

$$\frac{1}{\tau} = k_{ph} + k_{nr} + k_{act} \tag{2.5}$$

Therefore, temperature dependent emission lifetime measurements can be used to find the activation energy of temperature dependent non-radiative transitions (e.g. the transition associated with k_{act}).[31, 32]

To measure the lifetime of states that are not emissive, or to probe products and intermediates formed in reactions with excited Ru(bpy)$_3^{2+}$, TCSPC is not enough. An alternative approach is to study the evolution of the sample absorption at different delay times after excitation, given that the involved species absorb in the probed wavelength range. This is often represented as differential spectra, i.e. the difference in absorption between an excited sample and the same sample when it was not excited. The technique is called transient absorption (TA) spectroscopy.[7, 11, 36, 45, 46] The differential spectrum can feature four different signal types, summarised in Figure 2.7a. These are i) ground state bleach (GSB) which is a characteristic of population missing from the ^{1}GS, ii) excited state absorption (ESA) which is the characteristic absorption from the ^{3}MLCT state to higher states, iii) stimulated emission (SE) which is a characteristic induced emission of the ^{3}MLCT state and iv) product absorption (PA) which is characteristic absorption appearing if a product is formed in reaction with the ^{3}MLCT state. The signals can be described by considering the three-state system consisting of the ^{1}GS, the excited ^{3}MLCT state and the product ground state (see Figure 2.7a). Each of these states has an extinction coefficient depending on the wavelength $\epsilon_{G,M,P}(\lambda)$, and a concentration ($c_{G,M,P}$) of Ru(bpy)$_3^{2+}$ at a given time after excitation (G - ^{1}GS, M - ^{3}MLCT and P - product). The Beer-Lambert law (Equation 2.3) is used to describe the absorbance of the excited sample at a certain delay time, shown in Equation 2.6.[7]

$$A_{exc} = l(\epsilon_G(c_0 - c_M - c_P) + \epsilon_M c_M - k\epsilon_G c_M + \epsilon_P c_P) \tag{2.6}$$

In Equation 2.6, l is the path length of the sample, k is a scaling factor, and c_0 the summed concentration of Ru(bpy)$_3^{2+}$ in all states in the sample. To form the differential absorption signal, the absorbance of the unexcited sample is subtracted, which results in Equation 2.7.[7]

$$\begin{aligned} \Delta A &= l(\epsilon_G(c_0 - c_M - c_P) + \epsilon_M c_M - k\epsilon_G c_M + \epsilon_P c_P) - \epsilon_G c_0 l \\ &= l(-\epsilon_G(c_M + c_P) + \epsilon_M c_M - k\epsilon_G c_M + \epsilon_P c_P) \end{aligned} \tag{2.7}$$

The first term describes GSB, which is a negative signal following the spectral shape of the steady-state absorption, with signal strength depending on the total missing

concentration in the ^{1}GS. The second term describes ESA, which is positive and depend on the concentration in the ^{3}MLCT state. The third term describing SE is negative, since light is emitted instead of absorbed. The SE signal depends on the concentration in the ^{3}MLCT state. Its theoretical shape can be calculated from the spontaneous emission measured in a steady-state emission measurement. In the case of a short-lived SE signal the theoretical shape, however, might not have the time to develop. Finally, the forth term describes PA, which is positive and depend on the concentration of the products formed. The PA signal at long delay times resembles the steady-state absorption of the product, which is typically used to identify what species is formed.[7]

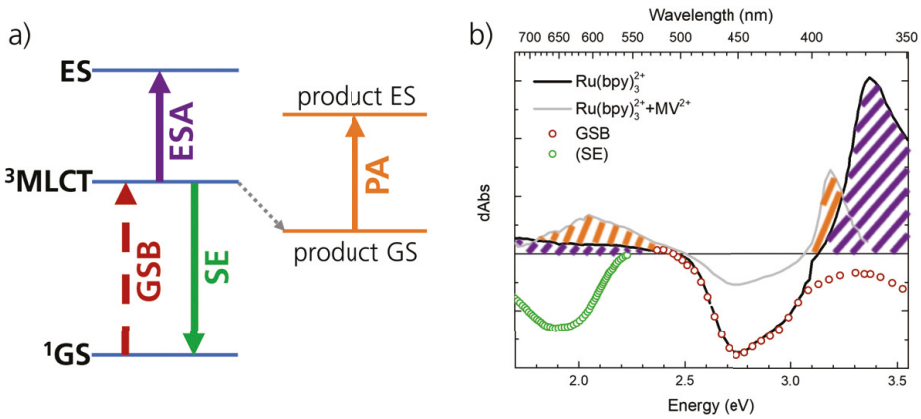

Figure 2.7: a) The possible signals in a differential spectrum exemplified by $Ru(bpy)_3^{2+}$. GSB - ground state bleach, ESA - excited state absorption, SE - stimulated emission, PA - product absorption (ES - excited state). b) A differential spectrum of $Ru(bpy)_3^{2+}$ in the ^{3}MLCT state, and $Ru(bpy)_3^{2+}$ after reaction with MV^{2+}. For comparison also the inverted steady-state absorption (GSB) and calculated stimulated emission (SE) spectra are shown. Adapted from Ha-Thi et al..[45]

In Figure 2.7b, a differential spectrum of $Ru(bpy)_3^{2+}$ in the ^{3}MLCT state, and after reaction with the methyl viologen di-cation (MV^{2+}), are shown. The ^{3}MLCT state displays the signals GSB (red) and ESA (purple), but no SE (its theoretical shape is however indicated in Figure 2.7b).[45] SE is not seen since the extinction coefficient of ESA is stronger than that of SE. By measuring how any of the characteristic signals of the ^{3}MLCT evolves over time, transients are retrieved (similar to those in Figure 2.6b) from which the lifetime can be fitted. If the TA setup is made for sub-ps time resolution, also how the ESA signal changes as the system forms the ^{3}MLCT state during ISC can be probed.[46] In charge-transfer reactions, such as that of $Ru(bpy)_3^{2+}$ and MV^{2+}, the TA measurement probes how intermediates and products appear (given they have strong enough absorption in the probed wavelength range). In Figure 2.7b, PA from the reduced MV^+ is detected.[45] To find the rates of the different steps in the reaction, a common analysis method is global analysis. This approach fits a sum of exponential decay functions with spectra $A_i(\lambda)$ and decay rates k_i to the TA data

$A(\lambda, t)$ according to Equation 2.8.

$$A(\lambda, t) = \sum_i A_i(\lambda) \mathrm{e}^{-tk_i} \tag{2.8}$$

Each fitted $A_i(\lambda)$ corresponds to a decay associated spectra (DAS), which is the spectral shape that changes with the fitted rate k_i. By identifying the shape of the DAS as a known differential spectrum assigned to a species, the fitted decay rates can be assigned to processes in the reaction (or in the decay pathway).[47]

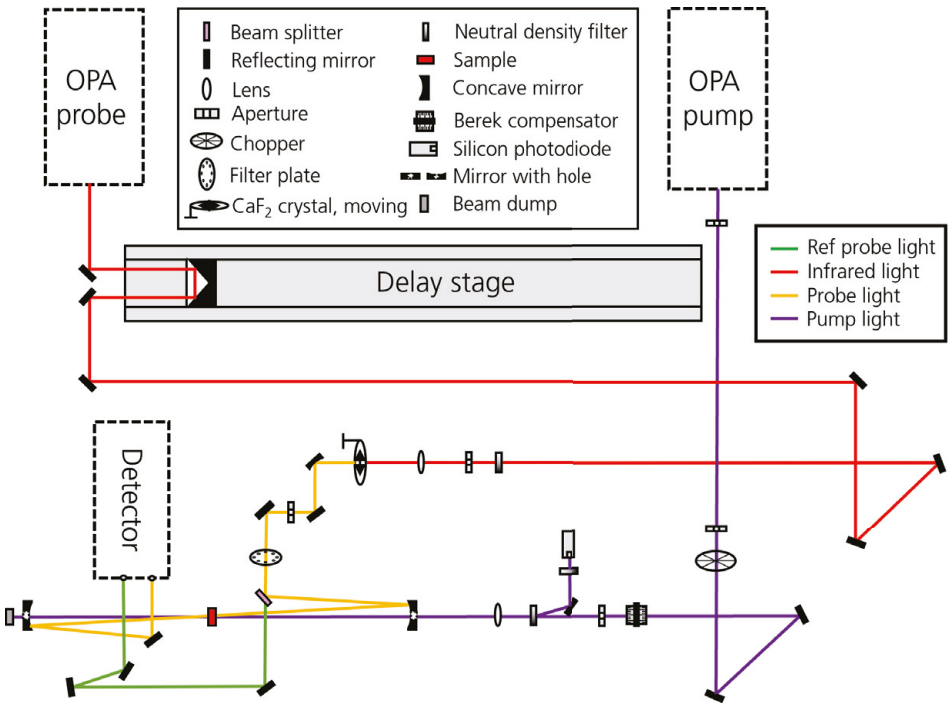

Figure 2.8: A simplified TA setup for measurements from 100 fs to 10 ns, and white light detection in UV to NIR wavelength range.

In TA spectroscopy, a detector monitors how light is transmitted through the sample at various times after excitation compared to the light transmittance of the unexcited sample. In Figure 2.8, a simple TA setup is shown (for measurements from 100 fs[6] to 10 ns). The setup relies on a pulsed laser producing a fundamental beam (not shown in Figure 2.8), which is split and fed into two optical parametric amplifiers (OPA). These devices can alter the wavelength of the light by using non-linear optical phenomena. In the pump OPA, a wavelength that can excite the sample is selected and then this light is guided and focused to the sample position. Important is that

[6]The time resolution is largely depending on the pulse duration of the laser, but also other factors.

every other pump pulse is blocked by a chopper to measure both the excited and unexcited sample, from which the differential absorption signal is calculated. In the probe OPA, an infrared wavelength is selected that is sent to a CaF_2 crystal for generating a white light continuum. This allows the TA setup to measure absorbance in a wavelength range from UV to near infrared (NIR). The probe beam is delayed with respect to the pump beam (i.e. excitation), to introduce the time dependence in the measurement. The probe beam is commonly split before the sample, to have one probe that transverses the sample and one reference probe relayed directly to a detector for monitoring fluctuations in the light intensity. The reference measurement improves the signal-to-noise ratio of the experiment. Finally, the polarisation between the pump and probe beams can be set so that either polarisation effects are avoided, or for measuring anisotropy.[7]

2.5 Quantum Chemical Calculations

Hypotheses about the excited state landscape and nature of the different transitions found by spectroscopy on $Ru(bpy)_3^{2+}$, can be confirmed by comparing measurements to theory.[43] The time-independent Schrödinger equation (Equation 2.9) describes the energy (E) and wave function (Ψ) of molecular electronic states.

$$\hat{H}\Psi = E\Psi \tag{2.9}$$

In Equation 2.9, $\hat{H}$ is the Hamiltonian operator.[48] Solving the Schrödinger equation for molecules such as $Ru(bpy)_3^{2+}$ is however not possible with either analytical or computational methods to date, thus simplifications are needed. As a first approximation, only the electronic part of the equation is solved if the atomic nuclei are kept at fixed positions and are described by an external potential. This is called the Born-Oppenheimer approximation, which states that there is no coupling between the nuclear and electronic coordinates (since the electrons are moving four orders of magnitude faster than the nuclei).[48]

Still, the time-independent electronic Schrödinger equation is too complex to solve since molecules have many electrons, each described by a set of three spatial coordinates and one spin coordinate. To further simplify, the electronic wave function can be replaced by the electron density. The electron density $\rho(\vec{r})$ is defined according to Equation 2.10, which integrates over the spin coordinates ($\vec{s}$) and all but one spatial coordinate ($\vec{x}$) of all N electrons in the molecule.[48]

$$\rho(\vec{r}) = N \int ... \int |\Psi(\vec{x_1}, \vec{x_2}, ..., \vec{x_N})|^2 d\vec{s_1} d\vec{x_2} ... \vec{x_N} \tag{2.10}$$

The electron density treats all electrons collectively, and thus only depends on three spatial coordinates ($\vec{r}$). The simplification does not contain all information about

the system (e.g. the spin of the electrons) as is the case of the wave function. The electron density is, however, an observable and can be measured. According to the Hohenberg-Kohn theorems, $\rho(\vec{r})$ is just as the wave function uniquely defined for a given electronic state. Furthermore, the Hohenberg-Kohn theorems state that there is a functional that given $\rho(\vec{r})$ returns the energy of the system.[48, 49]

The problem has thus been reduced to finding the correct functional that describes molecular systems. Given this functional, the energy of a system can be calculated from the electron density. A commonly used approach to this problem is Kohn-Sham density functional theory (DFT), where electrons are assumed to be non-interacting particles with single electron orbitals. In this method, Equation 2.11 is the functional returning the system energy E from the electron density ($\rho(\vec{r})$).[48]

$$E[\rho(\vec{r})] = T_S[\rho(\vec{r})] + E_{ne}[\rho(\vec{r})] + J[\rho(\vec{r})] + E_{xc}[\rho(\vec{r})] \tag{2.11}$$

Analytical expressions exist for T_S, E_{ne} and J, which describe the kinetic energy for non-interacting electrons, the attraction between electrons and the nuclei, and Coulomb repulsion between the electrons respectively. E_{xc}, which is the exchange-correlation energy, must however be approximated and has to date several different implementations. In the DFT calculation settings, a functional approximating E_{xc} and a basis set describing the single electron orbitals are selected.[48]

In the DFT calculation routine, an initial guess of the electron density is created from which the energy is calculated based on the selected functional. An implication of the first Hohenberg-Kohn theorem is that the variational principle can be applied to find the geometry of a molecule in the ground state. Therefore, DFT algorithms are based on minimising the energy calculated from the electron density generated as the nuclei positions are moved stepwise (i.e. a self-consistent field approach). When convergence at a given accuracy is met, the geometry of the ground state has been optimised. By optimising states of different spin, also selected excited states of molecules can be calculated.[48]

With DFT calculations, the ^{1}GS and selected excited states of $Ru(bpy)_3^{2+}$ can be optimised. The optimisation returns the molecular geometry with bond lengths and angles but also quantities such as the system energy and the spin density. From this information, projected potential energy surfaces (PPES) can be constructed, to generate a computed version of Figure 2.3b. The nature of an optimised state is commonly determined by the bond distances and the spin on Ru(II).[50, 51] This is a viable strategy since MC states are highly distorted and have high spin on Ru(II), whereas MLCT states have similar geometry as the ^{1}GS and a spin of $\sim$1 on Ru(II).[51] To validate the DFT results, the calculated energy of the states are compared to experimental data (such as the energy of the ^{1}MLCT state relative to the ^{1}GS and the energy difference between the ^{1}GS and ^{3}MLCT minima, estimated from steady-state spec-

troscopy techniques). If these match, the computational method describes the system well. Information not accessible by measurements can then be calculated in a reliable way. One such example is the energy of a state along any given reaction coordinate, which provides information on deactivation pathways and state crossings.[50]

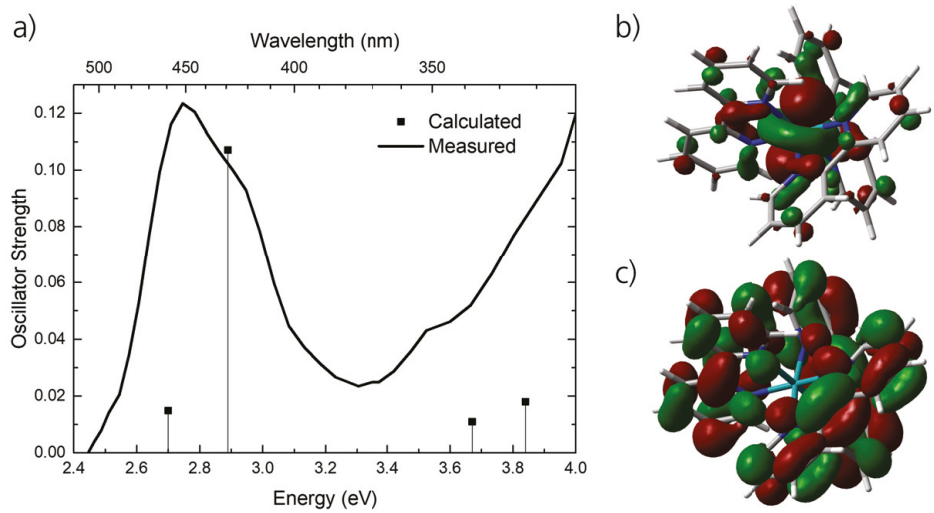

Figure 2.9: a) Calculated electronic singlet transitions of $Ru(bpy)_3^{2+}$, compared to the measured absorption spectrum. Adapted from Alary et al..[43] b) HOMO of $Ru(bpy)_3^{2+}$. c) LUMO of $Ru(bpy)_3^{2+}$. Courtesy of Petter Persson. All calculated by (TD)-DFT at the B3LYP level of theory.

To learn about electronic transitions in $Ru(bpy)_3^{2+}$, time-dependent density functional theory (TD-DFT) can be used. From a given state, the calculation returns the energy of possible electronic transitions to higher states of a given spin, as well as the oscillator strength of each transition.[48] The calculated transitions are then used to simulate the absorption spectrum of $Ru(bpy)_3^{2+}$ (see Figure 2.9a), and thereby cross-check the assigned transitions from Figure 2.4a.[43, 50, 52, 53] An assignment can be made by analysing the natural transition orbitals (NTOs) involved in each electronic transition. From an NTO analysis, the charge-separated nature of the ^{3}MLCT state can also be seen. The NTOs involved in the MLCT transition describe where the electron density is located before the transition, and to where the electron density is moved after the transition.[54] The lowest MLCT transition can also be approximated by analysing the highest occupied molecular orbital (HOMO) and the lowest unoccupied molecular orbital (LUMO).[43, 50] HOMO and LUMO for $Ru(bpy)_3^{2+}$ are shown in Figure 2.9b-c.

2.6 Earth-Abundant Photosensitisers

Ru polypyridyl complexes have been studied for decades, in order to adapt the ligand structure to suit different applications.[31] Ru-complexes are used as photosensitisers in solar cells,[55] solar fuel devices,[14] light emitting diodes,[56] molecular sensors[57] and medical applications.[58] There is, however, one major drawback with Ru polypyridyl complexes, and that is the availability and therefore cost of ruthenium. In Figure 2.10, the abundance of all elements accessible in Earth's crust are compared.[59] The group named "rarest metals" includes the least abundant elements, which from the logarithmic scale are shown to be several orders of magnitude scarcer than other elements. Elements such as gold and platinum belong to this group, but also ruthenium.

The low availability of ruthenium would lead to it becoming more and more expensive as the solar energy conversion technologies scale up, until it finally runs out. Therefore, much new photosensitiser research focuses on Earth-abundant elements including Cr, Mn, Fe, Co, Ni, Cu and Zn (see Figure 2.10) that are all first-row transition metals.[60–65] Fe-based photosensitisers is the scope of this thesis work, and the following chapters discuss the research conducted on this topic. This chapter has laid a solid foundation for understanding this work by discussing the properties of a good photosensitiser, how they are measured and how the electronic structure enables these properties.

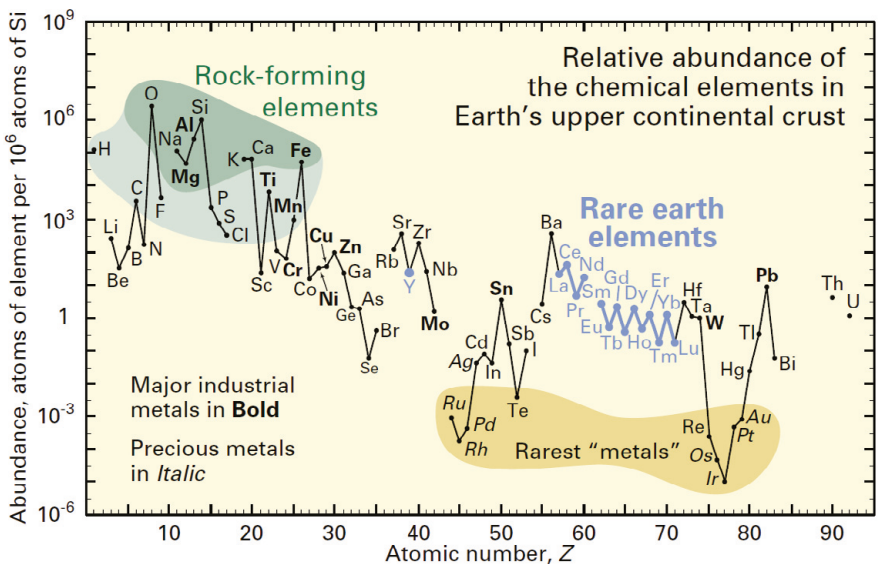

Figure 2.10: An overview of the abundance of all elements present in Earth's crust. On the vertical axis abundance is plotted on a logarithmic scale, normalised to Si. On the horizontal axis the atomic number of the element is plotted. The figure is courtesy of the U.S. Geological Survey.[59]

Chapter 3

Photophysics of Iron Carbene Complexes

You can't be healthy and rich.
Or can you?[1]

3.1 d^6 Fe Carbene Complexes

There are several options to realise Earth-abundant photosensitisers, but perhaps Fe has always been the dream candidate to replace Ru. The reason for this is that Fe is among the ten most abundant elements and also that Ru and Fe are in the same group in the periodic system.[59, 66, 67] This means that Ru(II) and Fe(II) are isoelectronic, i.e. both have a d^6 electronic configuration. Due to the primogenic effect, their respective frontier *d*-orbitals are, however, significantly different. The primogenic effect states that in the first shell a new set of orbitals is populated, the orbitals will not have a node in their radial distribution function.[68, 69] This leads to an electron density distributed closer to the centre of the atom, which is the case for the 3*d*-orbitals. This weakens the binding interaction with ligands, and makes the influence of the ligand field much lower in an Fe(II)-complex compared to the same Ru(II)-complex.[70] Therefore, in the case of $Fe(bpy)_3^{2+}$, the electronic state arrangement is very different compared to $Ru(bpy)_3^{2+}$ (see Figure 3.1).[70, 71]

In $Fe(bpy)_3^{2+}$, there is only a minor energy barrier for the transition from ^{3}MLCT to ^{3}MC, since the MC states are lower in energy than the MLCT states. This means that

[1] Traditional Russian expression, or communication between prof. Yartsev and PhD student.

after excitation into the ^{1}MLCT state, follows a rapid deactivation cascade through the ^{3}MLCT and ^{3}MC states to the ^{5}MC state (with the ^{3}MLCT excited state lifetime being <100 fs). The major excited state of $Fe(bpy)_3^{2+}$ is thus the ^{5}MC state, which has a lifetime of ~650 ps. The ^{5}MC state in $Fe(bpy)_3^{2+}$ is not a photofunctional state according to the definition in Chapter 2, since it does not participate in charge- or energy transfer reactions and does not display emission.[72–78] This means that just exchanging Ru(II) for Fe(II) is not a viable approach to yield an Fe-based photosensitiser.

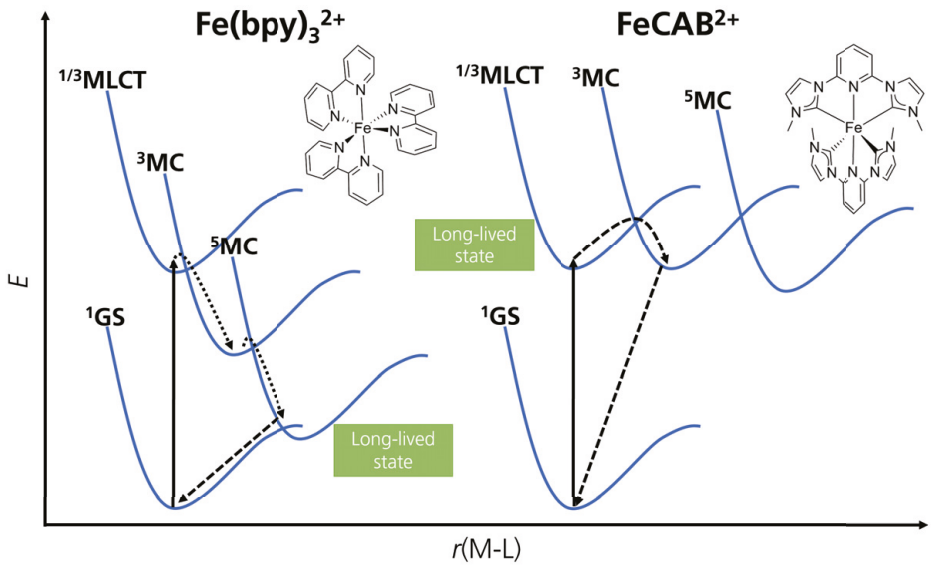

Figure 3.1: Schematic comparing the excited state landscape in $Fe(bpy)_3^{2+}$ to a representative Fe carbene complex ($FeCAB^{2+}$).

The first step towards an Fe-based photosensitiser would be to instead have a long-lived ^{3}MLCT state, since this is the photofunctional state in $Ru(bpy)_3^{2+}$. In order to achieve this goal, the excited state landscape needs to be rearranged so that instead the ^{3}MLCT state has lower or similar energy as the MC states. This would create an energy barrier that can slow down the transition from the ^{3}MLCT state to the MC states seen for $Fe(bpy)_3^{2+}$.[66, 67, 71, 79, 80] Early attempts at making the ^{3}MLCT state photofunctional in Fe-complexes include Fe cyanide complexes, where a ^{3}MLCT state was observed for a few ps in certain solvents, but the lifetime only quantified many years later.[81–83] More recent strategies include HOMO-inversion,[84] high strain,[85] improved octahedricity,[86] and coherent control.[87]

This thesis is devoted to the study of Fe carbene complexes, which resulted in a new class of Fe-complexes that did not rapidly deactivate into the ^{5}MC state.[88]

The carbene-ligands rearranged the excited state landscape to such an extent that the ^{3}MLCT state finally became the state of longest lifetime, see Figure 3.1.[66, 71, 88, 89] The ligand design strategies and their implications to the photophysics will be explained in the following sections. This will be exemplified by Fe carbene complexes from the research conducted in this thesis, however several other groups have also published Fe carbene complexes advancing the field.[66, 67, 80, 90] Note that Sections 3.1.1-3.1.3 present the Fe carbene complexes within the original photophysics model, which assigned all $>$1 ps lifetimes to the ^{3}MLCT state. This model will be revised in Section 3.1.4.

3.1.1 Strategy: Destabilising MC States

The destabilisation of the MC states is the major effect that the carbene-ligands have on the excited state landscape. When the MC states are moved up in energy relative to the ^{3}MLCT state, the energy barrier to go from ^{3}MLCT to ^{3}MC is increased, which is illustrated in Figure 3.2. Eventually, the barrier becomes substantial enough so that the excited population can stay in the ^{3}MLCT state. Thereafter, further ^{3}MC destabilisation prolongs the lifetime of the ^{3}MLCT state. The energetic position of the ^{3}MC state is mainly determined by the LF strength, since the MC transition entails moving one electron from a t_{2g}-orbital to an e_g-orbital (see Figure 3.3). The strongly σ-donating effect of the carbene-ligands create a strong LF in the Fe carbene complex, thus destabilising the MC states.[89]

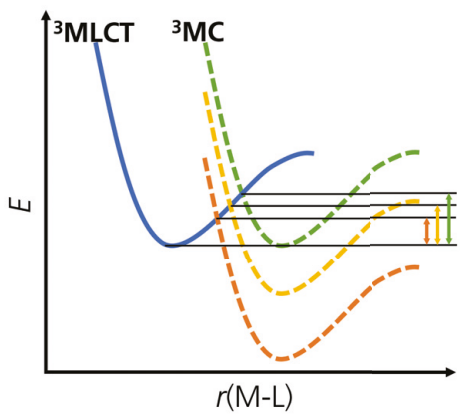

Figure 3.2: The effect on the ^{3}MLCT to ^{3}MC energy barrier by varying the energetic position of the ^{3}MC state.

In a more thorough picture, the frontier orbitals on the metal and on the ligands mix since the metal-ligand bond is not purely ionic. There are three different kinds of mixing interactions (illustrated in Figure 3.3), which involve both σ- and π-orbitals

of the ligand.[66, 71] σ-donation was already mentioned, and this is an effect of mixing the ligand carbene sp^2-orbital with the metal e_g-orbital. The new e_g-like orbital ($\sim e_g$) formed is the antibonding orbital between sp^2 and e_g, which is higher in energy than the pure e_g-orbital (effect A in Figure 3.3). Therefore, this effect increases the LF splitting. A similar mixing between the ligand π^*-orbital and the metal t_{2g}-orbital leads to the lowering of the bonding t_{2g}-like orbital ($\sim t_{2g}$) (effect B in Figure 3.3). This effect therefore also increases the LF splitting. The third type of interaction actually increases the energy of the t_{2g}-like orbital ($\sim t_{2g}$) which leads to a smaller LF splitting (effect C in Figure 3.3). This effect is, however, only slightly counteracting the other two, and the net outcome is an increased LF splitting and thus MC energy.[66, 71]

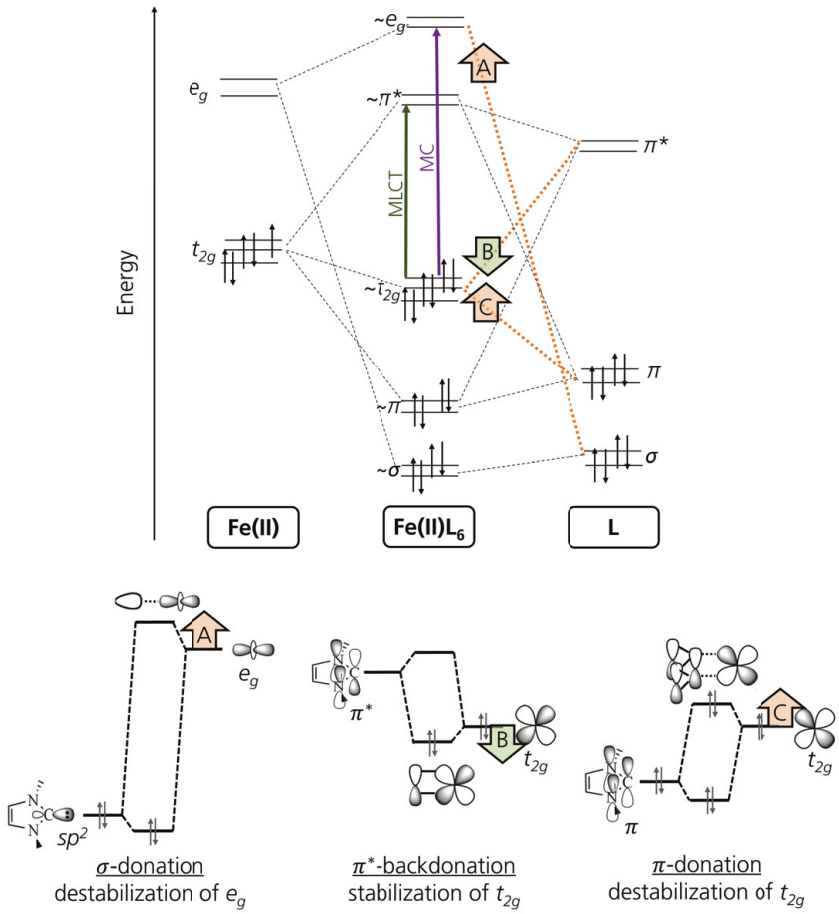

Figure 3.3: Frontier orbitals and their resulting mixed orbitals for an Fe(II) carbene complex (d^6 electronic configuration). The three different effects of the carbene ligand (L) on these orbitals are shown by the cases A, B and C. Furthermore, the electronic transitions giving rise to the excited MLCT and MC states are indicated. Adapted with permission from Lindh et al..[66]

Figure 3.4a shows the molecular structure of the first published iron carbene complex FeCAB, that resulted in an excited state lifetime of 9 ps assigned to the ^{3}MLCT state.[2][88] With this initial molecule as the "parent complex", several similar structures with 1-30 ps excited state lifetime have been published.[66, 67, 91–97] One of the related complexes is FeCABIm discussed in paper I, with molecular structure also shown in Figure 3.4a. The excited state landscape of FeCABIm (Figure 3.4b) provides a nice example for the changes introduced by the carbene-ligand, and is similar also for FeCAB.[89] In FeCABIm, the MC states have been destabilised to such an extent so that the ^{5}MC state minimum has a similar energy as the ^{3}MLCT minimum, and the ^{3}MC minimum is only slightly below them. This arrangement of the excited states is very different compared to $Fe(bpy)_3^{2+}$ (Figure 3.1) where all MC states were well below the ^{3}MLCT state in energy. In FeCABIm, there is now an energy barrier to go from the ^{3}MLCT to the ^{3}MC state, and also an energy barrier to go from the ^{3}MC state to the ^{5}MC state. Systematic studies of early Fe carbene complexes with similar structure as FeCAB investigated how many Fe-carbene bonds are required to avoid rapid deactivation into the ^{5}MC state. Zimmer et al. and Duchanois et al. found that a minimum of four Fe-carbene bonds are needed (which is the case of FeCAB and FeCABIm) and furthermore that the excited state lifetime depends on the number of such bonds.[96, 97]

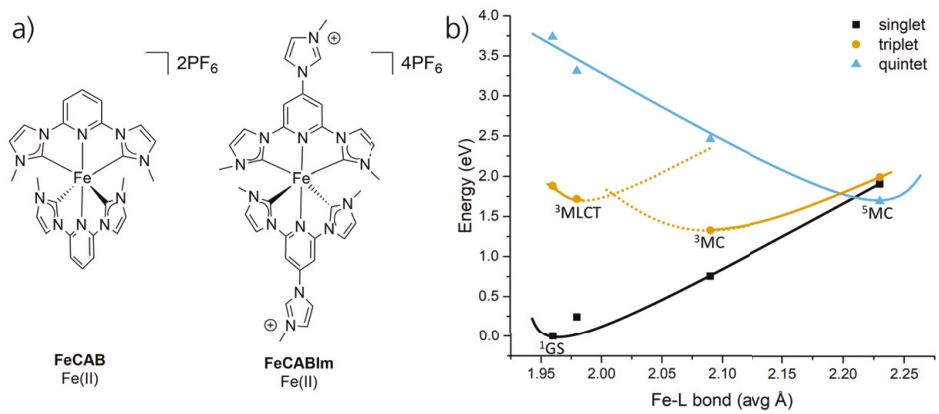

Figure 3.4: a) Molecular structure FeCAB discussed in papers I-IV, together with FeCABIm discussed in paper I. b) Projected potential energy surfaces showing the relevant excited state landscape for FeCABIm. Points are calculated by DFT at the B3LYP* level of theory, lines represent a guide to the interpretation.

[2]NB will be reassigned in Section 3.1.4.

3.1.2 Strategy: Stabilising MLCT States

A complementary strategy to increase the ^{3}MLCT lifetime is to stabilise the ^{3}MLCT state. Figure 3.5 illustrates how this strategy indeed increases the energy barrier between the ^{3}MLCT and ^{3}MC states. Lowering the ^{3}MLCT energy also results in lowering the ^{1}MLCT energy. This strategy can therefore expand the absorption spectrum of the photosensitiser towards the red spectral range, and enable harvesting of a larger part of the solar spectrum.[98] There is, however, a trade-off between extending the red absorption and maintaining a high redox potential in the excited state, which must be taken into account.

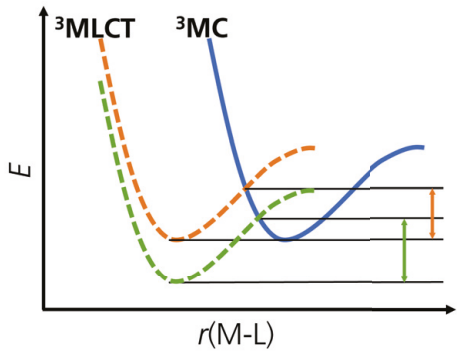

Figure 3.5: The effect on the ^{3}MLCT to ^{3}MC energy barrier by varying the energetic position of the ^{3}MLCT state.

The energy of the ^{3}MLCT state is within the orbital formalism the energy difference between the t_{2g}-like ($\sim t_{2g}$) and π^*-like ($\sim \pi^*$) orbitals, see Figure 3.3. Furthermore, in most d^6 Fe carbene complexes these are the frontier orbitals; $\sim t_{2g}$ is the highest occupied molecular orbital and $\sim \pi^*$ is the lowest unoccupied molecular orbital. To stabilise the MLCT states, both increasing the energy of HOMO or lowering the energy of LUMO are viable strategies. But if the energy of HOMO is increased, this can also cause a smaller ligand field splitting affecting the MC states in an undesirable way. Therefore, the main strategy to stabilise the MLCT states should be that of lowering LUMO.

Since the nature of LUMO is $\sim \pi^*$, strategies to lower the energy includes to expand the π-system or to introduce electron-withdrawing groups. FeCABIm discussed in paper I, belongs to the former of these strategies. The imidazole-groups attached to the para-position on the pyridine-moieties (see Figure 3.4a) increase the number of atoms in the π-system, and thus lower the energy of LUMO. That the energy of LUMO was decreased is seen in the calculations (Figure 3.6b) but also in the red-shift of the absorption spectrum compared to FeCAB (Figure 3.6c). Since the ligand

π-system interacts with the metal t_{2g}-orbitals (see Figure 3.3) the energy of HOMO has decreased too (Figure 3.6b), but not to as large extent as LUMO. Expanding π-systems generally increases the extinction coefficient of the absorption, which is observed in the case of FeCABIm (see Figure 3.6c).

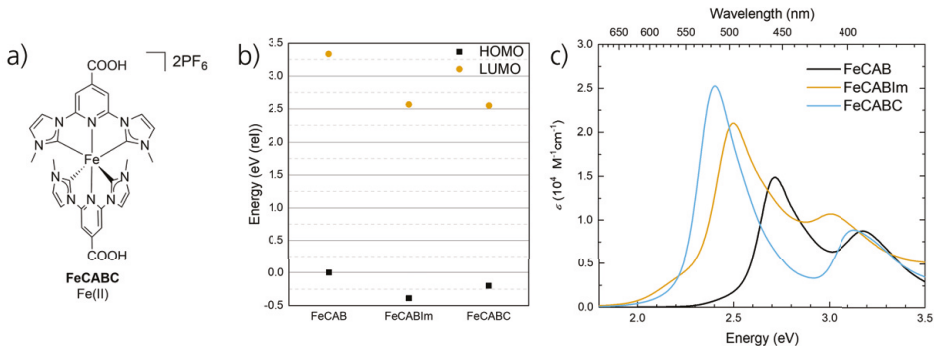

Figure 3.6: a) Molecular structure of FeCABC, discussed in papers I-IV. b) Calculated relative HOMO and LUMO energies for complexes FeCAB, FeCABIm and FeCABC by DFT at the B3LYP* level of theory. The HOMO energy of FeCAB is used as a reference point to which 0 eV is assigned. c) Compared extinction coefficient of complexes FeCAB, FeCABIm and FeCABC.

With complex FeCABC (see Figure 3.6a), Harlang et al. and Duchanois et al. explored the strategy of introducing an electron-withdrawing group.[99, 100] The carboxylic groups attached to the para-position on the pyridine-moieties have electron-withdrawing character, which accepts electron density and thus lowers the energy of LUMO. Compared to FeCABIm, the LUMO stabilisation is similar in both complexes, but in FeCABC HOMO is less affected (see Figure 3.6b). This leads to a smaller HOMO-LUMO gap, which is reflected in the yet further red-shifted absorption of FeCABC (see Figure 3.6c). The trend of red-shifted absorption is in agreement with an increasing trend in excited state lifetime of these complexes, see Table 3.1.

Table 3.1: Photophysical properties of FeCAB, FeCABIm and FeCABC compared. HOMO-LUMO gap calculated by DFT at the B3LYP* level of theory. Abs - MLCT absorption maximum, ϵ - extinction coefficient, τ - excited state lifetime.

Complex	HOMO-LUMO gap (eV)	Abs (nm)	$\epsilon\ 10^3$ ($M^{-1}cm^{-1}$)	τ (ps)
FeCAB	3.34	457	15	9
FeCABIm	2.95	496	21	16
FeCABC	2.75	516	25	19

3.1.3 Strategy: Increasing Charge Separation

A third strategy to increase the ^{3}MLCT lifetime of Fe-complexes, is to increase the charge separation in the excited state. The separation slows down deactivation process-

es,[32] and is furthermore one of the criteria for the ideal photosensitiser from Chapter 2. Charge separation can be realised in a heteroleptic complex, meaning that two different ligands coordinate to Fe(II) that have different properties.[3] In this case, one of the ligands should have low electron density and therefore "pull" the excited electron, and the other should have high electron density and thus "push" it away. Similarly, the ligands would push and pull the hole to the opposite ligand with respect to the electron. This type of design is called "push-pull complexes", and has been employed in both organic[101], Ru-based[102–104] and Zn porphyrin photosensitisers.[105, 106]

In paper II, a series of push-pull Fe carbene complexes were introduced, see Figure 3.7, but also examples of push-pull Fe-complexes from other groups have been presented.[107][108] For complexes FeCABCN1 and FeCABCN2, the intended push-pull functionality should result in the carboxylic group receiving the excited electron and the amine-substituted carbene-ligand receiving the hole. To realise this, the π-orbitals should be raised in energy to an extent where they approach the t_{2g}-orbitals and therefore contribute in sharing the hole density in the excited ^{3}MLCT state (see Figure 3.3). Alternatively, the complex should, after coming to the ^{3}MLCT state, access yet another state that is further charge-separated.

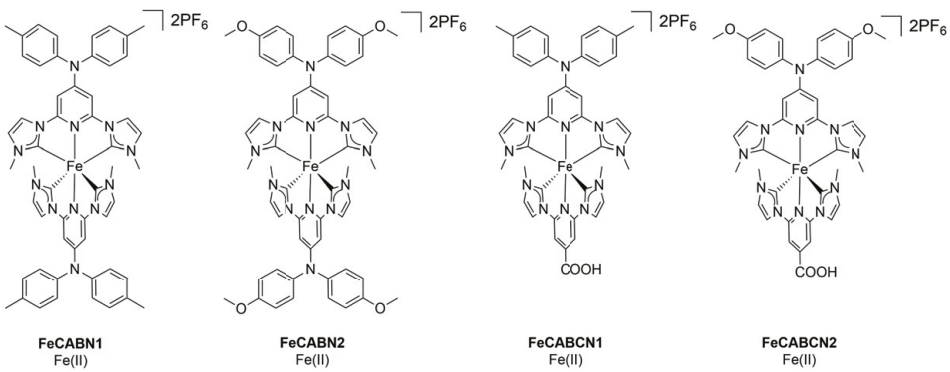

Figure 3.7: Molecular structure of the push-pull complexes (FeCABCN1 and FeCABCN2), discussed in papers II and III. Also shown are the homoleptic reference complexes with the amine-substituted ligands (FeCABN1 and FeCABN2).

Paper II investigated to what extent the push-pull effect was realised in FeCABCN1 and FeCABCN2 (Figure 3.7), which will here be exemplified by FeCABCN1. In Figure 3.8, the NTOs of the transition in the lowest energy MLCT absorption band are shown. Figure 3.8a represent the electron density before the transition and 3.8b after. The NTO analysis shows that electron density is moved to the carboxylic group in the transition, which is according to the intended push-pull strategy. There is, however, no involvement of the amine-substituted carbene-ligand in this transition.

[3]All complexes shown up to this point have been homoleptic, i.e. having only one type of ligand.

In Figure 3.8c, the spin density of the optimised ^{3}MLCT state is shown, which displays the combined density of the electron and the hole after ISC and relaxation. Here, some density (presumably of the hole) extends to the amine-substituted ligand, which is a step towards the intended charge separation. The majority of the hole density is however still on iron, which agrees with that the first oxidation of the complex is Fe(III)/Fe(II). What the push-pull structures in Figure 3.7 accomplished is therefore rather a preferential excitation, ensuring that the electron goes to the carboxylic-substituted ligand, but with the hole remaining on the metal. This is an improvement compared to the parent complex FeCABC (Figure 3.6a), where two degenerate LUMOs render excitation to both ligands similarly probable.[98]

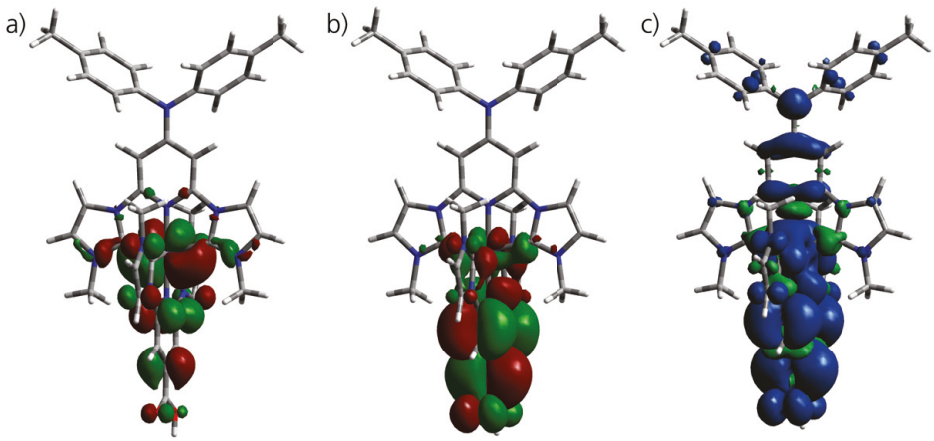

Figure 3.8: a) Initial NTO of the strong transition from TD-DFT in the lowest energy MLCT absorption band of FeCABCN1. b) Final NTO of the strong transition from TD-DFT in the lowest energy MLCT absorption band of FeCABCN1. c) Spin density contour plot of the optimised ^{3}MLCT state of FeCABCN1. All calculated by (TD-)DFT at the B3LYP* level of theory.

The push-pull complexes FeCABCN1 and FeCABCN2 are in many other aspects very similar to FeCABC, e.g. in terms of the HOMO-LUMO gap, the absorption spectrum and excited state lifetime (see Table 3.2). When comparing the absorption spectra also to the reference complexes in Figure 3.7, it is seen that the lowest energy peak red-shifts $\sim$0.3 eV for complexes with carboxylic group compared to complexes without carboxylic group[4] (see Table 3.2 and Figure 3.9b). Furthermore, the peak at 3.1-3.2 eV is consistently present in all complexes. The only change made to the ligand structure of the different complexes is to change the substituent in the para-position on the pyridine-moieties. The substituents seem to influence the lowest energy absorption peak significantly more than other absorption peaks, which suggests that the absorption peaks of the Fe carbene complexes in Figure 3.9b originate from different electronic transitions. Furthermore, complexes with carboxylic groups

[4]Deprotonated carboxylic group will in this thesis be counted as without carboxylic group, since it is then a carboxylate group.

were easily deprotonated which generated a species with distinctly different absorption spectrum (also shown in Figure 3.9b). When the complexes FeCABCN1 and FeCABCN2 are deprotonated (here denoted FeCABCN1- and FeCABCN2-), their absorption spectra instead become similar to the absorption spectrum of the unsubstituted FeCAB.

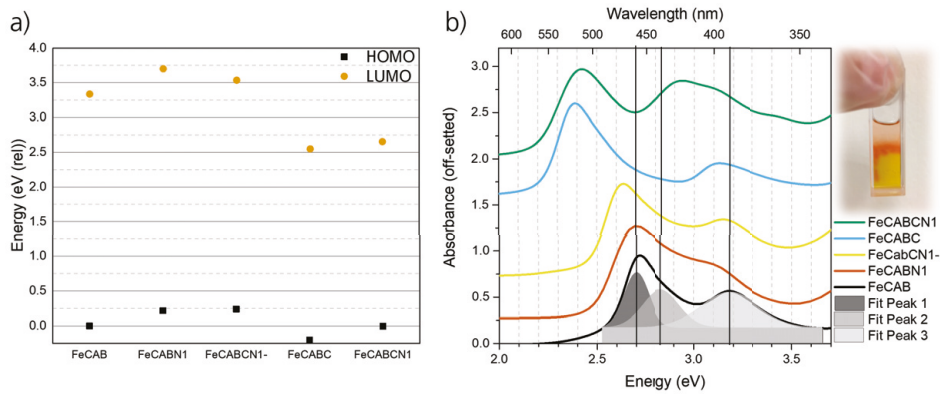

Figure 3.9: a) Relative HOMO and LUMO energies for FeCABCN1 with related complexes. The HOMO energy of FeCAB is used as a reference point to which 0 eV is assigned. Calculated by DFT at the B3LYP* level of theory. b) Compared absorption spectra for the same set of complexes, off-setted and scaled to facilitate qualitative comparison. A Gaussian fit to the absorption spectrum of FeCAB is shown by filled contours. The inset shows the colour change of FeCABCN1 as it changes protonation state.

To explain the nature of the underlying electronic transitions contributing to the absorption spectra in Figure 3.9b, all absorption spectra were simulated with TD-DFT in paper III. Here, the conclusions will be exemplified by FeCABCN1 shown in Figure 3.10. Based on a NTO analysis of the calculated transitions of FeCABCN1, two distinctly different electronic transitions were identified. These involve π^*-orbitals of different symmetry here labelled A and B, shown in Figure 3.10. The electronic transition contributing to the lowest energy peak in all complexes (i.e. at 2.4 eV for complexes with carboxylic group and at 2.6-2.7 eV for others) has the symmetry of π^*A. Since π^*A extends to the pyridine para-position, this orbital is influenced by the substituents. The electronic transitions contributing to the peaks in the higher energy absorption band in all complexes instead have the symmetry of π^*B. The π^*B-orbital does not extend on the pyridine para-position, and is therefore not influenced by the substituents. This explains why the peaks at 3.1-3.2 eV display so little shifts between the complexes in Figure 3.9b. Other peaks in Figure 3.9b result from electronic transitions involving both symmetries, e.g. the peak at $\sim$2.8 eV in FeCAB.

The different symmetries of the electronic transitions contributing to the MLCT absorption band explain the observations in Figure 3.9b. Especially interesting is the change in colour induced by deprotonating complexes with carboxylic groups, i.e.

Table 3.2: Photophysical properties of the push-pull complexes with reference complexes compared. HOMO-LUMO gap calculated by DFT at the B3LYP* level of theory. Abs - MLCT absorption maximum, ϵ - extinction coefficient, τ - excited state lifetime.

Complex	HOMO-LUMO gap (eV)	Abs (nm)	$\epsilon\ 10^3$ ($M^{-1}cm^{-1}$)	τ (ps)
FeCAB	3.34	457	15	9
FeCABN1	3.48	459	34	11
FeCABN2	3.56	454	32	12
FeCABCN1-	3.30	470	-	12
FeCABCN2-	3.29	470	-	14
FeCABC	2.75	516	25	19
FeCABCN1	2.66	511	16	19
FeCABCN2	2.65	512	14	19

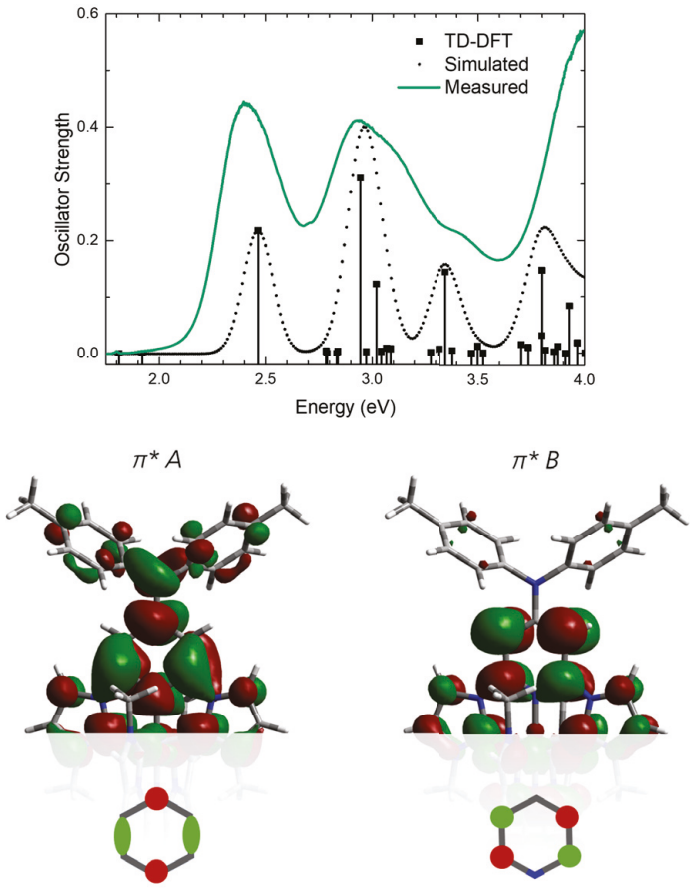

Figure 3.10: Absorption spectrum of FeCABCN1 compared to a simulated absorption spectrum calculated by TD-DFT at the B3LYP* level of theory (corrected by -0.16 eV). Below is a representation of the relevant NTOs of different symmetries, here called $\pi^* A$ and $\pi^* B$.

acidochromism. The carboxylic group is an electron-withdrawing substituent, but the carboxylate group is an electron donating substituent. This leads to a stabilised LUMO in the former case, and a destabilised LUMO in the latter case (see Figure 3.9a), which explains the colour change. To conclude, the sidegroup substitution on FeCAB influenced mainly the properties of the lowest MLCT state. To also influence higher MLCT states, substituting the pyridine para-position is not enough unless the substituent extends the π-system. In the case of the imidazole-substituted FeCABIm, the entire ligand π-system was affected which leads to a red-shift of all MLCT absorption peaks (see Figure 3.6c). On a final note, Liu et al. showed that substitution on the imidazole-moiety of FeCAB also resulted in a red-shift of all MLCT absorption peaks.[88]

3.1.4 Revising d^6 Fe Carbene Photophysics

As indicated in the introductory Section 3.1, papers III and IV propose a new photophysics model for FeCAB and derivatives without carboxylic group (FeCABN1, FeCABN2, FeCABCN1-, FeCABCN2-). This model (shown in Figure 3.11b) implies that their excited state lifetimes (ranging from 9-14 ps, see Table 3.2) should be assigned to the ^{3}MC state instead of the ^{3}MLCT state. FeCAB derivatives with carboxylic groups (FeCABC, FeCABCN1, FeCABCN2) are, however, still assigned to the original Fe carbene model (shown in Figure 3.11a). This section will motivate the reassignment of a rather large selection of complexes to the new model, and explain why the carboxylic group distinguishes what complex belongs to which model.

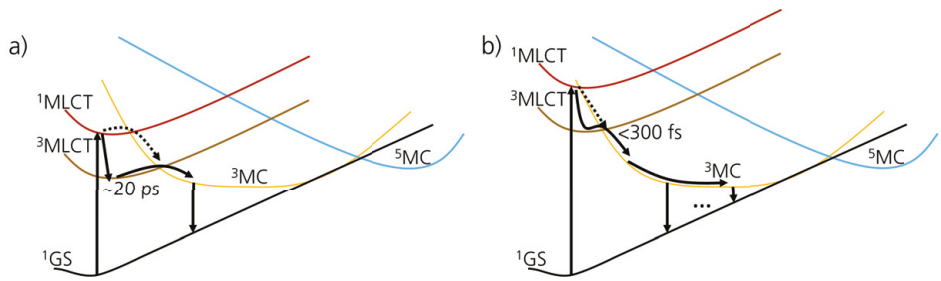

Figure 3.11: a) The original Fe carbene photophysics model, valid for FeCAB-derivatives with a carboxylic group. b) The new Fe carbene photophysics model suggested for FeCAB and derivatives without carboxylic group. The dotted lines represent a minor branching process.

To begin with, the TA data of FeCABCN1 and FeCABCN1- are compared in Figure 3.12. FeCABCN1 and its deprotonated analogue differ structurally only by a proton, still they display large differences in their photophysics. In Figure 3.12, both complexes show a similarly broad ESA spectrum at early times (100 fs). For FeCABCN1-, however, this broad ESA converts to a narrower, blue-shifted spectrum already after

200 fs. Since the GSB region display no recovery on a similar timescale, the observed process is assigned to a change of excited state. In FeCABCN1 there is no similar spectral evolution at early times, and the initial broad ESA spectrum remains during the lifetime of the complex. This broad ESA spectrum narrows somewhat, which is assigned to relaxation within the same excited state. The spectral evolutions of FeCABCN1 and FeCABCN1- are also different at longer delay times (>1 ps), see Figure 3.12. In FeCABCN1-, the ESA spectra blue-shift at the expense of the GSB signal. In FeCABCN1, the spectral shape remains constant which manifests as an isosbestic point ∼2.2 eV (after 1 ps delay time).

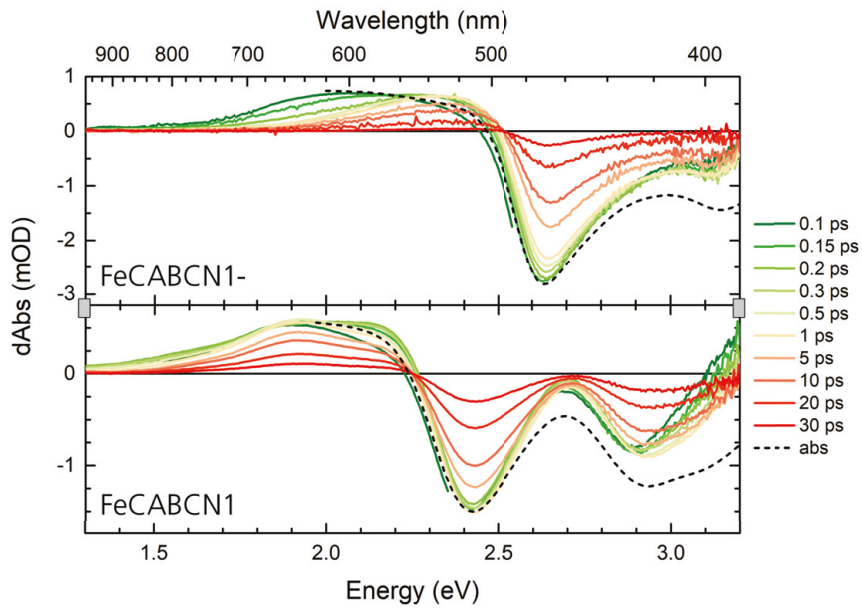

Figure 3.12: Differential spectra measured at different delay times of FeCABCN1 and FeCABCN1-. In dashed lines are the steady-state absorption spectra to compare to the GSB.

The TA data in Figure 3.12 shows that FeCABCN1 stays in the first probed excited state, whereas FeCABCN1- changes excited state. In all investigated FeCAB derivatives (paper III), the initially probed differential spectra are similar. It is therefore reasonable to assign them to the same state. After excitation into the ^{1}MLCT state ISC takes place, which happens in <50 fs for $Fe(bpy)_3^{2+}$ according to measurements from Gawelda et al..[75] Assuming the ISC rate depends mainly on the spin-orbit coupling, it should be similar in all Fe-complexes. The initially probed ESA spectra, measured at ∼100 fs delay time, are therefore assigned to the ^{3}MLCT state. This assignment confirms that FeCABCN1 (together with FeCABC1 and FeCABCN2 that display similar dynamics) stay in the ^{3}MLCT state during their 19 ps lifetime (see Table 3.2). FeCABCN1-, on the other hand, leaves the ^{3}MLCT state and enters another excited state with continuously blue-shifting ESA spectrum (Figure 3.12). Further-

more, a similar spectral evolution was observed for all FeCAB-derivatives without carboxylic group.

To identify the nature of the second excited state, TA spectroscopy of FeCABtBu was measured with improved time-resolution in paper IV (see Figure 3.13). FeCABtBu was shown to leave the ^{3}MLCT and ^{3}MC states on sub-ps timescale to then reside in the ^{5}MC state for ∼200 ps by Liu et al..[88] FeCABtBu is an Fe carbene complex of similar structure as FeCAB (see Figure 3.13a), and is therefore a relevant reference complex for the spectroscopic signature of the ^{5}MC state in Fe carbenes. Comparing the TA dynamics of FeCABtBu (Figure 3.13b) to FeCABCN1- (Figure 3.12), there are striking similarities on the ultrafast timescale, but also differences on the longer timescale. For FeCABtBu the first probed ESA spectrum is broad, which fits with a ^{3}MLCT state assignment. After 1 ps delay time, no positive ESA signal remains in the visible wavelength range, which by Liu et al. was assigned as the signature of the ^{5}MC state.[88] The spectroscopic signature of the ^{5}MC state is clearly different to the >1 ps ESA for FeCABCN1- (Figure 3.12). The lifetime of the ^{5}MC state (∼200 ps) is also substantially longer compared to the lifetime of the FeCAB-derivatives (9-19 ps, see Table 3.2). The comparison of the spectral evolution between FeCABCN1- and FeCABtBu therefore strengthens that the broad ESA observed corresponds to the ^{3}MLCT state, and rules out the second excited state as ^{5}MC.

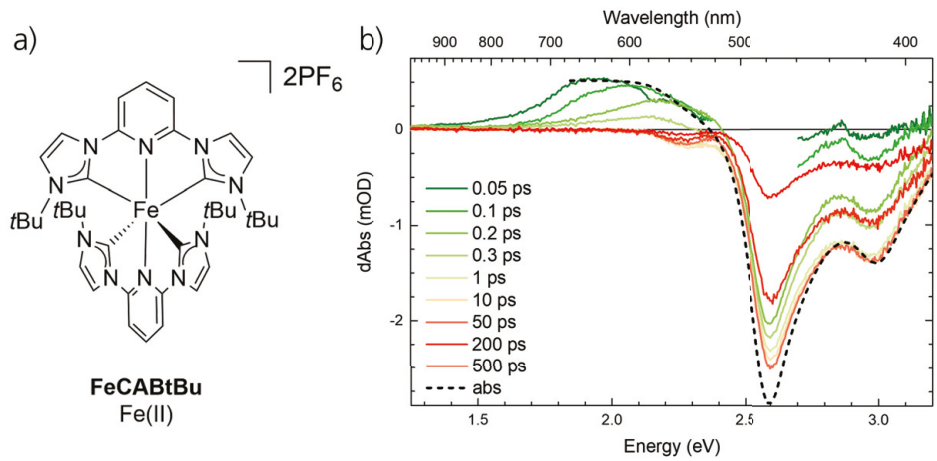

Figure 3.13: a) Molecular structure of FeCABtBu, discussed in paper IV. b) Differential spectra measured at different delay times of FeCABtBu. In dashed line is the steady-state absorption spectrum to compare to the GSB.

Since the ^{3}MLCT and ^{5}MC states were ruled out, the blue-shifted ESA observed for FeCABCN1- and other FeCAB-derivatives without carboxylic group is assigned to the ^{3}MC state. The 9-14 ps lifetime, together with a narrow ESA spectrum in the visible range overlapping with GSB, are similar to reports of ^{3}MC states in other Fe- and Ru-complexes.[107, 109–113] The ^{3}MC state is in the FeCAB-derivatives populated far

from its energetic minimum, due to the difference in geometry between the ^{3}MLCT and ^{3}MC states (see Figure 3.11b). The observed ESA blue-shift at >1 ps delay times is then explained by the structural relaxation within the ^{3}MC state. The same argument can explain why the ESA of the ^{3}MC state is blue-shifted compared to the ESA of the ^{3}MLCT state. The ESA was tentatively assigned to ligand-to-metal charge-transfer (LMCT) transitions, since LMCT transitions of oxidised FeCAB-derivatives are red-shifted compared to the Fe(II) GS absorption. LMCT transitions blue-shift when a MC state is populated, since this increases the energy of the empty t_{2g}-orbital involved in the LMCT transition. Finally, the shallow ^{3}MC potential surface commonly consists of contributions from many different electronic MC states, and can therefore have multiple local energy minima.[51, 114–119] This can explain why some of the studied molecules (i.e. FeCAB) show multiple ^{3}MC excited states of slightly different ESA and lifetime.

Several research groups have investigated the photophysics of FeCAB and FeCABC, not only by TA spectroscopy but also by complementary techniques. For FeCABC, the new results are in agreement with such previous studies including measurements of fluorescence up-conversion and vibrational coherence spectroscopy.[99, 100, 120, 121] For FeCAB, the original model was replaced and therefore the new results refine not only the first TA study but also an X-ray follow-up study.[88, 122] Why these papers can not fully explain the TA dynamics of FeCAB, and thus a new model is needed, is discussed in paper IV. The discussion is summarised as:

- The initial broad ESA spectrum is assigned to the ^{1}MLCT state by Liu et al.,[88] alternatively a hot MLCT state of mixed character by Kunnus et al..[122] This can not explain why such a state would have a 19 ps lifetime in FeCAB-derivatives with carboxylic group.
- Liu et al. assigned the narrow ESA to the ^{3}MLCT state based on its extinction coefficient and solvatochromism.[88] A ^{3}MC state receiving the majority population can, however, also posses such characteristics.
- Kunnus et al. identified a branching of 40% of the population from a hot MLCT state to the ^{3}MC state, the latter was assigned a lifetime of 1.5 ps.[122] The GSB dynamics, however, does not recover with a 1.5 ps component.
- Kunnus et al. assigned an even more blue-shifted ESA spectrum of 16 ps lifetime to GS cooling.[122] This spectral feature was in paper IV assigned to the ^{3}MC state, since time-resolved anisotropy measurements found the dipole moment of the ESA feature different to that of the GSB.
- The photophysical model proposed by Kunnus et al.[122] could not be fitted to the TA data using target analysis.

To explain why complexes without carboxylic groups leave the ^{3}MLCT state, the projected potential energy surfaces of FeCABCN1 and FeCABCN1- are compared in Figure 3.14 The calculations show that the position of the ^{3}MLCT state differ by $\sim$0.6 eV in the two complexes. For FeCABCN1, the ^{3}MLCT state minimum is $\sim$0.2 eV above the ^{3}MC state minimum, and the PPES suggests an energy barrier between the states. For FeCABCN1-, the ^{3}MLCT state minimum was estimated $\sim$0.9 eV above the ^{3}MC state minimum, and it is in this reaction coordinate hard to get an indication of any barrier between the states.[5] The stabilisation of the ^{3}MLCT state is consistent with the HOMO-LUMO analysis in Section 3.1.3 (Figure 3.9a). The carboxylic group stabilises the ^{3}MLCT state whereas the ^{3}MC state is unaffected (see Figure 3.14). The ^{3}MC state is actually the lowest excited state in both complexes, even though it is destabilised compared to complexes such as $Fe(bpy)_3^{2+}$. The relatively high energy of the ^{3}MC state ($\sim$1.2 eV) together with an even higher ^{5}MC state, allows for a ^{3}MC lifetime of 10-14 ps. To summarise, the FeCAB-derivatives have ^{3}MLCT and ^{3}MC states that are close in energy and therefore small influences from sidegroups can determine which of these states will host the majority population for a lifetime of 9-19 ps.

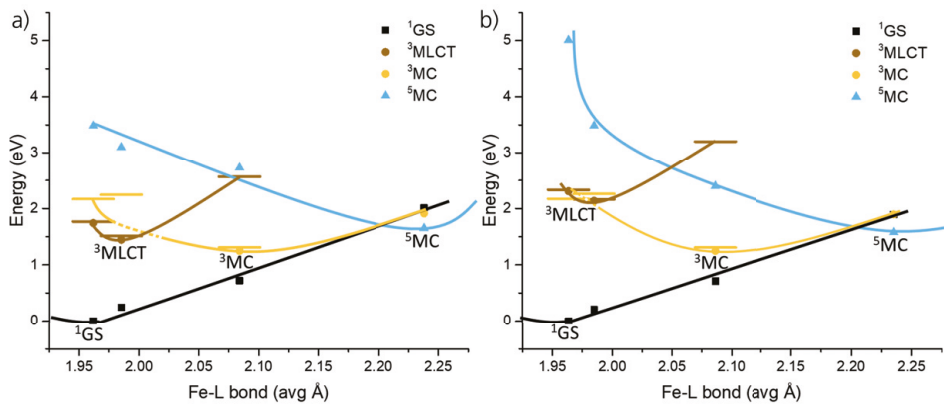

Figure 3.14: Projected potential energy surfaces showing the relevant excited state landscape for a) FeCABCN1 and b) FeCABCN1-. Points are calculated by DFT and bars with TD-DFT at the B3LYP* level of theory, lines represent a guide to the interpretation. Note that the two graphs are plotted on the same energy- and reaction coordinate-scale.

3.1.5 CoChamp - a Photofunctional ^{3}MC State

Following the sections about d^6 Fe(II) carbene complexes, in this last section a d^6 Co(III) carbene complex is presented. The complex is shown in Figure 3.15a, and

[5]The average Fe-L bond length is here the reaction coordinate, since it reflects the expansion of these bonds when changing from GS/MLCT states to MC states. It is however not necessary that this reaction coordinate represents the highest energy barrier on the multidimensional potential energy surface.

is not based on the same ligand as FeCAB. The ligand in this complex is called "Champ", since it has yielded complexes with most spectacular performance in this thesis work. This includes the CoChamp molecule presented here and in paper V (the Fe(III)Champ complex will be discussed in Section 3.2). The two Champ-ligands coordinate six carbenes to Co(III), which means that the σ-donation is stronger compared to FeCAB. This leads to increased LF splitting, and further MC state destabilisation. In CoChamp, the ^{3}MC minimum is $\sim$2.1 eV above the GS minimum (Figure 3.15b). In FeCABCN1 and FeCABCN1-, the same number is $\sim$1.2 eV (Figure 3.14).[6] Due to the large LF splitting, the ^{5}MC state is above the ^{3}MC state similar to the FeCAB-derivatives. The Champ-ligand is however negatively charged, which increases the energy of the π^*-orbitals, destabilising also the MLCT states. In CoChamp the ^{3}MLCT minimum could not be optimised, but based on TD-DFT calculations it is approximately $\sim$4 eV above the GS (see Figure 3.15b). This means that the ^{3}MC state is by far the lowest excited state in this complex, and other states appear nested within this state (i.e. do not have a crossing with it). The PPES of CoChamp is thus very different compared to the FeCAB-derivatives, which yields strikingly different photophysics.

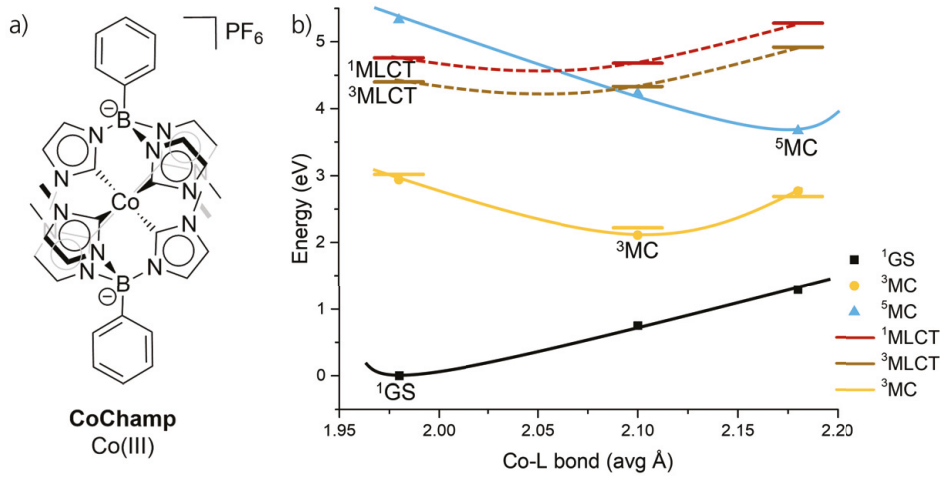

Figure 3.15: a) Molecular structure of CoChamp, discussed in paper V. b) Projected potential energy surfaces showing the relevant excited state landscape for CoChamp. Points are calculated by DFT and bars with TD-DFT at the B3LYP* level of theory, lines represent a guide to the interpretation.

As a consequence of the excited state landscape in CoChamp, the MLCT absorption bands are in the UV wavelength range (>4.5 eV), see in Figure 3.16a. The different absorption bands were assigned based on their extinction coefficient.[42] MC absorption bands were identified extending from the UV into the visible range, but are

[6]This comparison of the ligand-induced LF strength is however not completely fair, since the change of metal will also have an effect.

too weak to give CoChamp any visible colour. Furthermore, CoChamp shows weak emission centred at 1.8 eV (690 nm) with quantum yield 0.01%, see Figure 3.16a. The emission was attributed to the ^{3}MC state based on several considerations. First, the energy of the emission (1.8 eV) is more similar to the calculated vertical energy gap between the ^{3}MC state and ^{1}GS (1.4 eV) than the gap between the ^{3}MLCT state and ^{1}GS ($\sim$4 eV), see Figure 3.15b. Second, the excitation spectrum match not only the ^{1}MLCT absorption band but also the ^{1}MC lower energy absorption around $\sim$4 eV (see Figure 3.16a). Third, the emission was proven to come from a triplet state since it was quenched by an energy transfer reaction with $^3O_2$, and subsequently displayed emission from $^1O_2$ in the infrared (see Figure 3.16b). CoChamp is therefore one of the few examples of d^6 complexes displaying emission from a MC state. The reason why the emission is so red-shifted compared to the MLCT absorption band is also explained by the PPES, since most of the energy is lost in the internal conversion and ISC processes to reach the lowest excited ^{3}MC state.

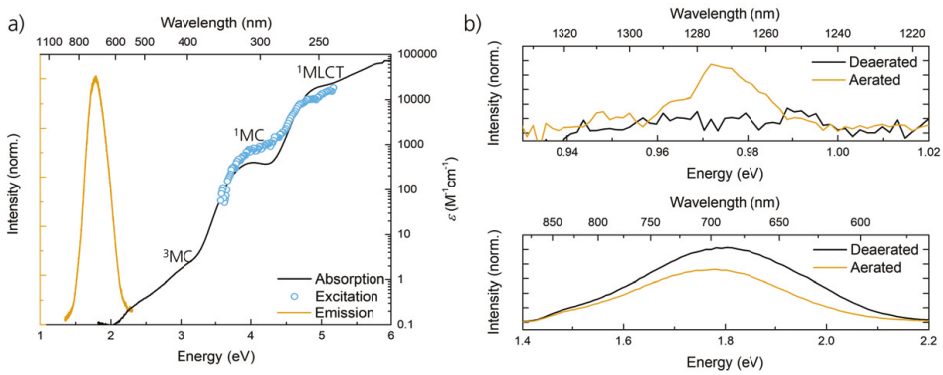

Figure 3.16: a) Extinction coefficient (NB logarithmic scale), emission spectrum and emission excitation spectrum of CoChamp. b) The triplet state energy transfer test with oxygen. In the bottom panel, the emission intensity of CoChamp is decreased aerated. At the same time, the emission intensity of $^1O_2$ appears in the top panel.

Not only the emission makes the ^{3}MC state in CoChamp remarkable, but also its lifetime of $\sim$1 µs.[7] Since the ^{3}MC state is emissive, the lifetime was confirmed both by time-resolved emission and absorption measurements. The excited state landscape in CoChamp is optimised so that the ^{3}MC state is high enough in energy to have a long lifetime (considering the energy-gap law) as well as other states are even higher and thus not provide a deactivation pathway to ^{1}GS. In the PPES of CoChamp (Figure 3.15b) there is no indication even for a crossing point between the ^{3}MC state and ^{1}GS, which indicates a high energy barrier for this conversion. CoChamp provides an example of a photofunctional ^{3}MC state, since it fulfils the criteria displaying emission and driving energy transfer reactions. The question is, however, if CoChamp

[7]The excited state lifetime depends on the solvent, e.g. in acetonitrile the lifetime is 0.8 µs and in methanol it is 1.3 µs.

qualifies as a photosensitiser, due to the lack of (strong) absorption in the visible wavelength range. Nevertheless, the complex nicely illustrates that it is not the nature of the excited state that decides whether it is photofunctional or not, it is the relative arrangement of the excited states.

3.2 d^5 Fe Carbene Complexes

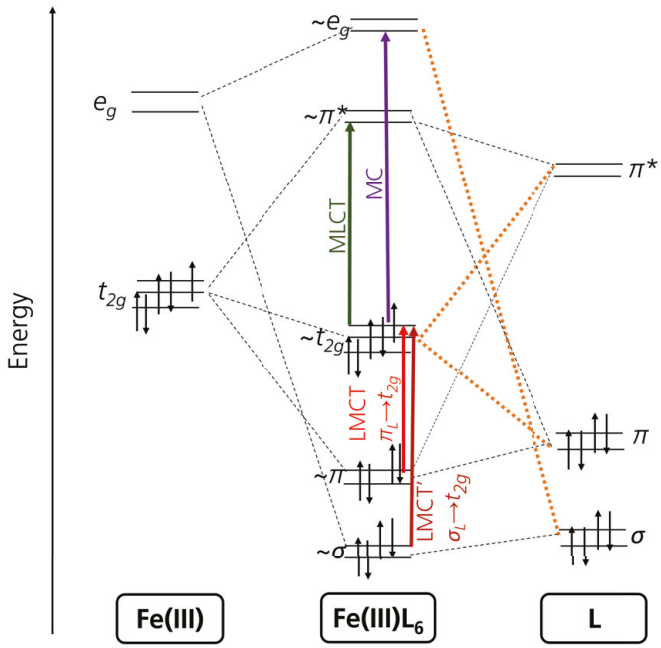

Figure 3.17: Frontier orbitals and their resulting mixed orbitals for an Fe(III) carbene complex (d^5 electronic configuration). (L - ligand) Furthermore, the electronic transitions giving rise to the excited LMCT, MLCT and MC states are indicated. Adapted with permission from Lindh et al..[66]

To improve the lifetime of Fe carbene complexes further, a stronger LF splitting than what the FeCAB-ligand can provide is required. A straightforward solution is to increase the number of carbenes from four to six, which indeed improved the ^{3}MLCT lifetime to ∼500 ps.[123] The bidentate hexa-carbene complex presented by Chábera et al. did however exist both as a d^6 Fe(II)-complex and as a d^5 Fe(III)-complex.[123, 124] This Fe(III) carbene complex became the first Fe-complex to display emission at room temperature.[124] Furthermore, the emissive state was of ^{2}LMCT nature which is to date only found in a few d^5 complexes (mainly Re(II) or Fe(III)).[125–128] Two families of Fe(III) carbene complexes with emissive ^{2}LMCT states have since then been introduced; paper VI presents a tridentate hexa-carbene complex and Steube et al. presented a cyclometalated complex.[128] In the following

sections, the properties of the ^{2}LMCT state in Fe(III)-complexes will be exemplified by the complex from paper VI and its derivatives.

The d^5 electronic structure implies other excited states with even spin-configurations (since there must be at least one unpaired electron already in the GS). Due to the large LF splitting, the Fe(III) carbene complexes all have low-spin ^{2}GS, i.e. all five electrons populate the t_{2g}-orbitals (see Figure 3.17). Since there is one vacant spot for an electron in the t_{2g}-orbitals, electronic transitions from the ground state can be of LMCT, MLCT and MC nature, see Figure 3.17. The ordering of the different excited state will, however, depend on the energy of the metal-centred and ligand-centred orbitals.

3.2.1 Introducing the ^{2}LMCT State

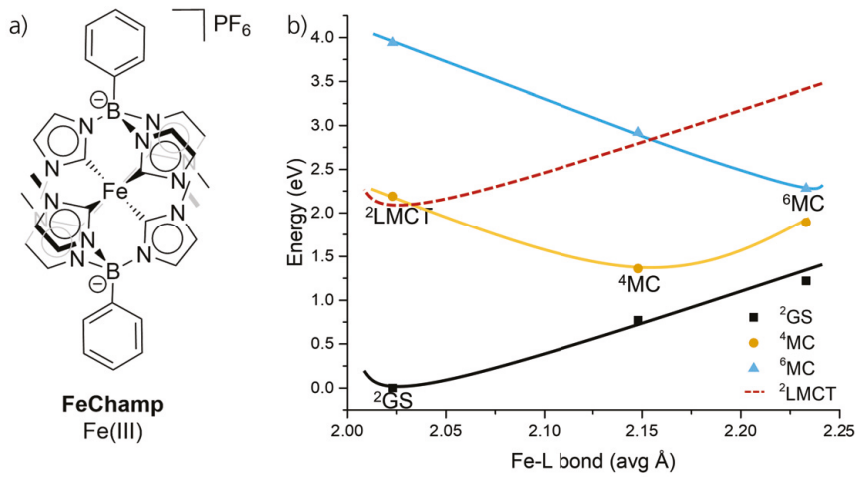

Figure 3.18: a) Molecular structure of FeChamp, discussed in papers VI-VIII. b) Projected potential energy surfaces showing the relevant excited state landscape for FeChamp. Points are calculated by DFT at the B3LYP* level of theory, lines represent a guide to the interpretation. The ^{2}LMCT state energy is estimated based on measured absorption and emission spectra.

The Champ-ligand, introduced in Section 3.1.5, is both a strong σ-donor and negatively charged. From paper VI, the resulting Fe(III)-complex[8] is shown in Figure 3.18a here referred to as FeChamp. Similar to CoChamp, both metal-centred and ligand-centred orbitals are destabilised in FeChamp compared to FeCAB. This is seen in the negative shift of the ligand reduction and metal oxidation potentials (Fe(III)/Fe(II)).

[8]The analogous Fe(IV)-complex is also stable shown by Prakash et al.,[129] but will not be discussed here.

The lowest excited state in FeChamp is the ^{4}MC state, identified by DFT calculations (see Figure 3.18b). Similar to the d^6 complexes, a higher spin MC state (here ^{6}MC) is also present at even more elongated Fe-L bond lengths and at higher energy due to the LF splitting.

FeChamp absorbs in the visible spectral range, see Figure 3.19a. Based on the extinction coefficient ($\sim$3000 $M^{-1}cm^{-1}$), this band is spin-allowed and of charge-transfer nature,[42] i.e. either ^{2}MLCT or ^{2}LMCT based on Figure 3.17. Furthermore, FeChamp is to date the Fe-complex with highest emission quantum yield: 2.1% at room temperature (see Figure 3.19a). The emission excitation spectrum matches the absorption spectrum, which suggests that both absorption and emission involves the same excited state (see Figure 3.19a). To judge whether this state is indeed a ^{2}MLCT or ^{2}LMCT state, the 2.1 eV E_{00} energy was compared to measured redox potentials from electrochemistry. Such a comparison is valid since charge-transfer transitions to a first approximation oxidises and reduces different parts of the molecule. In the case of a MLCT transition, the E_{00} energy is similar to the energy difference between the ligand reduction potential and the metal oxidation potential. In the case of a LMCT transition, the E_{00} energy is instead similar to the energy difference between the ligand oxidation potential and the metal reduction potential. For FeChamp, the LMCT transition results in 2.8 eV which matches better with 2.1 eV than the $>$3.6 eV approximated for the MLCT transition. Therefore, the emissive state in FeChamp was assigned as a ^{2}LMCT state.

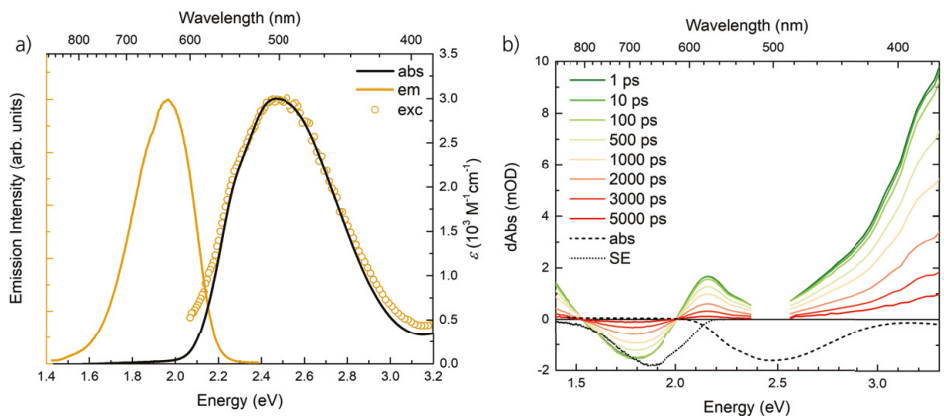

Figure 3.19: a) Extinction coefficient, emission spectrum and emission excitation spectrum of FeChamp. b) Differential spectra measured at different delay times of FeChamp. The absorption (abs) and calculated stimulated emission (SE) spectra are also shown for comparison.

The differential spectrum of the ^{2}LMCT state in FeChamp is shown in Figure 3.19b. The differential spectrum features strong ESA in the whole visible wavelength range also extending into the NIR and UV. In Figure 3.19b, the spectrum is only negative $\sim$1.8 eV which is assigned to stimulated emission. The ESA extinction coefficient is

stronger than the GSB, which explains why only a dip in the ESA is seen ∼2.5 eV where a GSB region is expected. The differential spectra in FeChamp do not change shape over the probed delay time, which means that no change of excited state is taking place. This is consistent with a simple model, where the excited ^{2}LMCT state after the lifetime of the complex returns to ^{2}GS. Both the TA data and time-resolved emission measurements found a single exponential decay time of 2.0 ns, which was assigned as the lifetime of the ^{2}LMCT state.

3.2.2 Deactivation of the ^{2}LMCT state

Both absorption and emission involve the same two states in FeChamp, that is ^{2}GS and ^{2}LMCT. This means that excitation is directly into the state of 2 ns lifetime. De-excitation of the ^{2}LMCT state then proceeds via three deactivation pathways, shown in Figure 3.20. These are fluorescence to the ^{2}GS, non-radiative decay to the ^{2}GS, and activated decay via the ^{4}MC state which then non-radiatively decays to the ^{2}GS. The deactivation via the ^{4}MC state thus requires an ISC event. The deactivation of the ^{2}LMCT state is clearly very different compared to the ^{3}MLCT state in d^6 Fe-complexes. To get more insights, a temperature dependent study of FeChamp was started in paper VI and continued in-depth in paper VII.

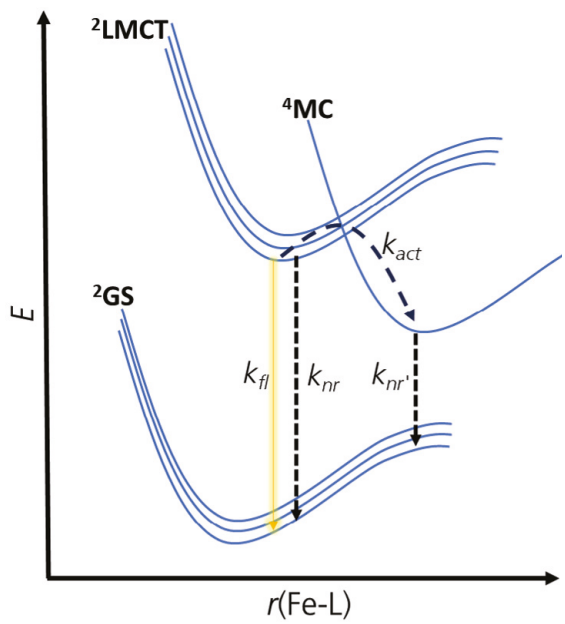

Figure 3.20: Schematic of the excited state landscape in FeChamp, together with the relevant deactivation rates. fl - fluorescence, nr - non-radiative, act - activation.

Starting with the steady-state data, temperature dependent absorption and emission of FeChamp are shown in Figure 3.21. Characteristic for low temperature data is that peak structure becomes more pronounced, which is seen both in the absorption and emission spectra. For FeChamp, the absorption spectrum does not shift with temperature, whereas the emission peaks blue-shift as the temperature is decreased. This means that the ^{2}GS and ^{2}LMCT state minima have different geometry, so when FeChamp is excited it enters a vibrationally hot ^{2}LMCT state. When the complex is cooled down, the relaxation is hindered which yields emission at higher energy. Yet another difference between the absorption and emission spectra is that the emission spectrum can be fitted by a vibrational progression model with four Gaussians, which clearly does not work for the absorption spectrum. This means that the emission spectrum indeed is produced by one electronic transition from the lowest ^{2}LMCT state to the ^{2}GS, and its vibrational sublevels. The absorption spectrum can only be fitted by a vibrational progression model (with three Gaussians) if two independent Gaussians are also included. This means that absorption involves transitions to multiple electronic states in the ^{2}LMCT manifold.

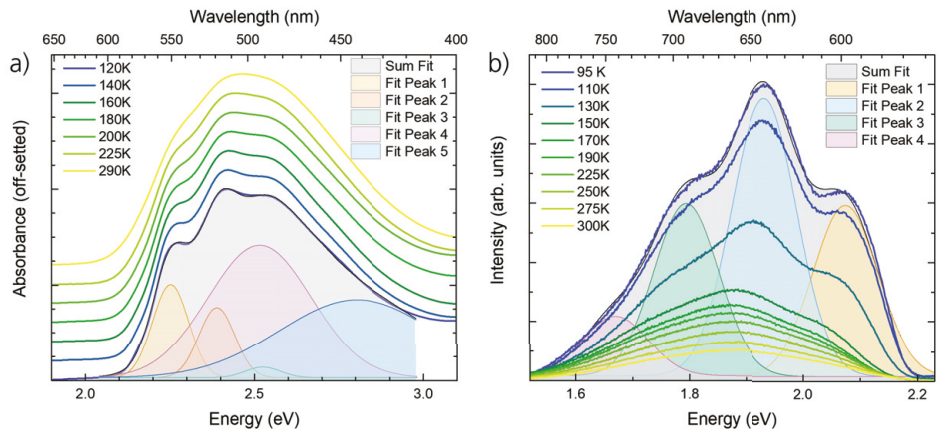

Figure 3.21: a) Absorption spectra measured at different temperatures of FeChamp (vertically off-setted for clarity). Also shown is a fit to the lowest temperature absorption spectrum by a sum of Gaussian functions. b) Emission spectra measured at different temperatures of FeChamp. Also shown is a fit to the lowest temperature emission spectrum by a sum of Gaussian functions of shared width (i.e. a vibrational progression model).

The lowest ^{2}LMCT state responsible for the fluorescence in FeChamp, shows a temperature dependent excited state lifetime, see Figure 3.22a. At 80 K the lifetime has extended to 12 ns, and the emission quantum yield has increased to 25%. The improved properties indicate that there are non-radiative deactivation processes that are hindered when FeChamp is cooled down. These processes have an activation energy, such as the conversion to the ^{4}MC state with rate k_{act} in Figure 3.20. The fluorescence process is not governed by an activation energy, and its rate k_{fl} is therefore temperature independent. Finally, the direct non-radiative deactivation from ^{2}LMCT to ^{2}GS

(rate k_{nr} in Figure 3.20) is a collection of many different processes, and must therefore be divided in one temperature dependent and one temperature independent part. Derived from these processes, Equation 3.1 is an Arrhenius expression describing how the ^{2}LMCT lifetime τ depends on the temperature T.[31]

$$\frac{1}{\tau} = k_0 + A_1 e^{-\frac{\Delta E_1}{kT}} + A_2 e^{-\frac{\Delta E_2}{kT}} + \frac{M}{1 + e^{C(1/T - 1/T_m)}} \tag{3.1}$$

In Equation 3.1, there are two Arrhenius terms which consist of a pre-exponential factor A and an exponential decay function that relates an activation energy ΔE to the temperature T (k is the Boltzmann constant). The first of these terms is associated with the temperature dependent part of the direct non-radiative deactivation (k_{nr}) from ^{2}LMCT to ^{2}GS, the second one with the deactivation pathway via the ^{4}MC state (k_{act}), see Figure 3.20. k_0 represents the temperature independent processes, including fluorescence (k_{fl}) and part of the direct non-radiative deactivation (k_{nr}). Furthermore, the temperature independent deactivation rate k_0 increases by a step-function above the glass transition temperature (T_m), since the solvent melts. This is corrected for by the last term including the empirically fitted constants M and C, as well as T_m.

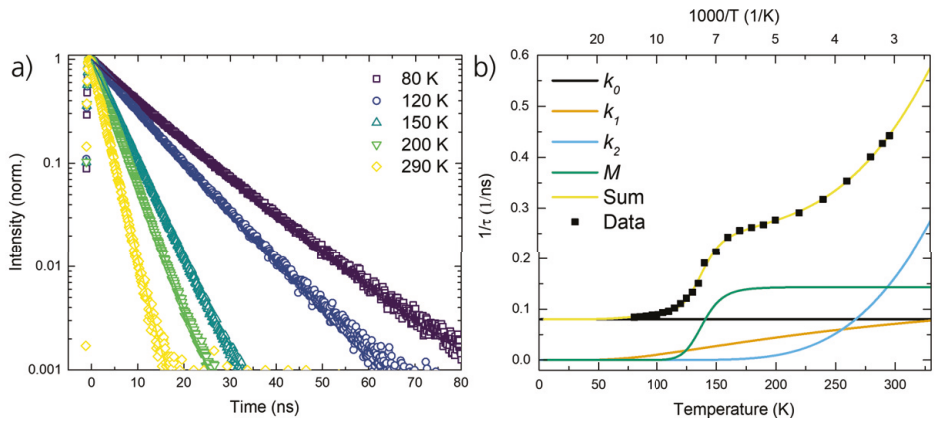

Figure 3.22: a) Time-resolved emission kinetics of FeChamp measured by TCSPC at different temperatures. Fits are given by the solid lines. b) Emission lifetime of FeChamp as a function of temperature, fitted by Equation 3.1. The relative contribution of the different terms in Equation 3.1 are also shown.

Equation 3.1 indeed fit the temperature dependent ^{2}LMCT lifetime data, shown in Figure 3.22b. The same model has been applied to several Ru-complexes[31], although the states associated with each process are in the case of FeChamp different. To interpret the result of the model, the relative significance of the different terms in Equation 3.1 are plotted in Figure 3.22b. Especially interesting is of course the deactivation pathways at room temperature, i.e. ∼300 K. At 300 K, the temperature independent pathway (k_0 together with M in Figure 3.22b) is the major contribu-

tion to the deactivation rate, followed by the pathway via the ^{4}MC state (k_2 in Figure 3.22b). The smallest contribution comes from the direct activated non-radiative pathway (k_1 in Figure 3.22b). This means that in FeChamp it is not the deactivation pathway via a MC state that is dominating. The result is very different to the deactivation model for the ^{3}MLCT state in d^6 Fe-carbenes such as FeCABC. The result also implies that improvement to the lifetime can not be accomplished by the usual strategies of stabilising the charge-transfer state and destabilising the MC states.

Table 3.3: Temperature dependent lifetime (τ) and fit results to Equation 3.1 comparing FeChamp, Ru(dqp)$_2$[130] and Coumarine 47 (fitted with only the first two terms in Equation 3.1).[131] k_0 - temperature independent rate, T_m - glass transition temperature, A - pre-exponential factor, ΔE - activation energy.

Complex	τ 80 K (ns)	τ 300 K (ns)	k_0 (s^{-1})	T_m (K)	A_1 (s^{-1})	ΔE_1 (cm^{-1})	A_2 (s^{-1})	ΔE_2 (cm^{-1})
FeChamp$^+$	12	2	8.0E7	139	1.8E8	200	4.9E10	1190
Ru(dqp)$_2^{2+}$	8500	3000	1.2E5	119	3.0E5	260	1.5E10	2600
Coumarine 47	5[a]	4	2.0E8	-	4.3E9	850	-	-

[a]Measured at 115 K.

To put the fitted parameters in context, FeChamp is compared to one of the best performing Ru-based d^6 photosensitisers, Ru(dqp)$_2^{2+}$, see Table 3.3. This complex behaves similarly to FeChamp in the way that the lifetime is only prolonged by a factor of $<$10 when cooled down, and not several orders of magnitude. For Ru(dqp)$_2^{2+}$, a high activation energy (2600 cm^{-1}) together with a low pre-exponential factor (1.5E10 s^{-1}) for deactivation via the ^{3}MC state (see Table 3.3) has stopped this process from limiting the ^{3}MLCT lifetime. In the case of FeChamp, the activation energy is somewhat lower (1190 cm^{-1}), but the pre-exponential factor (4.9E10 s^{-1}) is of the same order of magnitude compared to Ru(dqp)$_2^{2+}$, see Table 3.3. The low pre-exponential factor in FeChamp is explained by the spin-forbidden nature of the transition from ^{2}LMCT to ^{4}MC. This enables FeChamp to stay in the ^{2}LMCT state despite the ^{4}MC state being lower in energy (see Figure 3.18b).

What is really limiting the lifetime of FeChamp, is the non-radiative temperature independent deactivation from ^{2}LMCT directly to ^{2}GS. The non-radiative processes are governed by factors such as the extinction coefficient, vibrational modes, the energy gap law etc. Especially important is the fact that the transition is spin-allowed, which increases the rate of both fluorescence and non-radiative processes. In this regard, a good comparison to FeChamp is an organic photosensitiser exemplified by Coumarine 47 in Table 3.3. In both photosensitisers, it is actually the temperature independent deactivation processes that limit the excited state lifetime to the ns timescale. What has stopped the deactivation via MC states in the d^5 configuration is therefore also limiting the lifetime and emission quantum yield of the ^{2}LMCT state. Strategies to further improve the ^{2}LMCT properties should therefore target the non-radiative

decay. This can be done by hindering vibrational modes, a strategy used in some Fe-complexes.[87] In FeChamp, the N-B bond generates strong infrared stretching modes which are possibly involved in deactivating the ^{2}LMCT state.

3.2.3 The robust ^{2}LMCT state

One strategy to influence the ^{2}LMCT state in FeChamp would be to attach sidegroups, similar to the push-pull complexes for FeCAB. This idea was explored in paper VIII. Three different sidegroups were incorporated in the outmost phenyl rings of FeChamp creating the homoleptic complexes FeChampBr (with Br sidegroups), FeChampOM (with methoxy sidegroups) and FeChampC (with carboxylic sidegroups) shown in Figure 3.23a. In Figure 3.23b the absorption spectra of all FeChamp-derivatives are shown. In stark contrast to the FeCAB-derivatives, the FeChamp-derivatives show only minor differences in their absorption spectra if any. Two derivatives show slightly higher extinction coefficient than FeChamp, but within the experimental accuracy no clear trends could be observed taking into account also steady-state emission, oxidation/reduction potentials and excited state lifetimes (see Table 3.4). All photophysical characteristics are virtually unchanged between the parent complex FeChamp and its derivatives. This suggests that there is no communication between the ^{2}LMCT state and the outmost phenyl ring with substituents.

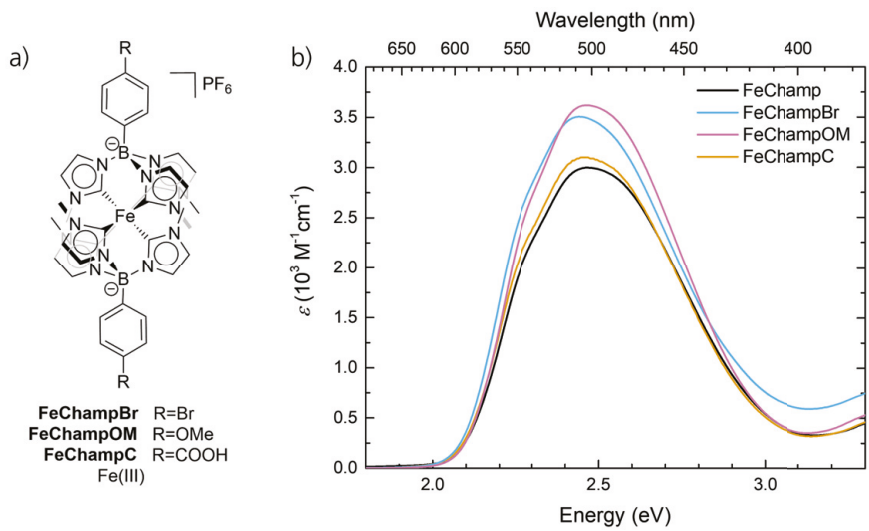

Figure 3.23: a) Molecular structure of the FeChamp-derivatives (FeChampBr, FeChampOM, FeChampC), discussed in paper VIII. b) Comparison of the extinction coefficients of the FeChamp-derivatives.

Table 3.4: Photophysical properties of the FeChamp-derivatives compared. Abs - LMCT absorption maximum, ϵ - extinction coefficient, Em - LMCT emission maximum, Φ - emission quantum yield, $Fe^{III/II}$ - Fe reduction potential, $Fe^{IV/III}$ - Fe oxidation potential, L_{ox} - ligand oxidation potential, τ - excited state lifetime.

Complex	Abs (nm)	$\epsilon\ 10^3$ ($M^{-1}cm^{-1}$)	Em (nm)	Φ (%)	$Fe^{III/II}$ (V)	$Fe^{IV/III}$ (V)	L_{ox} (V)	τ (ns)
FeChamp	502	3.0	655	2.1	-1.16	0.26	1.67	2.0
FeChampBr	508	3.5	658	1.8	-1.14	0.28	1.75	1.8
FeChampOM	503	3.6	658	1.7	-1.19	0.24	1.39	1.7
FeChampC	505	3.1	661	1.9	-1.13	0.29	>1.9	1.9

The ^{2}LMCT state involves transitions from ligand π-orbitals to metal t_{2g}-orbitals (seen in Figure 3.17). This means that if the sidegroups should influence the ^{2}LMCT state, the ligand π-orbitals must extend on the outmost phenyl ring. The highest singly occupied molecular orbital is shown in Figure 3.24b, which clearly has contributions only on the inner imidazole-moieties. Also ligand π-orbitals of lower energy (contributing to higher ^{2}LMCT states) never extend past the boron atoms. As the metal t_{2g}-orbital (Figure 3.24a) naturally resides on iron, this means that the sidegroups in the FeChamp-derivatives can not influence the ^{2}LMCT state.

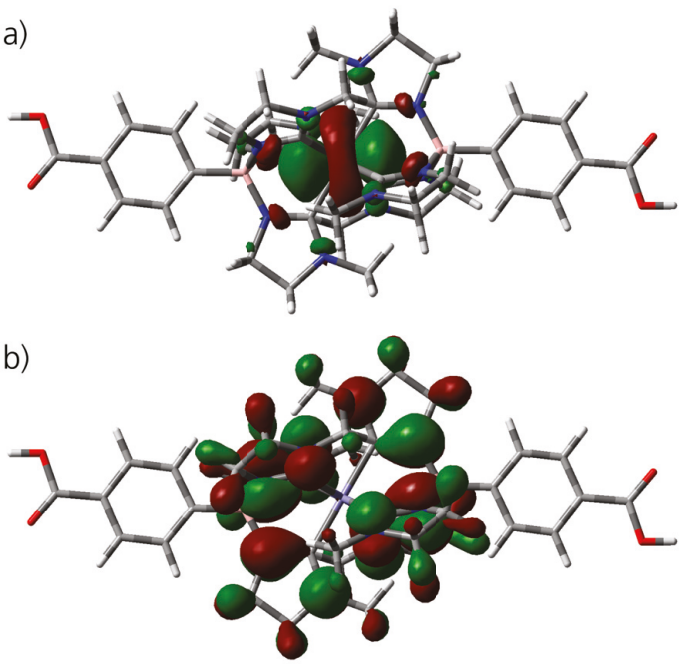

Figure 3.24: a) Lowest singly unoccupied molecular orbital of FeChampC. b) Highest singly occupied molecular orbital of FeChampC. Calculated by DFT at the B3LYP* level of theory.

The introduction of sidegroups in this series of FeChamp-derivatives did not improve the ^{2}LMCT lifetime nor the emission quantum yield (see Table 3.4). Even though the intended strategy did not work, the result is still useful as it shows an integrity of the ^{2}LMCT state to sidegroup substitution. That can be useful in applications where FeChamp is incorporated in a larger supramolecular structure or where FeChampC is attached to a semiconductor. By only modifying the outmost phenyl rings the already good properties of the ^{2}LMCT state can be maintained. In order to further improve or modify the photophysical properties of the ^{2}LMCT state, modifications should target the inner structure of the ligand (such as the imidazole-moieties, see Figure 3.23a).

3.3 Conclusions

This chapter has described how the classical picture of Fe-complexes, ultrafast deactivation to the ^{5}MC state, changed due to the carbene-ligands. The Fe carbene complexes presented show a rich variation of excited states, featuring both ^{3}MLCT, ^{3}MC and ^{2}LMCT states with lifetimes varying from $\sim$10 ps to $\sim$2 ns. Therefore, the Fe carbene complexes have paved the way to an Earth-abundant photosensitiser library where Fe-complexes are indeed included. The development was here presented based on the two ligand-templates FeCAB and FeChamp, but as stated previously there are many more structures from other researchers that were thus not included in this thesis.[66, 67, 80, 90]

Sidegroup substitution on the FeCAB- versus the FeChamp-framework yielded very different results. The FeChamp-derivatives hardly differed in their photophysical properties. This was due to the lack of electronic communication between the ^{2}LMCT state and the position where the sidegroup was attached. The FeCAB-derivatives were instead largely influenced by the sidegroup, which could even determine if the major excited state resulted in ^{3}MLCT or ^{3}MC. The sidegroups were however found to mainly influence the lowest ^{3}MLCT state, due to the different symmetry between ^{3}MLCT states. For designing new complexes, calculations can give a pointer to the position where sidegroup substitution is efficient.

In this work, many of the short-lived Fe carbene complexes were reassigned to have the ^{3}MC state as the major excited state. MC states are known in the field for being hard to observe spectroscopically, potentially due to their short lifetimes and weak absorption.[121] Recent studies (including those presented here) show that the ^{3}MC state indeed can have lifetimes ranging from 2-450 ps and can be observed by TA spectroscopy.[86, 107, 109–113] This thesis work therefore contributes to disproving the myth of the "elusive MC states". Even though the ^{3}MC state is not a charge-

separated state, complexes with photofunctional MC states have started to appear, displaying emission and engaging in photocatalytic reactions.[132, 133] CoChamp presented here constitutes one such example.

Comparing the d^6 and d^5 approach, both the ^{3}MLCT and ^{2}LMCT states have their own advantages and disadvantages. For the ^{2}LMCT state, the spin-allowed nature of the transition to ^{2}GS enables strong emission. Furthermore, the spin-forbidden transition to the ^{4}MC state significantly slowed this deactivation pathway down resulting in a long ^{2}LMCT lifetime. The same spin-considerations, however, also imply that it will be hard to further improve the ^{2}LMCT state properties by the strategies described for d^6 complexes. For the d^5 Fe carbenes, the fight for longer lifetime is against non-radiative spin-allowed internal conversion from ^{2}LMCT to ^{2}GS. This includes blocking vibrational modes with strong Franck-Condon factors, and potentially other strategies from the organic photosensitiser field since this type of molecules face similar challenges.

For the d^6 Fe carbenes, this work has shown that four Fe-carbene bonds seldom guarantee the ^{3}MLCT state as the major excited state. The ligand field strength of the FeCAB-ligand does not destabilised the MC states enough to ensure the ^{3}MLCT state as the major excited state. To accomplish that, also a strategy of stabilising the ^{3}MLCT state is needed, such as adding an electron-withdrawing substituent. For the FeCAB-derivatives studied here, the ^{3}MLCT and ^{3}MC states are so close in energy that the influence of a sidegroup can dictate the photophysics. More carbenes or other ligands introducing an even stronger LF are needed to fully move the MC states out of the way, which was explored e.g. by Chábera et al. and Braun et al..[123, 134] The good thing with d^6 complexes is after all that the ^{3}MLCT state has different spin compared to the ^{1}GS, which means that the challenge to prolong the ^{3}MLCT lifetime is to block the non-radiative decay via the ^{3}MC states. To meet this challenge there are many strategies to apply, and it will be interesting to learn what will ultimately limit the lifetime for d^6 Fe-complexes.

Chapter 4

Photochemistry of Iron Carbene Complexes

Temperature dependence,
and more points![1]

4.1 Intermolecular Charge-Transfer

Chapter 3 laid a firm foundation for understanding the photophysics of Fe carbene photosensitisers. In Chapter 4, some of the introduced Fe carbene complexes will be evaluated in terms of photofunctionality. Here, this entails if their excited states can participate in charge-transfer reactions. Charge-transfer reactions are generally the first step towards the solar harvesting applications discussed in Chapter 1. The first half of this chapter (Section 4.1) will discuss intermolecular charge-transfer. That is a reaction between two molecules, where in this case one is the Fe carbene photosensitiser. The intermolecular charge-transfer reaction is often the first step in photocatalysis schemes for making solar fuels. At the end of this section, some early examples of photocatalysis with Fe carbene photosensitisers will be shown. Before that, a theoretical background is presented together with insights from fundamental studies of intermolecular charge-transfer reactions with Fe carbene photosensitisers.

FeChamp is the Fe carbene photosensitiser of longest excited state lifetime discussed in this thesis (Figure 4.1). The lifetime is important in photocatalysis applications, since the intramolecular deactivation should be significantly slower compared to the

[1]Communication between prof. Persson and PhD student.

intermolecular reaction rate. Furthermore, the ^{2}LMCT state in FeChamp has both high reduction and oxidation potential. This means that it can participate in potentially both oxidative and reductive photocatalysis schemes. The presented examples in this section will mainly involve FeChamp, which is in line with the scope of this thesis. In this case, the selection actually represents the overall literature on Fe carbenes in intermolecular charge-transfer, where this complex is well represented due to its great photophysical properties.[135]

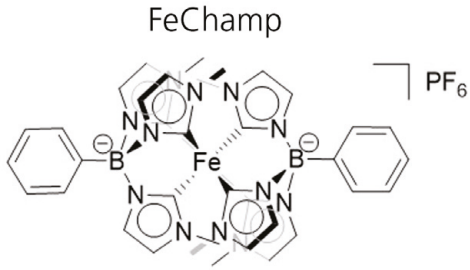

Figure 4.1: The Fe carbene photosensitiser mainly investigated for photocatalysis applications, that will be discussed in the intermolecular charge-transfer section.

4.1.1 Marcus Electron-Transfer Theory

The rate of an intermolecular charge-transfer process (k_{CT}) is classically described by Marcus electron-transfer[2] theory.[136, 137] The following presentation of this theory is inspired by that of Balzani et al..[7] In Marcus theory, it is assumed that the collective state of the two reacting molecules before and after charge separation can be described by parabola, see Figure 4.2a. The transition from the initial to the final state is associated with a free thermodynamic driving force (ΔG^0). For the transition to occur, a free activation energy needs to be overcome ($\Delta G^\ddagger$). The relative positions of the parabola (i.e. states) are described by the free reorganisation energy (λ). The three quantities are related via Equation 4.1.

$$\Delta G^\ddagger = \frac{1}{4\lambda}(\Delta G^0 + \lambda)^2 \tag{4.1}$$

The reorganisation energy describes the energy the system needs to gain to reorganise to the charge-separated state at its initial optimal geometry, without making the charge-transfer reaction (see Figure 4.2a). This energy difference has two contributions: i) the change in arrangement of the solvent surrounding the molecules, ii) the change in the structure of the two reacting molecules.

[2]The theory is named Marcus electron-transfer, but in most practical cases electron-transfer and charge-transfer (that is used in this thesis) are identical.

The Arrhenius Equation 4.2 describes the charge-transfer rate k_{CT} of the system in Figure 4.2a.

$$k_{CT} = \nu_N \kappa_{el} e^{\frac{-\Delta G^{\ddagger}}{RT}} \tag{4.2}$$

The rate is clearly temperature dependent, which means that the activation energy $\Delta G^{\ddagger}$ can be determined by temperature dependent studies of k_{CT}. Equation 4.2 has two pre-exponential factors, ν_N and κ_{el}. ν_N is the nuclear frequency factor, which describes how often the initial state comes to the crossing point between the parabola (see Figure 4.2a). κ_{el} is the electronic transmission coefficient, which describes how likely it is to change state once the system comes to the crossing point. This depends on the overlap between the electronic wave functions of the two states, and is very distance dependent.

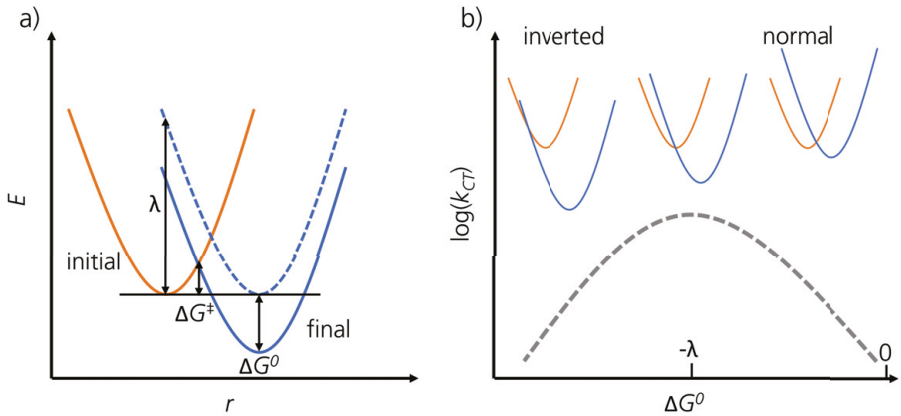

Figure 4.2: a) The classical picture of Marcus theory. The initial state (orange) and final charge-separated state (blue) have a quadratic energy dependence on the reaction coordinate r. Three energy quantities are associated with the charge-transfer reaction: the free thermodynamic driving force ΔG^0, the free activation energy $\Delta G^{\ddagger}$ and the free reorganisation energy λ. b) The relation between the charge transfer rate k_{CT} and ΔG^0, indicating the normal and inverted Marcus regimes.

k_{CT} does not necessarily increase with increasing thermodynamic driving force (ΔG^0), illustrated by the three cases in Figure 4.2b. In the normal regime, an increase of driving force indeed leads to increased charge-transfer rate. When the reorganisation energy exactly matches the thermodynamic driving force, the reaction is barrierless. This is the optimal condition for creating as fast charge-transfer rate as possible. By increasing the thermodynamic driving force further, the charge-transfer rate will instead decrease. As seen in Figure 4.2b, this is because a barrier between the states is reintroduced. This is known as the inverted Marcus regime, and in this regime the initial state is nested within the charge-separated state. Experimental studies of how k_{CT} depends on ΔG^0 have indeed identified the inverted regime in some systems including natural photosynthesis.[138–140] For other systems, k_{CT} was found to stagnate in the inverted regime rather than to decrease.[141, 142]

4.1.2 Bimolecular Charge-Transfer

In a bimolecular charge-transfer reaction, the excited photosensitiser either reduces or oxidises another molecule. In the case of oxidation, the photosensitiser (PS) receives an electron from the other molecule which is then called a donor (D). In the case of reduction, the photosensitiser (PS) gives an electron to the other molecule which is then called an acceptor (A). The reaction takes place if there is a thermodynamic driving force for either of the charge-transfer reactions generating PS^+ and A^- or PS^- and D^+ (see Figure 4.3a).[7]

$$PS^* + A \rightarrow PS^+ + A^-$$
$$PS^* + D \rightarrow PS^- + D^+$$

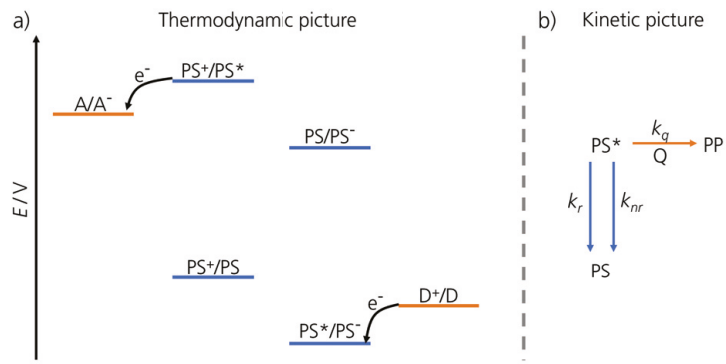

Figure 4.3: Illustration of a) the thermodynamic picture verses b) the kinetic picture of bimolecular charge-transfer. The excited photosensitiser PS^* is quenched by an acceptor A or donor D (collectively called quenchers, Q) to form photoproducts PP. The quenching rate k_Q will compete with the intramolecular deactivation rates k_r (radiative) and k_{nr} (non-radiative).

The charge-transfer reaction opens up yet another pathway for the excited state of the photosensitiser to deactivate (with rate k_Q), apart from radiative (k_r) and non-radiative (k_{nr}) deactivation (see Figure 4.3b). The donor and acceptor can therefore collectively be called quenchers (Q), as they quench the emission from the excited state of the photosensitiser. This makes the emission quantum yield (Φ) of the photosensitiser dependent on the concentration of the quencher ([Q]) according to Equation 4.3.[7]

$$\Phi([Q]) = \frac{k_r}{k_r + k_{nr} + k_Q * [Q]} \tag{4.3}$$

This means that Φ without quencher (i.e. the quencher concentration [Q] is put to 0) divided by Φ with quencher will vary linearly with the concentration of the quencher, shown in Equation 4.4.[7]

$$\frac{\Phi([0])}{\Phi([Q])} = 1 + \frac{k_Q}{k_r + k_{nr}} * [Q] \tag{4.4}$$

Equation 4.4 is the Stern-Volmer equation, which allows for a simple way to study charge-transfer reactions by measuring the emission quantum yield at various concentrations of the quencher. The equation can also be formulated for the emission intensity at a given wavelength, or for the observed emission lifetime. These quantities are both easily accessible via steady-state and time-resolved emission techniques, respectively.[7, 41, 143]

For two molecules to engage in a bimolecular charge-transfer reaction, they have to physically meet in solution. This means that diffusion plays a role, and will limit the reaction if the diffusion time is similar or longer than the excited state lifetime of the photosensitiser. Typically, photosensitisers with excited state lifetimes on the ns-µs timescale are used.[135] In paper VI, FeChamp was observed to participate in bimolecular charge-transfer reactions despite the 2 ns lifetime. In Stern-Volmer type quenching experiments the quenching rate was, however, found to be diffusion controlled. At high enough photosensitiser concentration, the product yield was ∼5%.

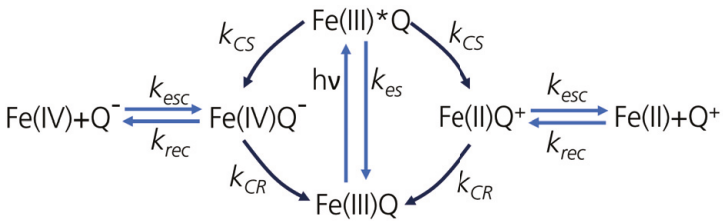

Figure 4.4: The possible bimolecular charge-transfer reaction steps for the system of Fe(III)Champ and a quencher Q in close contact (Fe(III)Q). After excitation (hν), intramolecular relaxation (k_{es}) or charge separation (k_{CS}) takes place. The charge-separated state (Fe(II)Q^+ or Fe(IV)Q^-) either undergo cage-escape (k_{esc}) or charge recombination (k_{CR}). If cage-escape indeed happens, also the generated photoproducts (Fe(II) and Q^+ or Fe(IV) and Q^-) can recombine if they meet again (k_{rec}).

Since then, two follow-up studies by Rosemann et al. and Aydogan et al. focused on finding the reason for such a low photoproduct yield despite efficient quenching.[144, 145] If the concentration is high enough, the photosensitiser will always be in contact with the quencher basically being the solvent. In this way, the "intrinsic charge-transfer rates" independent of diffusion are studied, shown in Figure 4.4. FeChamp (Fe(III)) and the quencher are therefore shown in contact from the beginning when FeChamp is excited (Fe(III)*). In the excited state, Fe(III)Champ reacts with the quencher in a charge-transfer reaction going to right or left in Figure 4.4 depending on whether the quencher is a donor or an acceptor. The rate of the charge-transfer reaction is here called k_{CS}, i.e. the charge separation (CS) rate. The charge-transfer reaction forms a charge-separated state, where the positive and negative species are still bound to each other. This state can proceed to escape the solvent cage (k_{esc}), or can recombine to reform the photosensitiser and quencher (k_{CR}), i.e. charge recombination (CR). If cage-escape happens, photoproducts are formed (Fe(II) and Q^+ or

Fe(IV) and Q^-) which can sometimes be observed spectroscopically or even isolated if surviving long enough. There is, however, also the possibility that the photoproducts recombine (k_{rec}). From a photocatalysis application point of view, the goal is generally to form photoproducts at highest possible yield.[66]

Rosemann et al. and Aydogan et al. found that in general, the charge separation rate (k_{CS}) is high compared to systems with $Ru(bpy)_3^{2+}$ as the photosensitiser.[144, 145] Rosemann et al. found that a fast charge recombination rate (k_{CR}) limits the photoproduct yield, in a case study of two donors.[144] This means that it is not only the diffusion that limits the cage-escape yield, but also the trade-off between k_{CS}, k_{CR} and k_{esc} (see Figure 4.4). Aydogan et al. found the k_{CR} to be dependent both on the specific donor and also on the solvent, to a larger extent than k_{CS}. Therefore, the cage-escape yield was improved to a final record value of 63%.[145] The factors governing the k_{CR} and k_{esc}, and thus the cage-escape yield, are still poorly understood. Hypotheses discussed by Aydogan et al. includes: i) the dielectric constant of the solvent (that determines the electrostatic forces influencing cage-escape), ii) the direction of the charge-transfer (and how screened the charges are by the molecular structure), and iii) the spin of the different states involved in the reaction.[145]

4.1.3 Light-Induced Charge-Disproportionation

The ground and excited state redox potentials of FeChamp are shown in Figure 4.5. In the excited state (Fe(III)*), it is thermodynamically favourable for FeChamp to both oxidise and reduce another FeChamp complex at ground state (Fe(III)). This process is called light-induced charge-disproportionation (LICD). Regardless if the excited Fe(III)* complex accepts or donates an electron the end result is the same: from two Fe(III) complexes one Fe(IV) and one Fe(II) complex is generated.

$$\mathrm{Fe(III)^* + Fe(III) \rightarrow Fe(IV) + Fe(II)}$$

The LICD reaction can happen if the excited Fe(III)Champ has a neighbouring ground state Fe(III)Champ to react with. Since the lifetime of Fe(III)Champ is 2 ns, diffusion should also in this case be overcome by using a high concentration of the photosensitiser. The reaction was identified and first characterised by Kaul et al., that measured Fe(III)Champ at high concentration (70 mM) in solution.[146] The reaction was, however, also found to take place at low temperatures (<170 K) when Fe(III)Champ was dissolved in alcohol solvents with limited solubility. This enabled high local concentration of aggregated Fe(III)Champ. The LICD reaction at low temperatures, including the temperature dependence of the involved rates, was investigated in paper VII. Note that the solvent was frozen at virtually all probed low temperatures where

the LICD reaction was seen, which means that in this system the diffusion parameter is excluded.

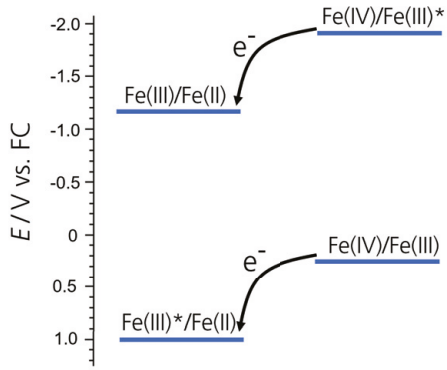

Figure 4.5: Ground and excited state redox potentials of FeChamp, versus the ferrocene reference electrode (FC). The diagram indicates the thermodynamic driving forces for the LICD reaction. Note that there is a driving force both for a reductive and an oxidative mechanism.

Since the species Fe(II)Champ, Fe(III)Champ and Fe(IV)Champ have drastically different absorption spectra (indicated in Figure 4.6) the LICD reaction can be studied by transient absorption spectroscopy. In Figure 4.6, differential spectra probed at 100 ps delay time for a selection of different temperatures are shown. For temperatures $\geq$170 K, the spectra resemble the characteristic differential spectrum of the excited ^{2}LMCT state in Fe(III)Champ. Especially prominent is the negative SE feature $\sim$1.8 eV ($\sim$670 nm), and the positive ESA in the rest of the probed spectral range. For temperatures $<$170 K, the differential spectra instead display a negative GSB feature $\sim$2.5 eV ($\sim$500 nm) and two positive bands at 1.5-1.8 eV (700-850 nm) and $>$3 eV ($<$410 nm). The positive band at 1.5-1.8 eV nicely overlaps with the Fe(IV)Champ absorption. The band $>$3 eV overlaps with the Fe(II)Champ absorption, but is harder to assess as also Fe(IV)Champ and the excited Fe(III)Champ absorbs here. Since the same time components for build up and decay of the Fe(II) and Fe(IV) bands were fitted, the observed dynamics are safely assigned to the LICD reaction.

From the transient absorption analysis, the Fe(IV) and Fe(II) absorption bands form with the rate 1 ps^{-1}. This is therefore attributed to the rate of charge separation (k_{CS}) in the LICD reaction (see Figure 4.7), and agrees well with the results published by Kaul et al..[146] Moreover, k_{CS} is temperature independent over the studied range of temperatures (80-170 K). This means that the CS process is in principle barrierless (fitted activation energy 3 meV) and should be the highest possible k_{CS} for the reaction according to Marcus theory. Based on quantum chemical calculations, a barrierless CS process was indeed identified if the LICD reaction proceeds via an excited

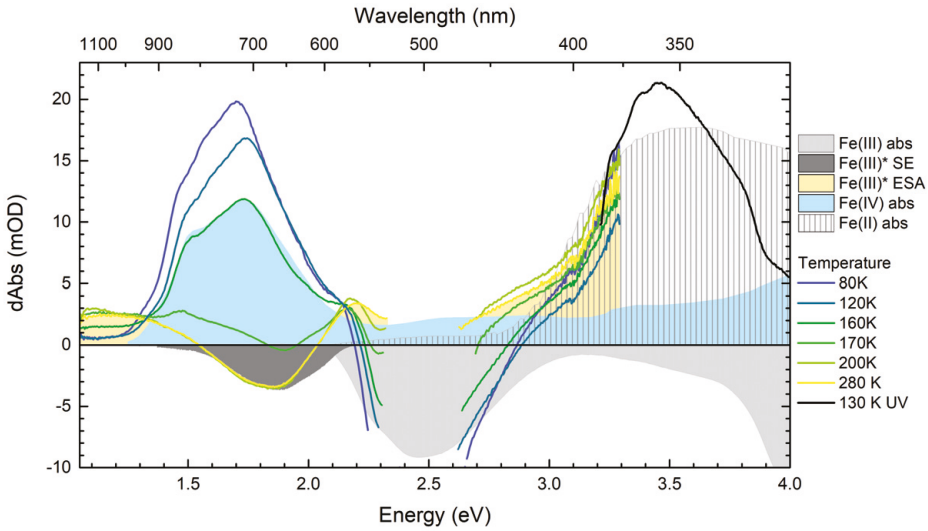

Figure 4.6: Differential spectra measured of FeChamp in alcohol solution at different temperatures. A differential spectrum measured in the UV wavelength range (3.2-4.0 eV) is also included for one low temperature. The differential spectra are compared to typical spectral profiles such as the Fe(II), Fe(III) and Fe(IV) species absorption (abs), and the characteristic SE and ESA of the excited Fe(III)* species.

state of Fe(IV)Champ (see Figure 4.7).

$$\mathrm{Fe(III)^* + Fe(III) \rightarrow Fe(IV)^* + Fe(II) \rightarrow Fe(IV) + Fe(II) + 0.5\,eV}$$

Since Fe(IV)Champ is an open-shell system, there are two excited states just ∼0.5 eV above ground state where the electrons in the t_{2g}-orbitals only rearrange. Furthermore, the CS reaction outcompetes the intramolecular deactivation of the ^{2}LMCT state in Fe(III)Champ (rate 0.0005 ps^{-1}). The quantum yield for CS in the LICD reaction is thus 99.95% under the condition that there is a ground state Fe(III)Champ neighbour to react with.

The majority of the generated Fe(II) and Fe(IV) species recombine with the rate 0.0125 ps^{-1} (80 ps lifetime) extrapolated to room temperature. The rate is in good agreement with the results published by Kaul et al., who also suggested that the recombination takes place in the inverted Marcus regime. This was based on the observation that CR proceeds with a lower rate than CS, despite a ∼2 times higher thermodynamic driving force compared to CS.[146] k_{CR} was in paper VII found to be temperature dependent, resulting in the fitted activation energy ∼60 meV. Furthermore, the quantum chemical calculations presented in Figure 4.7 shows that the charge-separated state of one Fe(II) and one Fe(IV) is indeed nested within the ground state potential of two Fe(III) species. This confirmed that CR takes place in the inverted Marcus regime, and explains why CR is significantly slower than CS in this

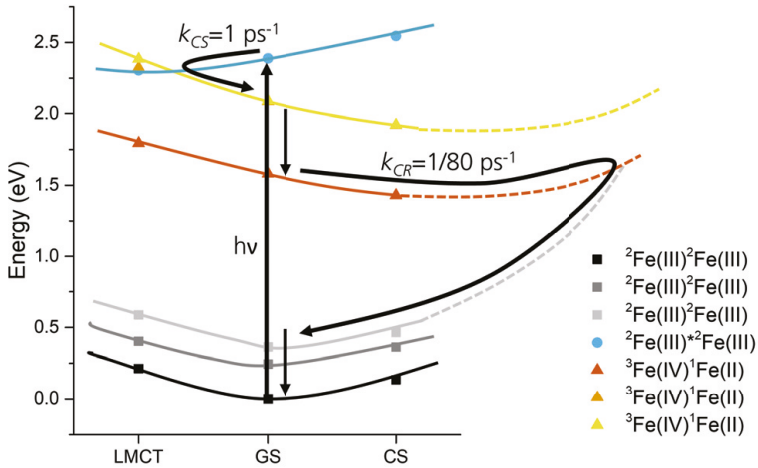

Figure 4.7: Projected potential energy surfaces for the system of two FeChamp molecules. The horizontal axis does not represent a true reaction coordinate, but show the states LMCT (Fe(III)Fe(III)*), GS (Fe(III)Fe(III)) and CS (Fe(II)Fe(IV)). Indicated by arrows is the proposed LICD reaction pathway: hν - light excitation, CS - charge separation, CR - charge recombination. Points are calculated by DFT or TD-DFT at the B3LYP* level of theory, lines represent a guide to the interpretation.

system. The generated photoproduct of Fe(II)Champ and Fe(IV)Champ actually recombines one order of magnitude slower compared to the bimolecular reactions published by Rosemann et al..[144] No photoproduct of Fe(II) and Fe(IV) species was however observed at low temperatures, tentatively attributed to the frozen positions of the generated species which hinders cage-escape. In the high concentration solution study, however, Kaul et al. observed a small part of the photoproduct (quantum yield 4%) survive to the µs-timescale.[146]

4.1.4 First Demonstrations of Photocatalysis

Intermolecular charge-transfer reactions were here exemplified by bimolecular reactions and light-induced charge-disproportionation. These reactions can be incorporated as the first step in a photocatalysis reaction scheme, that forms the reactive charge-separated intermediates. Photocatalysis where FeChamp or FeChampBr have been utilised involve dehalogenation reactions,[145, 147] cyclisation reactions[147] and borylation reactions.[148] Another Fe(III) carbene photosensitiser has been employed in radical cationic cycloadditions[149] and atom transfer radical additions.[150]

Hydrogen evolution, perhaps the number one solar fuel reaction, has also been investigated with Fe carbene complexes as the photosensitiser. Early attempts included complexes based on the FeCAB-structure, of d^6 electronic configuration and excited state lifetimes in the ps-range. Hydrogen evolution was shown to take place

by Zimmer et al., however at very low yields.[92] Zimmer et al. also synthesised a supramolecular dyad complex consisting of an Fe carbene photosensitiser connected to a Co-based catalyst, but unfortunately there was no suitable electronic communication between the two parts.[91] With FeChamp as the photosensitiser, hydrogen evolution was clearly demonstrated by Schwarz et al. using Pt colloids alternatively a Co-complex as the hydrogen evolution catalyst.[151] In order to get high turnover numbers (>1000), the strategy of using high donor concentration from the bimolecular studies was applied. Actually, the reaction mechanism was shown to indeed start with the reductive quenching of the excited FeChamp by a donor, just as in the bimolecular reactions.[151]

Even though Fe carbene photosensitisers are not yet competitive with Ru-based alternatives in photocatalysis, the stability has in general been higher of FeChamp compared to $Ru(bpy)_3^{2+}$. Still, too low cage-escape yields are considered to limit the performance of FeChamp in photocatalysis.[135] Aydogan et al. has, however, shown that FeChamp can participate in electron transfer reactions that do generate substantial cage-escape yields if the conditions are right.[145] Overall, the progress in photocatalysis is enabled by the success to create Fe carbene photosensitisers with long excited state lifetimes.

4.2 Interfacial Charge-Transfer

In this second section of Chapter 4, interfacial charge-transfer reactions will be discussed. These are reactions between a photosensitiser and a semiconductor (in this thesis TiO_2), that the photosensitiser is attached to. The interfacial charge-transfer reactions are relevant for applications such as dye-sensitised solar cells (shown in Section 1.3) and heterogeneous catalysis (e.g. the DSPEC shown in Section 1.2). In the DSSC and DSPEC systems, an electron is transferred from the photosensitiser into the conduction band of TiO_2 upon excitation.[3] Such an interfacial charge-transfer reaction is often referred to as injection, whereas the back-charge-transfer of an injected electron is called recombination.[23]

Fe carbene photosensitisers have so far been employed in DSSCs. In general, these complexes enabled solar cells of better performance than the early attempts using other Fe-based photosensitisers.[152, 153] The photosensitiser needs an anchor group that binds to TiO_2, and the carboxylic group is one such group. The Fe carbene complexes discussed in this section are mainly FeCABC, FeCABCN1, FeCABCN2 (see Figure 4.8), according to the scope of this thesis. These are all d^6 complexes with an excited

[3]This is valid for a n-type device. For a p-type device, instead a positive hole is transferred into the valence band of a suitable semiconductor.[23]

^{3}MLCT state lifetime of ∼20 ps. Also some initial steps of functionalising the d^5 FeChampC complex on surfaces have been made, which is discussed towards the end of this section.

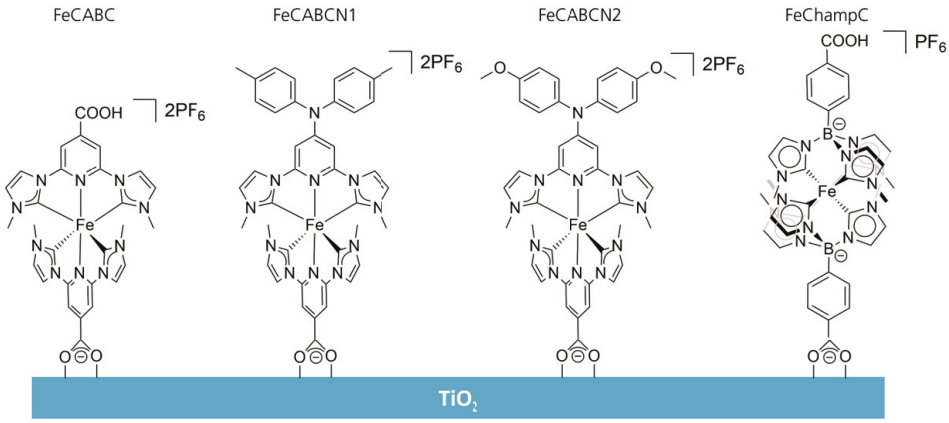

Figure 4.8: The Fe carbene photosensitisers that will be discussed in the interfacial charge-transfer section. The figure illustrates the bonding between the photosensitisers and TiO_2.

4.2.1 Interfacial Charge-Transfer Theory

To describe interfacial charge-transfer reactions, Marcus electron-transfer theory can be expanded to account for charge-transfer from one state to a band of acceptor states. The acceptor is the CB of TiO_2, which has a density of available states depending on the redox potential $\rho(E)$ (depicted in Figure 4.9). Figure 4.9a shows two possible arrangements: one where the excited state redox potential of the photosensitiser (PS*) is above the CB edge, and one where it is below the CB edge.[4] In the former case, injection is not limited by the density of available acceptor states and this is called the "wide-band limit". In the latter case, the photosensitiser has much fewer acceptor states to interact with, and typically there is also an activation energy for injection to take place. The injection will therefore depend on the excitation energy, i.e. vibrationally hot states of PS* will be better at injecting.[154]

In Figure 4.9b, the bonding between the PS and the CB instead results in a new charge-separated state PS^+CB^-. This case is mainly seen for small organic photosensitisers that have no absorption in the visible spectral range, but with strong interaction between the frontier orbitals of the PS and the CB.[28, 154, 155] It has, however, also been observed for transition metal complexes e.g. with cyanide-ligands, including

[4]The conduction band edge is here defined as the redox potential where the derivative of $\rho(E)$ is maximum. This means that there are also states below the CB edge, but the density decreases rapidly.

$Fe(CN)_6^{4-}$.[156] In this case, a new charge-transfer band will appear in the absorption spectrum of the PS attached to TiO_2, that was not present in the absorption spectrum of any of the individual compounds.[28, 154, 155] When exciting into this band, a metal-to-particle charge-transfer (MPCT) transition takes place, which directly excites the system into the injected, charge-separated state.[28]

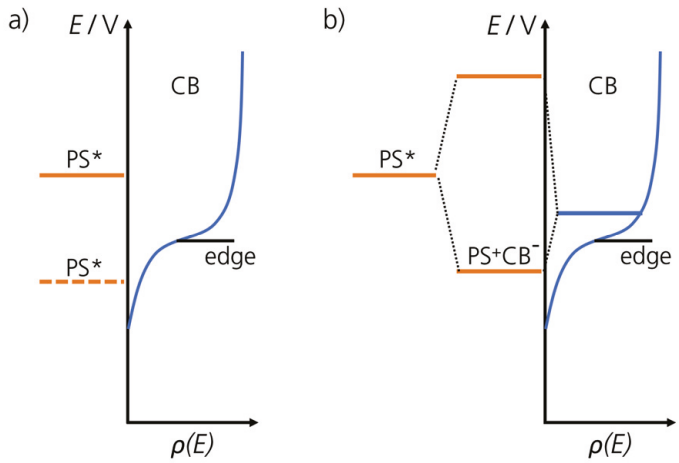

Figure 4.9: Two different mechanisms of injection; a) injection succeeding excitation and b) injection via excitation. What determines the mechanism is the coupling between the excited photosensitiser state PS^* and the conduction band of TiO_2 (CB). In the right case, they bind to form a new, charge-separated state PS^+CB^-. In the left case, injection will instead depend on the density of available states in the CB ($\rho(E)$).

The rate of interfacial charge-transfer, here mainly considering injection as depicted in Figure 4.9a, is composed of a sum of rates. This is because the transfer can happen between the PS and a manifold of acceptor states, each interaction having a slightly different rate. Taken together with the fact that TiO_2 substrates are often inhomogeneous means that it is common to measure multiexponential injection rates or a distributed injection rate. Equation 4.5 describes the injection rate k_{inj} based on Fermi's golden rule.[154]

$$k_{inj} = \frac{2\pi}{\hbar} \sum_a |V'_{da}|^2 \rho(E) \tag{4.5}$$

k_{inj} depends on a coupling term $|V'_{da}|^2$ between the donor (which is the PS) and the acceptor (which is the TiO_2 CB), and the density of available states in the acceptor $\rho(E)$.[154] By combining Fermi's golden rule and Marcus theory, a more elaborate

expression for the injection rate is obtained in Equation 4.6.[5][28]

$$k_{inj} = \frac{2\pi}{\hbar} \int_{-\infty}^{\infty} |V_{da}|^2 \rho(E) \frac{1}{\sqrt{4\pi\lambda kT}} e^{-\frac{(\lambda+\Delta G^0+E)^2}{4\lambda kT}} dE \tag{4.6}$$

What is added to Equation 4.6 is the donor distribution as a function of energy (E) which is a Gaussian function depending on the reorganisation energy (λ), the free thermodynamic driving force (ΔG^0) and the temperature (T) (k is the Boltzmann constant).[28, 157–159] The donor has a Gaussian energy distribution due to fluctuations in the solvation and the many binding configurations between the photosensitiser and TiO_2.[28] In Figure 4.10, a Marcus theory interpretation of interfacial charge-transfer is shown with the definition of λ and ΔG^0.[157]

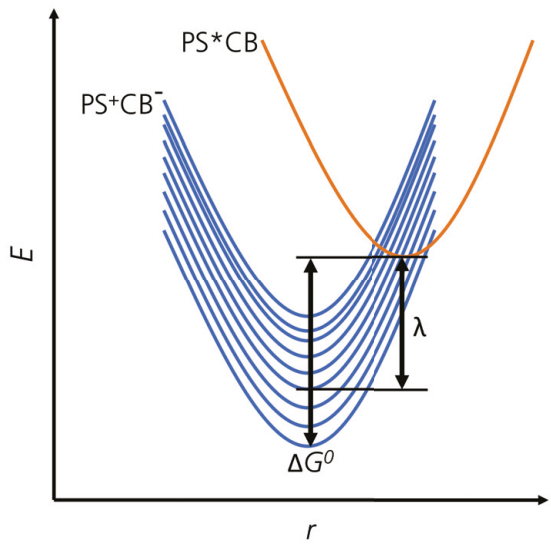

Figure 4.10: Interfacial charge-transfer from a Marcus theory interpretation. The initial state PS^*CB can here transition to a band of charge-separated final states PS^+CB^-. Both states have a quadratic energy dependence on the reaction coordinate (r) within the Marcus formalism. Also indicated in the figure is the free thermodynamic driving force ΔG^0 and the free reorganisation energy λ.

To summarise, the injection rate depends on three key parameters: i) the electronic coupling between acceptor and donor, ii) the density of states in the acceptor, and iii) the donor distribution function. These parameters are in turn dependent on system specific factors such as the distance and binding geometry between the PS and TiO_2,

[5]The density of available states in the acceptor, $\rho(E)$, can also be expressed as $\rho(E)(1-f(E,E_F))$. Then the Fermi function $f(E,E_F)$ with the Fermi energy E_F as parameter ensures that the acceptor states are available and not filled. For a conduction band in a semiconductor of bandgap $>> kT$ such as TiO_2, this is virtually always the case and the Fermi function can be omitted.[28]

the alignment between the PS* and the CB of TiO_2, the temperature, etc. If the redox potential of PS* is close to the CB edge, the density of acceptor states will play an especially large role, whereas in the wide-band limit there are many available acceptor states to interact with.[28, 154]

4.2.2 The Fe-Based Solar Cell: Current Limitations

DSSCs with photosensitisers based on the FeCABC framework (Figure 4.8) have to date reached a power-conversion efficiency of 2.0%, demonstrated by Marri et al..[160] This is low in comparison with the currently best performing DSSCs with efficiencies around 13%.[29] To understand what limits the performance in Fe carbene DSSCs, paper II investigated the fundamental charge-transfer steps crucial for DSSC operation. The photosensitisers tested were FeCABCN1 and FeCABCN2 (see Figure 4.8), but since the results are qualitatively similar FeCABCN1 will be used as an illustrative example. The spectroscopic signal of FeCABCN1 in the excited ^{3}MLCT state is different to the oxidised FeCABCN1 generated after injection. The processes of electron injection and recombination can thus be studied by measuring transient absorption spectroscopy of FeCABCN1 attached to TiO_2 substrates. Sensitised Al_2O_3 substrates were measured as a reference, since the conduction band of Al_2O_3 is too high for any interfacial charge-transfer to take place.

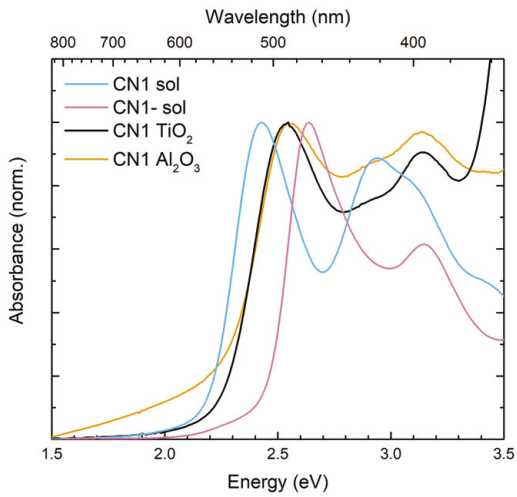

Figure 4.11: Steady-state absorption spectra comparing FeCABCN1 in solution in the protonated (CN1) and deprotonated (CN1-) form, to FeCABCN1 attached to Al_2O_3 or TiO_2.

The steady-state absorption spectrum of FeCABCN1 attached to semiconductors display a shifted lowest energy peak compared to in solution, see Figure 4.11. The absorption on semiconductors blue-shifts compared to the protonated FeCABCN1 in

solution, since FeCABCN1 is deprotonated when it binds to a semiconductor (see Figure 4.8). The absorption on semiconductors is, however, not as blue-shifted as the spectrum of FeCABCN1-. This is because the MLCT state is stabilised to some extent when FeCABCN1- binds to TiO_2. Finally, no MPCT transitions are expected for this system since no new absorption feature (apart from scattering) is present red-shifted to the absorption in solution.

To find the rate of injection and possibly recombination, global analysis was applied to fit the transient absorption data of FeCABCN1 on TiO_2.[47] Three major decay times were fitted with decay associated spectra shown in Figure 4.12a. The DAS with decay times 100 fs and >10 ns display positive broad ESA features between 1.2-1.9 eV (650-1000 nm), that very much resemble the absorption of the oxidised FeCABCN1 (measured by spectroelectrochemistry). Both components are therefore related to recombination processes, as they have a positive amplitude signifying the decay of a positive signal. A decay time >10 ns, however, means that the population did not decay during the time frame of the experiment, which is 10 ns. The third DAS of decay time 18 ps instead displays ESA between 1.7-2.3 eV (540-750 nm). This ESA is assigned to the ^{3}MLCT state, both based on measurements of FeCABCN1- in solution (see Figure 4.12a, CN1- 100 fs) and measurements of FeCABCN1 attached to Al_2O_3. The assignment is further confirmed by a similar lifetime (18 ps) as the ^{3}MLCT lifetime of FeCABCN1 in solution (19 ps).

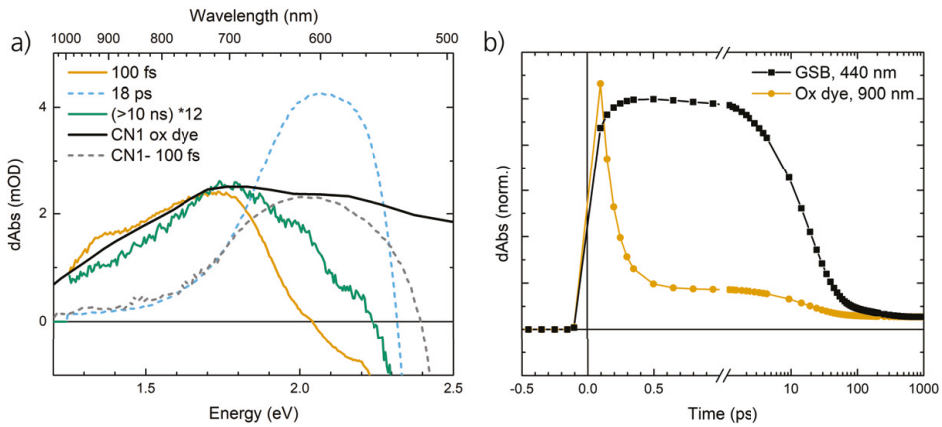

Figure 4.12: Transient absorption data of FeCABCN1 attached to TiO_2. a) The DAS resulting from a global analysis fit are compared to the absorption of the oxidised FeCABCN1 (CN1 ox dye) and the ^{3}MLCT ESA from FeCABCN1- (CN1- 100 fs). Spectra are plotted on the red side of the ground state bleach. b) Kinetics from the ground state bleach (GSB) and oxidised dye (Ox dye) spectral regions are compared.

The ideal outcome for the solar cell performance would be that all injected electrons stay in the CB of TiO_2, which means the >10 ns component dominates. The presence of the 100 fs recombination process signifies that this is not the case. It was

estimated from the GSB kinetic in Figure 4.12b that 90-95% of the injected electrons recombined with the 100 fs time component, and only 5-10% remained after 10 ns. The process is of course detrimental to the solar cell performance, and was identified as a key bottleneck explaining the low efficiency. In Figure 4.12b, only the oxidised dye kinetic decays with a 100 fs time component, i.e. it is not accompanied by a similar recovery of the GSB kinetic. This suggests that the recombination returns the photosensitiser to the excited state. This is also indicated by the negative amplitude in the 100 fs DAS around ∼2.1 eV, where the 18 ps DAS has its peak.

The injection rate was not resolved in the study, but an lower limit of 13 ps^{-1} was estimated. For FeCABC, the injection yield was determined to be as high as 92% by Harlang et al., however proceeding at a slower injection rate.[99] Comparing the estimated injection time component of <75 fs to the excited state lifetime of FeCABCN1 (19 ps), the injection yield should be close to 100%. However, with a recombination reaction being both ultrafast and very efficient (90-95%), that returns population to the excited state, the question is whether the classical injection as described in Section 4.2.1 indeed happened. Three hypotheses could potentially explain the observed dynamics. One is summarised in Figure 4.13, which shows that the position of the ^{3}MLCT state is just below the CB edge of TiO_2. In this picture, the ultrafast injection takes place from the ^{1}MLCT state, and recombination instead goes to the ^{3}MLCT state. This explains why the recombination returns population to the excited state, and fits with the observed ultrafast timescales.

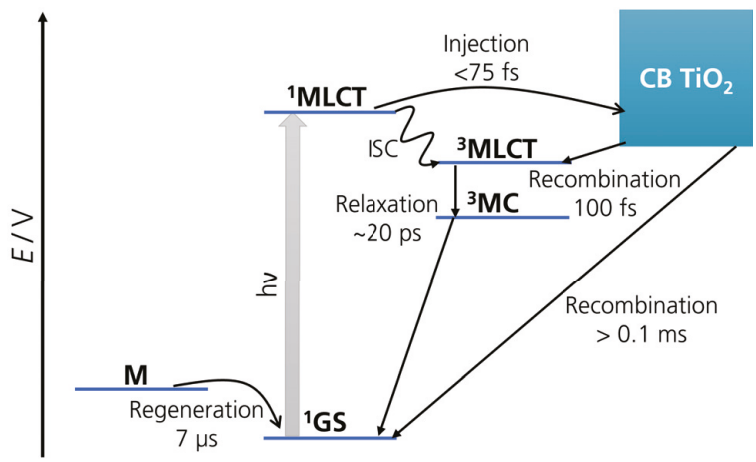

Figure 4.13: Schematic of all characterised processes relevant for the DSSC, in the system FeCABCN1 on TiO_2. CB - conduction band, M - redox mediation, hν - light excitation. Adapted with permission from paper II.

An alternative explanation is that injection creates a charge-separated state where the electron and hole are still bound. This would mean that in <75 fs, interfacial charge

separation takes place to the bound state between the photosensitiser and the TiO_2 CB. In this case, such a state must have a spectral signature similar to oxidised FeCABCN1. 90-95% of the bound charge-separated states would then quickly recombine, whereas 5-10% would escape and become truly charge-separated. Such processes have, however, mainly been observed for photosensitisers bound to ZnO, since ZnO has lower permittivity and thus screens charge less efficiently compared to TiO_2.[161–163] A third hypothesis is that the ultrafast process with decay time 100 fs instead is the transition from the ^{3}MLCT to the ^{3}MC state. In paper III, this was found to take place on the sub-ps timescale for FeCABCN1-, identified by an initial broad ESA turning into a narrow blue-shifted ESA (see Section 3.1.4). This explanation, however, seems unlikely since the 100 fs DAS matches well with the broad oxidised dye spectrum, and the 18 ps DAS matches well with the early ^{3}MLCT ESA for FeCABCN1- (see Figure 4.12a).

Mainly injected electrons that stay in TiO_2 to the ms-timescale can be extracted as a current in DSSC. In solar cells with FeCABCN1 and FeCABCN2 this is only a small part of the efficiently injected electrons, due to the ultrafast recombination process. Furthermore, no slower recombination process was identified that was as prominent as the ultrafast recombination (see Figure 4.13). This implies that there is a large potential to increase the solar cell performance if the ultrafast recombination is hindered. Since the power-conversion efficiency for the best published photosensitisers based on the FeCABC motif lie within the range 1-2%,[97, 108, 160, 164–169] the ultrafast recombination could be a general problem.

4.2.3 Towards Heterogeneous Catalysis

FeChampC has retained the favourable excited state properties of FeChamp, and can be functionalised on semiconductors. This molecule is therefore a top candidate for DSSCs and DSPECs. The carboxylic anchor group is, however, situated in the outer part of the ligand (see Figure 4.8), which was shown in Section 3.2.3 to have bad electronic communication with the ^{2}LMCT state. Furthermore, since the ^{2}LMCT state locates the excited electron in a metal-centred orbital it needs to tunnel through the ligand for injection to take place. These considerations suggests that injection should be slower in this system, compared to FeCABCN1. Furthermore, the high local concentration generated when bound to semiconductors could enable the LICD reaction present for FeChamp at high concentrations (see Section 4.1.3). To find out what the dominant process is, transient absorption spectroscopy of FeChamp bound to TiO_2 and Al_2O_3 was measured in paper IX.

As a first consideration, the absorption spectra of FeChampC attached to semiconductors are shown in Figure 4.14. All spectra shown in Figure 4.14 share the same

peak position, also the different protonation states of FeChampC. Only broadening of the absorption spectrum when bound to semiconductors is observed, which could be due to aggregation effects. The system thus displays a different behaviour compared to FeCABCN1 in the previous section (see Figure 4.11). The observed result is, however, consistent with the bad electronic communication established in Section 3.2.3. Binding to semiconductors also does not influence the ^{2}LMCT state.

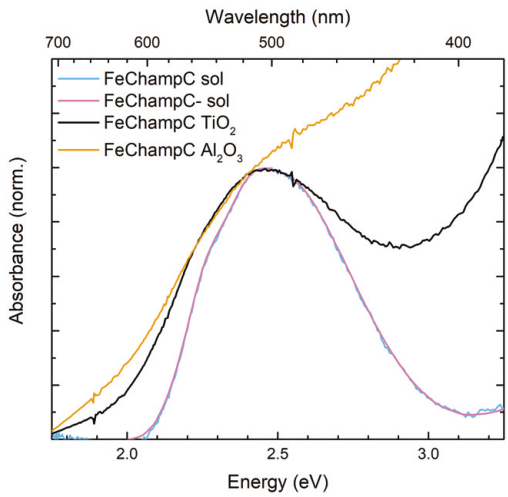

Figure 4.14: Steady-state absorption spectra comparing FeChampC in solution in the protonated (FeChampC) and deprotonated (FeChampC-) form, and FeChampC attached to Al_2O_3 or TiO_2.

The transient absorption data of FeChampC on TiO_2 and Al_2O_3 in fact display very similar dynamics, showcased here by the data on TiO_2. The earliest probed spectrum at 150 fs (see Figure 4.15) is well described by the ESA and SE associated with the ^{2}LMCT state. This means that injection in this system, if present, is much slower than for FeCABCN1. At 10 ps delay time, the differential spectrum displays the features of Fe(IV)Champ absorption (at 1.5-1.8 eV), Fe(II)Champ absorption (>3 eV) and GSB of Fe(III)Champ ~2.5 eV. This is similar to the differential spectrum generated in case of LICD (see Figure 4.6). To reconstruct the differential spectrum at 10 ps, however, also the ^{2}LMCT differential spectrum is added to the linear combination shown in Figure 4.15. This confirms that part of the excited FeChampC complexes did participate in LICD, whereas others did not have a suitable neighbour to react with and therefore remained in the ^{2}LMCT state.

On both semiconductors, the spectral regions corresponding to Fe(II), Fe(IV) and GSB rise biexponentially with the time components 600-700 fs and 3 ps. The same set of features also decay with the major time component 30 ps. The similarity on both semiconductors, together with the fact that the Fe(II) signal should not share dynamics with interfacial charge-transfer processes, suggest that the observed dynamics are

associated with LICD. Furthermore, the identified rates of CS and CR respectively, are similar to what was found in paper VII and by Kaul et al..[146] On semiconductor the CS and CR processes are multiexponential due to the inhomogenity, i.e. there exist many unique binding geometries between the semiconductor nanoparticles and FeChampC. The inhomogenity further explains why the lifetime of the ^{2}LMCT state is multiexponential (130-1000 ps) for the fraction of FeChampC molecules not participating in LICD.

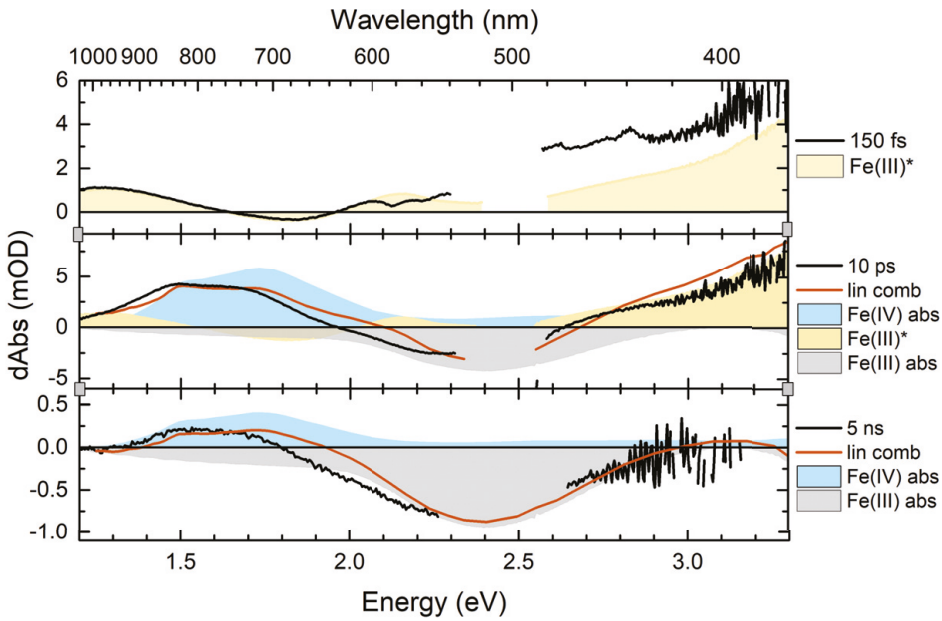

Figure 4.15: Differential spectra measured of FeChampC on TiO_2 at 150 fs, 10 ps and 5 ns delay time. The differential spectra are compared to the typical spectral profile of the excited Fe(III)* species and the absorption (abs) of Fe(III) and Fe(IV) species. A linear combination (lin comb) of these signals were used to reconstruct the measured differential spectra.

One substantial difference between the TiO_2 and Al_2O_3 systems is that on TiO_2, part of the signal remains at the end of the probed time window (>10 ns). This signal is represented by the differential spectrum at 5 ns delay time shown in Figure 4.15, and displays features of GSB and Fe(IV) absorption. The signal therefore fits the expected outcome of an injection process. The multiexponential charge separation and recombination processes of LICD makes it impossible to distinguish the minor process of potential slow injection (and recombination) in the TiO_2 system. The upper limit of the injection rate can, however, be estimated in relation to the CS rate of LICD, which results in 0.3 ps^{-1}. The presence of an injection process was thus not proven by the studied system.

Since LICD efficiently outcompetes injection, an alternative application could be to use the generated Fe(IV) and Fe(II) species in a heterogeneous catalysis scheme. For

such an application, the lifetime of the charge-separated species should ideally be longer than ∼30 ps. This was accomplished by adding triethylamine (TEA) to the semiconductor samples, see Figure 4.16. In this system, after the initial ^{2}LMCT differential spectrum was probed at 150 fs, the spectra evolved to only resemble the charge-separated species at 10 ps. This was corroborated by the reconstruction of the 10 ps differential spectrum, which does not need the differential spectrum of the ^{2}LMCT state in the linear combination (see Figure 4.16). Furthermore, at 5 ns delay time still a signal resulting from charge-separated species remain. The signal from Fe(II)ChampC (>3 eV) is however lower than expected at 10 ps delay time, and not present at 5 ns. Since both the TiO_2 and Al_2O_3 systems displayed the same dynamics, the observed dynamics are related to the LICD reaction and the reactivity of TEA.

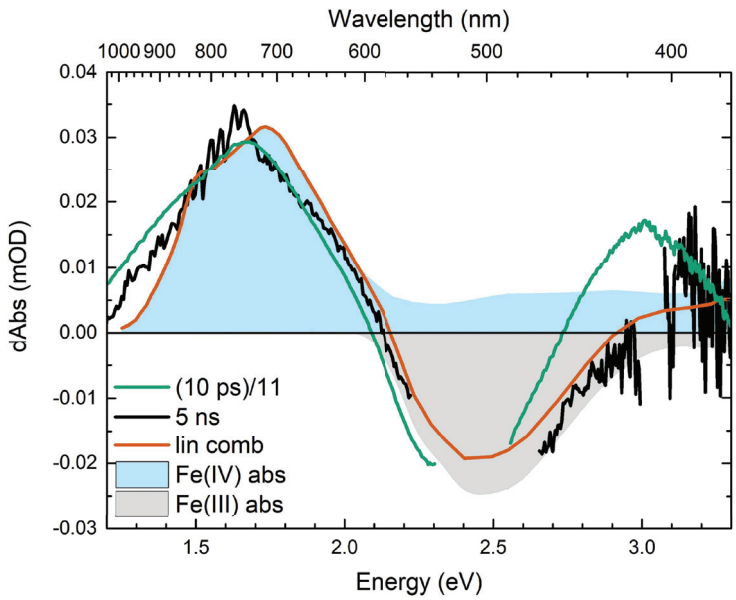

Figure 4.16: Differential spectra measured of FeChampC on Al_2O_3 with added TEA, at 10 ps and 5 ns delay time. The differential spectra are compared to the absorption (abs) of Fe(III) and Fe(IV) species. A linear combination (lin comb) of these signals were used to reconstruct the measured differential spectra.

Rosemann et al. showed that TEA can react with the excited ^{2}LMCT state in FeChamp, but no photoproduct (Fe(II)Champ, TEA+) was observed since the CR rate was faster than the CS rate.[144] The same reactivity was observed for FeChampC in solution with TEA in paper IX. It is therefore reasonable to assume that TEA reacts with part of the excited FeChampC molecules attached to the semiconductor, and quenches their excited state. This can explain why no remaining excited FeChampC signal is observed for the samples where TEA was added. A corresponding decay component of 5 ps with DAS matching this assignment was also identified from global analysis. Further-

state since all signal >3 eV decayed (see Figure 4.16). The disappearance of only Fe(II) species leaves a fraction of Fe(IV)ChampC with no neighbour Fe(II)ChampC to recombine with. Likely, this is what enables a photoproduct only consisting of Fe(IV) species. Why the Fe(II) species disappear is not understood yet, but worth to note is that Fe(II)Champ is unstable under ambient conditions observed in paper VI. The observation is, however, different to Kaul et al. who measured Fe(II) species surviving in solution to the μs timescale.[146] More investigations are therefore needed to understand the system and to optimise the yield of the long-lived photoproduct.

4.2.4 Ideas to Improve the Solar Cell Performance

Since Duchanois et al. first demonstrated Fe carbenes in DSSCs (FeCABC of power-conversion efficiency 0.1%),[100] a 20-fold improvement was enabled both by photosensitiser design and DSSC optimisation performed by different research groups.[97, 108, 160, 164–169] Many hypotheses have been proposed in order to explain the still low power-conversion efficiency compared to Ru-based dyes.[29] One consistent explanation in all studies, however, is that moving from a homoleptic design (FeCABC) to a heteroleptic design with directional excitation towards TiO_2 (such as for example FeCABCN1, see Section 3.1.3) was beneficial.[108, 167–169] For FeCABC anchored to TiO_2, Pastore et al. even found the excitation directed towards the ligand not facing TiO_2, as the carboxylic group is more electron-withdrawing than carboxylate bound to TiO_2.[108]

For heteroleptic complexes such as FeCABCN1, FeCABCN2 and other similar structures, separation on the semiconductor together with dye loading were important factors controlling the performance.[167] Marri et al. also found that different additives such as Mg^{2+} increased the performance by e.g. further enhancing directed excitation towards TiO_2.[168, 169] The main finding of paper II, that only 5-10% of the initially injected electrons remain in TiO_2 is, however, a key bottleneck that if resolved should allow for a big increase of the power-conversion efficiency. To block the ultrafast charge recombination, there are different strategies, and some suggestions are summarised in Figure 4.17. Since the push-pull structure did not work as fully intended (see Section 3.1.3) one approach would be to further strengthen the electron donating ability of the far-end substituent. Yet another strategy is to slow down recombination by increasing the distance between iron and the attaching carboxylic group with a bridge in the ligand structure. Both approaches were employed by Marri et al., who showed that they indeed can yield a better solar cell performance.[160, 168]

If the ultrafast recombination is indeed taking place due to the ^{3}MLCT state being below the CB edge of TiO_2, altering this alignment should lead to improvement (see Figure 4.17). This is accomplished by either increasing the redox potential of the

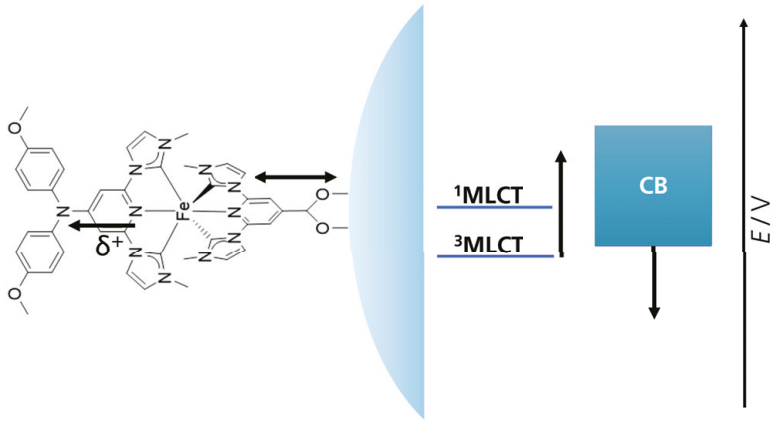

Figure 4.17: Suggestions to improve the performance for DSSCs with heteroleptic Fe carbene photosensitisers. From left to right: i) increasing the electron donating strength of the far-end substituent, ii) increasing the distance between iron and the semiconductor surface, iii) increasing the redox potential of the MLCT states, iv) decreasing the redox potential of the CB edge of the semiconductor.

^{3}MLCT state, or lowering the CB of TiO_2. The current best DSSC performance demonstrated by Marri et al. was reached with a photosensitiser of red-shifted absorption (i.e. lower MLCT states)[160] and with a mixed electrolyte of small cations (Mg^{2+} and Li^+) that each have an opposite influence on the CB of TiO_2.[170, 171] This is not in line with the strategy in Figure 4.17. However, the efficiency improvement found is not reflecting the order of magnitude improvement that could result if the ultrafast recombination was prevented.[160] One way to shift the CB of TiO_2 towards lower potentials is to change from anatase to rutile crystal structure.[172] Indeed, when FeCABCN1 on anatase TiO_2 from paper II was compared to a mixture of anatase and rutile sensitised with FeCABCN1, the dynamics changed. In Figure 4.18, the GSB kinetic of FeCABCN1 on anatase compared to the mixed substrate has shifted from having 5% of the signal amplitude left >1 ns to 25%. Even though Figure 4.18 provides a striking result, the safe conclusion is that the optimal system conditions have not been found yet, and should come with big room for improvement.

No results have to date been published for a DSSC with an Fe-based d^5 photosensitiser. Paper IX identifies one good reason for that, namely that injection is outcompeted by the LICD reaction. Therefore, injection could not be unambiguously identified and instead complementary techniques such as THz spectroscopy are needed to distinguish the signal of injected electrons.[99] FeChampC is not ideal for n-type DSSC application, since the lack of electronic communication with the sidegroup together with the electron placed on the metal in the ^{2}LMCT state slows injection down. To improve the injection yield, LICD must be mitigated by e.g. using co-

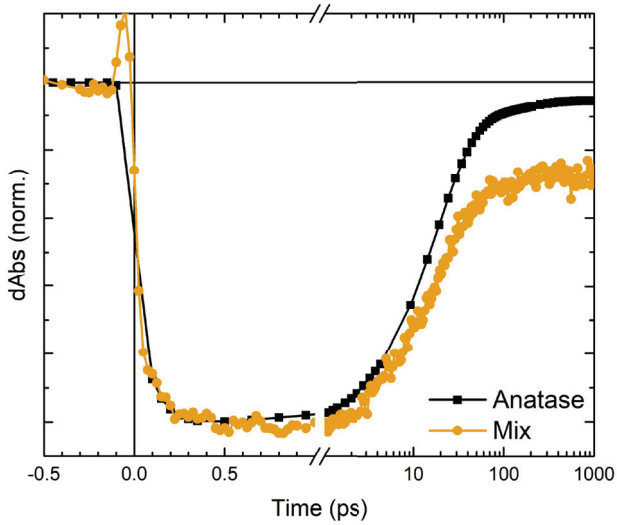

Figure 4.18: Kinetics from the GSB spectral region of two samples of FeCABCN1 on TiO_2. TiO_2 has either the crystal structure anatase or a mixture of the crystal structures anatase and rutile (Mix). This influences the amount of signal not decaying within the time frame of the experiment.

down. To improve the injection yield, LICD must be mitigated by e.g. using co-adsorbants or low dye loading. The question is, however, if this will allow for a good DSSC performance, since a solar cell should have strong absorbance enabled by high dye loading. An alternative approach is to try FeChampC in a p-type DSSC configuration, since the ^{2}LMCT state also has high reduction potential. In such a case, injection could be faster as the hole is placed on the ligand, however still not on the anchoring group.

Instead of blocking the LICD reaction, it can be used for heterogeneous catalysis applications. The sensitisation on semiconductors yielded a high enough local concentration of FeChampC for most molecules to participate in LICD. This enabled the LICD reaction at room temperature, and without using large amounts of the photosensitiser such as in solution. Furthermore, the initial attempts in paper IX illustrates that with the correct additives, long-lived charge-separated species for catalysis can be generated. More work in this direction is, however, needed to optimise and understand the system.

Chapter 5

Reflections and Outlook

You are never too small
to make a difference.[1]

How an ideal photosensitiser should behave, how it can be assessed and what strategies there are to tailor the photophysics of Fe-complexes, have been discussed in this thesis. All with the ultimate goal to replace Ru polypyridyl complexes with Earth-abundant Fe alternatives. The progress of the Fe carbene photosensitisers will here be assessed by the set of criteria for an ideal photosensitiser[31, 32] introduced in Chapter 2:

- strong visible absorption
- stability in all involved states
- high excited state redox potential
- long-lived excited state
- charge-separated excited state

Considering all of these points, the Fe carbene complexes are indeed approaching the ideal photosensitiser. All complexes investigated in this thesis (except CoChamp, paper V) have strong absorption in the visible, however with room for further improvement especially towards the NIR. The Fe carbene complexes are also very stable, and have redox potentials similar to those of $Ru(bpy)_3^{2+}$. Charge separation is realised in complexes with ^{3}MLCT or ^{2}LMCT as their major excited state, but perhaps not

[1] Greta Thunberg

in those with ^{3}MC (paper III). The excited state lifetime has improved tremendously from the first published Fe carbene of 9 ps, however in a ^{3}MC state, (paper IV) to the current best of 2 ns (paper VI). Although a great improvement, the current record is not yet competitive with $Ru(bpy)_3^{2+}$ and other Ru polipyridyl complexes. However, from a photofunctionality perspective a long lifetime is not everything. It is all a game of being faster than the competing processes, and for electron-transfer reactions even a 19 ps lifetime can be enough (paper II).

To further prolong the lifetime of Fe-based photosensitisers, thus remains an open research field. Still there are strategies to employ within the d^6 system, and in recent years long-lived Fe-complexes based on non-carbene ligands have started to appear.[84, 134] For the d^5 Fe carbene photosensitisers much is left to explore, as not many examples of photofunctional ^{2}LMCT states have yet been demonstrated.[127] This thesis work has, however, provided some progress in that direction by looking into the influence of sidegroup substitution and deactivation mechanisms (paper VII and VIII).

Parallel to the progress of Fe-based photosensitisers, many other Earth-abundant metals of various electronic configurations have been explored.[60–65] Only in the last five years d^6 complexes with other transition metals have reached excited state lifetimes on the order of ns, even with weak phosphorescence from the ^{3}MLCT state.[173] By changing electronic configuration to d^{10}, and thus removing the presence of MC states, even $>$10 μs ^{3}MLCT lifetimes have been reached with Cu(I)-complexes.[174, 175] The development of Earth-abundant photosensitisers is overall a promising and recognised research field, where Fe-complexes have a natural role to play.

Furthermore, this thesis work contributed to the emerging field of photofunctional MC states in transition metal complexes.[132, 133] Even though MC states are not charge-separated, they can still fulfil the other criteria from the ideal photosensitiser list. One of the most promising Earth-abundant photosensitisers to date actually feature a long-lived, photofunctional MC state. This is a Cr(III) d^3 complex referred to as "molecular ruby", which has μs lifetime and display emission.[176] In this thesis, CoChamp was provided as one example of a complex having a photofunctional ^{3}MC state (paper V). Several more complexes were assigned to have a $\sim$10 ps lifetime in the ^{3}MC state (paper III and IV). Such complexes constitute important cases for fundamental studies, that aim to investigate what excited state landscape can favour the ^{3}MC state.

The two light harvesting applications solar fuels and solar cells, which Fe carbene complexes have recently been employed in, were also discussed in this thesis. Both applications mainly show early demonstrations, rather than well-functioning devices.[145, 151, 160] In homogeneous photocatalysis schemes diffusion must be overcome, and in this case the 2 ns lifetime of FeChamp is still on the low side. Diffusion is, how-

ever, not the only factor controlling the photoproduct yield,[144, 145] and more investigations are needed to understand and control the intrinsic charge-transfer rates. For heterogeneous catalysis, the light-induced charge-disproportionation reaction of FeChampC bound to semiconductor surfaces could be a viable route forward (paper IX). In this scheme diffusion of the photosensitiser can not take place, which means that a smaller concentration of the photosensitiser and reactants are needed.

For Fe-based solar cells, the power-conversion efficiency has in recent years stagnated around 2%.[97, 108, 160, 164–169] In this thesis, an ultrafast recombination reaction is proposed as the main bottleneck for this performance (paper II). A substantial improvement of the solar cell performance should therefore be possible, and several strategies to resolve the recombination reaction have been discussed. Ultrafast spectroscopy is key to identify the relative contribution of injection and recombination in these systems. On a final note, a long lifetime does not necessarily yield the best solar cell performance.

References

[1] N. S. Lewis and D. G. Nocera, "Powering the planet: Chemical challenges in solar energy utilization," *Proceedings of the National Academy of Sciences*, vol. 103, pp. 15729–15735, 10 2006.

[2] N. Armaroli and V. Balzani, "Solar Electricity and Solar Fuels: Status and Perspectives in the Context of the Energy Transition," *Chemistry - A European Journal*, vol. 22, pp. 32–57, 1 2016.

[3] United Nations, "Paris Agreement," 55 Int'l Legal Materials 743, 2016.

[4] B. British Petroleum, "Statistical Review of World Energy," tech. rep., 2022.

[5] P. Alstone, D. Gershenson, and D. M. Kammen, "Decentralized energy systems for clean electricity access," *Nature Climate Change*, vol. 5, pp. 305–314, 4 2015.

[6] M. Perez and R. Perez, "Update 2022 – A fundamental look at supply side energy reserves for the planet," *Solar Energy Advances*, vol. 2, no. December 2021, p. 100014, 2022.

[7] V. Balzani, P. Ceroni, and A. Juris, *Photochemistry and Photophysics - Concepts, Research, Applications*. Weinheim: Wiley-VCH, 1st ed., 2014.

[8] J. Barber and P. D. Tran, "From natural to artificial photosynthesis," *Journal of The Royal Society Interface*, vol. 10, p. 20120984, 4 2013.

[9] R. E. Blankenship, D. M. Tiede, J. Barber, G. W. Brudvig, G. Fleming, M. Ghirardi, M. R. Gunner, W. Junge, D. M. Kramer, A. Melis, T. A. Moore, C. C. Moser, D. G. Nocera, A. J. Nozik, D. R. Ort, W. W. Parson, R. C. Prince, and R. T. Sayre, "Comparing Photosynthetic and Photovoltaic Efficiencies and Recognizing the Potential for Improvement," *Science*, vol. 332, pp. 805–809, 5 2011.

[10] R. Croce and H. van Amerongen, "Light-harvesting in photosystem I," *Photosynthesis Research*, vol. 116, pp. 153–166, 10 2013.

[11] D. Zigmantas, T. Polívka, P. Persson, and V. Sundström, "Ultrafast laser spectroscopy uncovers mechanisms of light energy conversion in photosynthesis and sustainable energy materials," *Chemical Physics Reviews*, vol. 3, p. 041303, 12 2022.

[12] Y. Wang, H. Suzuki, J. Xie, O. Tomita, D. J. Martin, M. Higashi, D. Kong, R. Abe, and J. Tang, "Mimicking Natural Photosynthesis: Solar to Renewable H2 Fuel Synthesis by Z-Scheme Water Splitting Systems," *Chemical Reviews*, vol. 118, no. 10, pp. 5201–5241, 2018.

[13] M. Đokić and H. S. Soo, "Artificial photosynthesis by light absorption, charge separation, and multielectron catalysis," *Chemical Communications*, vol. 54, no. 50, pp. 6554–6572, 2018.

[14] F. Puntoriero, A. Sartorel, M. Orlandi, G. La Ganga, S. Serroni, M. Bonchio, F. Scandola, and S. Campagna, "Photoinduced water oxidation using dendrimeric Ru(II) complexes as photosensitizers," *Coordination Chemistry Reviews*, vol. 255, pp. 2594–2601, 11 2011.

[15] F. Puntoriero, G. La Ganga, A. M. Cancelliere, and S. Campagna, "Recent progresses in molecular-based artificial photosynthesis," *Current Opinion in Green and Sustainable Chemistry*, vol. 36, p. 100636, 8 2022.

[16] D. W. Thompson, A. Ito, and T. J. Meyer, "[Ru(bpy)3]2+ and other remarkable metal-to-ligand charge transfer (MLCT) excited states," *Pure and Applied Chemistry*, vol. 85, pp. 1257–1305, 6 2013.

[17] J. H. Alstrum-Acevedo, M. K. Brennaman, and T. J. Meyer, "Chemical Approaches to Artificial Photosynthesis. 2," *Inorganic Chemistry*, vol. 44, pp. 6802–6827, 10 2005.

[18] D. Gust, T. A. Moore, and A. L. Moore, "Solar Fuels via Artificial Photosynthesis," *Accounts of Chemical Research*, vol. 42, pp. 1890–1898, 12 2009.

[19] Q. Wang and K. Domen, "Particulate Photocatalysts for Light-Driven Water Splitting: Mechanisms, Challenges, and Design Strategies," *Chemical Reviews*, vol. 120, pp. 919–985, 1 2020.

[20] L. Hammarström, "Accumulative Charge Separation for Solar Fuels Production: Coupling Light-Induced Single Electron Transfer to Multielectron Catalysis," *Accounts of Chemical Research*, vol. 48, pp. 840–850, 3 2015.

[21] J. A. Treadway, J. A. Moss, and T. J. Meyer, "Visible Region Photooxidation on TiO2 with a Chromophore–Catalyst Molecular Assembly," *Inorganic Chemistry*, vol. 38, pp. 4386–4387, 10 1999.

[22] S. Zhang, H. Ye, J. Hua, and H. Tian, "Recent advances in dye-sensitized photoelectrochemical cells for water splitting," *EnergyChem*, vol. 1, p. 100015, 11 2019.

[23] A. B. Muñoz-García, I. Benesperi, G. Boschloo, J. J. Concepcion, J. H. Delcamp, E. A. Gibson, G. J. Meyer, M. Pavone, H. Pettersson, A. Hagfeldt, and M. Freitag, "Dye-sensitized solar cells strike back," *Chemical Society Reviews*, vol. 50, no. 22, pp. 12450–12550, 2021.

[24] B. Zhang and L. Sun, "Artificial photosynthesis: opportunities and challenges of molecular catalysts," *Chemical Society Reviews*, vol. 48, no. 7, pp. 2216–2264, 2019.

[25] B. O'Regan and M. Grätzel, "A low-cost, high-efficiency solar cell based on dye-sensitized colloidal TiO2 films," *Nature*, vol. 353, pp. 737–740, 10 1991.

[26] B. E. Hardin, H. J. Snaith, and M. D. McGehee, "The renaissance of dye-sensitized solar cells," *Nature Photonics*, vol. 6, no. 3, pp. 162–169, 2012.

[27] A. Hagfeldt, G. Boschloo, L. Sun, L. Kloo, and H. Pettersson, "Dye-Sensitized Solar Cells," *Chemical Reviews*, vol. 110, pp. 6595–6663, 11 2010.

[28] S. Ardo and G. J. Meyer, "Photodriven heterogeneous charge transfer with transition-metal compounds anchored to TiO2 semiconductor surfaces," *Chem. Soc. Rev.*, vol. 38, no. 1, pp. 115–164, 2009.

[29] M. A. Green, E. D. Dunlop, M. Yoshita, N. Kopidakis, K. Bothe, G. Siefer, and X. Hao, "Solar cell efficiency tables (version 62)," *Progress in Photovoltaics: Research and Applications*, vol. 31, pp. 651–663, 7 2023.

[30] H. Michaels, M. Rinderle, R. Freitag, I. Benesperi, T. Edvinsson, R. Socher, A. Gagliardi, and M. Freitag, "Dye-sensitized solar cells under ambient light powering machine learning: towards autonomous smart sensors for the internet of things," *Chemical Science*, vol. 11, no. 11, pp. 2895–2906, 2020.

[31] A. Juris, V. Balzani, F. Barigelletti, S. Campagna, P. Belser, and A. von Zelewsky, "Ru(II) polypyridine complexes: photophysics, photochemistry, eletrochemistry, and chemiluminescence," *Coordination Chemistry Reviews*, vol. 84, pp. 85–277, 3 1988.

[32] M. Abrahamsson, *Tuning of the Excited State Properties of Ruthenium (II) - Polypyridyl Complexes*. PhD thesis, Uppsala University, 2006.

[33] J. P. Sauvage, J. P. Collin, J. C. Chambron, S. Guillerez, C. Coudret, V. Balzani, F. Barigelletti, L. De Cola, and L. Flamigni, "Ruthenium(II) and Osmium(II) Bis(terpyridine) Complexes in Covalently-Linked Multicomponent Systems: Synthesis, Electrochemical Behavior, Absorption Spectra, and Photochemical and Photophysical Properties," *Chemical Reviews*, vol. 94, pp. 993–1019, 6 1994.

[34] D. Pomeranc, V. Heitz, J.-C. Chambron, and J.-P. Sauvage, "Octahedral Fe(II) and Ru(II) Complexes Based on a New Bis 1,10-Phenanthroline Ligand That Imposes a Well Defined Axis," *Journal of the American Chemical Society*, vol. 123, pp. 12215–12221, 12 2001.

[35] D. M. Klassen and G. A. Crosby, "Spectroscopic Studies of Ruthenium(II) Complexes. Assignment of the Luminescence," *The Journal of Chemical Physics*, vol. 48, pp. 1853–1858, 2 1968.

[36] R. J. Watts, "Ruthenium polypyridyls: A case study," *Journal of Chemical Education*, vol. 60, p. 834, 10 1983.

[37] K. Kalyanasundaram, "Photophysics, photochemistry and solar energy conversion with tris(bipyridyl)ruthenium(II) and its analogues," *Coordination Chemistry Reviews*, vol. 46, pp. 159–244, 10 1982.

[38] B. N. Figgis and M. A. Hitchman, *Ligand Field Theory and Its Applications*. Weinheim: Wiley-VCH, 1st ed., 1999.

[39] D. M. Arias-Rotondo and J. K. McCusker, "The photophysics of photoredox catalysis: a roadmap for catalyst design," *Chemical Society Reviews*, vol. 45, no. 21, pp. 5803–5820, 2016.

[40] T. J. Meyer, "Photochemistry of metal coordination complexes: metal to ligand charge transfer excited states," *Pure and Applied Chemistry*, vol. 58, pp. 1193–1206, 1 1986.

[41] J. R. Lakowicz, *Principles of Fluorescence Spectroscopy*. New York: Springer, 3rd ed., 2006.

[42] C. Housecroft and A. G. Sharpe, *Inorganic Chemistry*. New York: Pearson Education, 5th ed., 2018.

[43] F. Alary, J.-L. Heully, L. Bijeire, and P. Vicendo, "Is the 3MLCT the Only Photoreactive State of Polypyridyl Complexes?," *Inorganic Chemistry*, vol. 46, pp. 3154–3165, 4 2007.

[44] W. Kaim and J. Fiedler, "Spectroelectrochemistry: the best of two worlds," *Chemical Society Reviews*, vol. 38, no. 12, p. 3373, 2009.

[45] M. Ha-Thi, G. Burdzinski, T. Pino, and P. Changenet, "Transient Absorption Spectroscopy in Inorganic Systems," in *Handbook of Inorganic Photochemistry* (D. Bahnemann and A. Patrocinio, eds.), ch. 5, pp. 107–130, Springer, Cham, 2022.

[46] J. K. McCusker, "Femtosecond Absorption Spectroscopy of Transition Metal Charge-Transfer Complexes," *Accounts of Chemical Research*, vol. 36, pp. 876–887, 12 2003.

[47] C. Müller, T. Pascher, A. Eriksson, P. Chabera, and J. Uhlig, "KiMoPack: A python Package for Kinetic Modeling of the Chemical Mechanism," *The Journal of Physical Chemistry A*, vol. 126, pp. 4087–4099, 6 2022.

[48] W. Koch and M. Holthausen, *A Chemist's Guide to Density Functional Theory*. Weinheim: Wiley-VCH, 2nd ed., 2000.

[49] P. Hohenberg and W. Kohn, "Inhomogeneous Electron Gas," *Physical Review*, vol. 136, pp. B864–B871, 11 1964.

[50] A. Vlček and S. Záliš, "Modeling of charge-transfer transitions and excited states in d6 transition metal complexes by DFT techniques," *Coordination Chemistry Reviews*, vol. 251, pp. 258–287, 2 2007.

[51] T. Österman, M. Abrahamsson, H.-C. Becker, L. Hammarström, and P. Persson, "Influence of Triplet State Multidimensionality on Excited State Lifetimes of Bis-tridentate RuII Complexes: A Computational Study," *The Journal of Physical Chemistry A*, vol. 116, pp. 1041–1050, 1 2012.

[52] T. Österman and P. Persson, "Excited state potential energy surfaces of bistridentate RuII complexes – A TD-DFT study," *Chemical Physics*, vol. 407, pp. 76–82, 10 2012.

[53] C. Daniel, "Photochemistry and photophysics of transition metal complexes: Quantum chemistry," *Coordination Chemistry Reviews*, vol. 282-283, pp. 19–32, 1 2015.

[54] R. L. Martin, "Natural transition orbitals," *Journal of Chemical Physics*, vol. 118, no. 11, pp. 4775–4777, 2003.

[55] S. Shalini, R. Balasundaraprabhu, T. S. Kumar, N. Prabavathy, S. Senthilarasu, and S. Prasanna, "Status and outlook of sensitizers/dyes used in dye sensitized solar cells (DSSC): a review," *International Journal of Energy Research*, vol. 40, pp. 1303–1320, 8 2016.

[56] K. G. Cho, J. I. Lee, S. Lee, K. Hong, M. S. Kang, and K. H. Lee, "Light-Emitting Devices Based on Electrochemiluminescence Gels," *Advanced Functional Materials*, vol. 30, p. 1907936, 8 2020.

[57] S. E. Angell, C. W. Rogers, Y. Zhang, M. O. Wolf, and W. E. Jones, "Hemilabile coordination complexes for sensing applications," *Coordination Chemistry Reviews*, vol. 250, pp. 1829–1841, 7 2006.

[58] M. Mital and Z. Ziora, "Biological applications of Ru(II) polypyridyl complexes," *Coordination Chemistry Reviews*, vol. 375, pp. 434–458, 11 2018.

[59] G. B. Haxel, J. B. Hedrick, and G. J. Orris, "Rare Earth Elements — Critical Resources for High Technology," tech. rep., Department of the Interior/USGS, 2002.

[60] O. S. Wenger, "Photoactive Complexes with Earth-Abundant Metals," *Journal of the American Chemical Society*, vol. 140, pp. 13522–13533, 10 2018.

[61] C. Förster and K. Heinze, "Photophysics and photochemistry with Earth-abundant metals – fundamentals and concepts," *Chemical Society Reviews*, vol. 49, no. 4, pp. 1057–1070, 2020.

[62] C. B. Larsen and O. S. Wenger, "Photoredox Catalysis with Metal Complexes Made from Earth-Abundant Elements," *Chemistry - A European Journal*, vol. 24, pp. 2039–2058, 2 2018.

[63] B. M. Hockin, C. Li, N. Robertson, and E. Zysman-Colman, "Photoredox catalysts based on earth-abundant metal complexes," *Catalysis Science & Technology*, vol. 9, no. 4, pp. 889–915, 2019.

[64] B. Bozic-weber, E. C. Constable, and C. E. Housecroft, "Light harvesting with Earth abundant d-block metals: Development of sensitizers in dye-sensitized solar cells (DSCs)," *Coordination Chemistry Reviews*, vol. 257, pp. 3089–3106, 11 2013.

[65] C. E. Housecroft and E. C. Constable, "Solar energy conversion using first row d-block metal coordination compound sensitizers and redox mediators," *Chemical Science*, vol. 13, no. 5, pp. 1225–1262, 2022.

[66] L. Lindh, P. Chábera, N. W. Rosemann, J. Uhlig, K. Wärnmark, A. Yartsev, V. Sundström, and P. Persson, "Photophysics and Photochemistry of Iron Carbene Complexes for Solar Energy Conversion and Photocatalysis," *Catalysts*, vol. 10, p. 315, 3 2020.

[67] S. Kaufhold and K. Wärnmark, "Design and Synthesis of Photoactive Iron N-Heterocyclic Carbene Complexes," *Catalysts*, vol. 10, p. 132, 1 2020.

[68] P. Pyykkö, "Relativistic Effects in Structural Chemistry," *Chem. Rev.*, vol. 88, no. 3, pp. 563–594, 1988.

[69] M. Kaupp, "The role of radial nodes of atomic orbitals for chemical bonding and the periodic table," *Journal of Computational Chemistry*, vol. 28, pp. 320–325, 1 2007.

[70] J. K. McCusker, "Electronic structure in the transition metal block and its implications for light harvesting," *Science*, vol. 363, pp. 484–488, 2 2019.

[71] Y. Liu, P. Persson, V. Sundström, and K. Wärnmark, "Fe N-Heterocyclic Carbene Complexes as Promising Photosensitizers," *Accounts of Chemical Research*, vol. 49, pp. 1477–1485, 8 2016.

[72] D. W. Fink and W. E. Ohnesorge, "Temperature Effects on Charge-Transfer Luminescence Intensity of Some Transition Metal Ion Chelates," *Journal of the American Chemical Society*, vol. 91, no. 18, pp. 4995–4998, 1969.

[73] C. Creutz, M. Chou, T. L. Netzel, M. Okumura, and N. Sutin, "Lifetimes, Spectra, and Quenching of the Excited States of Polypyridine Complexes of Iron (II), Ruthenium (II), and Osmium (II)," *Journal of the American Chemical Society*, vol. 1309, no. 18, pp. 1309–1319, 1980.

[74] J. K. Mccusker, K. N. Walda, R. C. Dunn, J. D. Simon, D. Magde, and D. N. Hendrickson, "Subpicosecond 1MLCT -» 5T2 Intersystem Crossing of Low-Spin Polypyridyl Ferrous Complexes," *J. Am. Chem. Soc.*, vol. 115, no. 4, pp. 298–307, 1993.

[75] W. Gawelda, A. Cannizzo, V.-T. Pham, F. van Mourik, C. Bressler, and M. Chergui, "Ultrafast Nonadiabatic Dynamics of [FeII(bpy)3]2+ in Solution," *Journal of the American Chemical Society*, vol. 129, pp. 8199–8206, 7 2007.

[76] A. Cannizzo, C. Milne, C. Consani, W. Gawelda, C. Bressler, F. van Mourik, and M. Chergui, "Light-induced spin crossover in Fe(II)-based complexes: The full photocycle unraveled by ultrafast optical and X-ray spectroscopies," *Coordination Chemistry Reviews*, vol. 254, pp. 2677–2686, 11 2010.

[77] W. Zhang, R. Alonso-Mori, U. Bergmann, C. Bressler, M. Chollet, A. Galler, W. Gawelda, R. G. Hadt, R. W. Hartsock, T. Kroll, K. S. Kjær, K. Kubiček, H. T. Lemke, H. W. Liang, D. A. Meyer, M. M. Nielsen, C. Purser, J. S.

Robinson, E. I. Solomon, Z. Sun, D. Sokaras, T. B. van Driel, G. Vankó, T.-C. Weng, D. Zhu, and K. J. Gaffney, "Tracking excited-state charge and spin dynamics in iron coordination complexes," *Nature*, vol. 509, pp. 345–348, 5 2014.

[78] G. Auböck and M. Chergui, "Sub-50-fs photoinduced spin crossover in [Fe(bpy)3]2+," *Nature Chemistry*, vol. 7, pp. 629–633, 8 2015.

[79] O. S. Wenger, "Is Iron the New Ruthenium?," *Chemistry – A European Journal*, vol. 25, pp. 6043–6052, 4 2019.

[80] P. Dierks, Y. Vukadinovic, and M. Bauer, "Photoactive iron complexes: More sustainable, but still a challenge," *Inorganic Chemistry Frontiers*, vol. 9, no. 2, pp. 206–220, 2022.

[81] J. R. Winkler, C. Creutz, and N. Sutin, "Solvent tuning of the excited-state properties of (2,2′-bipyridine)tetracyanoferrate(II): direct observation of a metal-to-ligand charge-transfer excited state of iron(II)," *Journal of the American Chemical Society*, vol. 109, pp. 3470–3471, 5 1987.

[82] J. Winkler and N. Sutin, "Lifetimes and spectra of the excited-states of cis-dicyanobis(2,2′-bipyridine)iron(II) and cis-dicyanobis(2,2′-bipyridine)ruthenium(II) in solution," *Inorganic Chemistry*, vol. 26, no. 2, pp. 220–221, 1987.

[83] W. Zhang, K. S. Kjær, R. Alonso-Mori, U. Bergmann, M. Chollet, L. A. Fredin, R. G. Hadt, R. W. Hartsock, T. Harlang, T. Kroll, K. Kubiček, H. T. Lemke, H. W. Liang, Y. Liu, M. M. Nielsen, P. Persson, J. S. Robinson, E. I. Solomon, Z. Sun, D. Sokaras, T. B. van Driel, T.-C. Weng, D. Zhu, K. Wärnmark, V. Sundström, and K. J. Gaffney, "Manipulating charge transfer excited state relaxation and spin crossover in iron coordination complexes with ligand substitution," *Chemical Science*, vol. 8, no. 1, pp. 515–523, 2017.

[84] J. D. Braun, I. B. Lozada, and D. E. Herbert, "In Pursuit of Panchromatic Absorption in Metal Coordination Complexes: Experimental Delineation of the HOMO Inversion Model Using Pseudo-Octahedral Complexes of Diarylamido Ligands," *Inorganic Chemistry*, vol. 59, pp. 17746–17757, 12 2020.

[85] S. M. Fatur, S. G. Shepard, R. F. Higgins, M. P. Shores, and N. H. Damrauer, "A Synthetically Tunable System To Control MLCT Excited-State Lifetimes and Spin States in Iron(II) Polypyridines," *Journal of the American Chemical Society*, vol. 139, pp. 4493–4505, 3 2017.

[86] L. L. Jamula, A. M. Brown, D. Guo, and J. K. McCusker, "Synthesis and Characterization of a High-Symmetry Ferrous Polypyridyl Complex: Approaching the 5T2/3T1 Crossing Point for FeII," *Inorganic Chemistry*, vol. 53, pp. 15–17, 1 2014.

[87] B. C. Paulus, S. L. Adelman, L. L. Jamula, and J. K. McCusker, "Leveraging excited-state coherence for synthetic control of ultrafast dynamics," *Nature*, vol. 582, pp. 214–218, 6 2020.

[88] Y. Liu, T. Harlang, S. E. Canton, P. Chábera, K. Suárez-Alcántara, A. Fleckhaus, D. A. Vithanage, E. Göransson, A. Corani, R. Lomoth, V. Sundström, and K. Wärnmark, "Towards longer-lived metal-to-ligand charge transfer states of iron(II) complexes: an N-heterocyclic carbene approach," *Chemical Communications*, vol. 49, no. 57, p. 6412, 2013.

[89] L. A. Fredin, M. Pápai, E. Rozsályi, G. Vankó, K. Wärnmark, V. Sundström, and P. Persson, "Exceptional Excited-State Lifetime of an Iron(II)–N-Heterocyclic Carbene Complex Explained," *The Journal of Physical Chemistry Letters*, vol. 5, pp. 2066–2071, 6 2014.

[90] C. Cebrián, M. Pastore, A. Monari, X. Assfeld, P. C. Gros, and S. Haacke, "Ultrafast Spectroscopy of Fe(II) Complexes Designed for Solar-Energy Conversion: Current Status and Open Questions," *ChemPhysChem*, vol. 23, 4 2022.

[91] P. Zimmer, L. Burkhardt, R. Schepper, K. Zheng, D. Gosztola, A. Neuba, U. Flörke, C. Wölper, R. Schoch, W. Gawelda, S. E. Canton, and M. Bauer, "Towards Noble-Metal-Free Dyads: Ground and Excited State Tuning by a Cobalt Dimethylglyoxime Motif Connected to an Iron N-Heterocyclic Carbene Photosensitizer," *European Journal of Inorganic Chemistry*, vol. 2018, pp. 5203–5214, 12 2018.

[92] P. Zimmer, P. Müller, L. Burkhardt, R. Schepper, A. Neuba, J. Steube, F. Dietrich, U. Flörke, S. Mangold, M. Gerhards, and M. Bauer, "N-Heterocyclic Carbene Complexes of Iron as Photosensitizers for Light-Induced Water Reduction," *European Journal of Inorganic Chemistry*, vol. 2017, pp. 1504–1509, 3 2017.

[93] T. Duchanois, T. Etienne, M. Beley, X. Assfeld, E. A. Perpète, A. Monari, and P. C. Gros, "Heteroleptic Pyridyl-Carbene Iron Complexes with Tuneable Electronic Properties," *European Journal of Inorganic Chemistry*, vol. 2014, pp. 3747–3753, 8 2014.

[94] L. Liu, T. Duchanois, T. Etienne, A. Monari, M. Beley, X. Assfeld, S. Haacke, and P. C. Gros, "A new record excited state 3MLCT lifetime for metalor-

ganic iron(II) complexes," *Physical Chemistry Chemical Physics*, vol. 18, no. 18, pp. 12550–12556, 2016.

[95] M. Darari, E. Domenichini, A. Francés-Monerris, C. Cebrián, K. Magra, M. Beley, M. Pastore, A. Monari, X. Assfeld, S. Haacke, and P. C. Gros, "Iron(II) complexes with diazinyl-NHC ligands: impact of π-deficiency of the azine core on photophysical properties," *Dalton Transactions*, vol. 48, no. 29, pp. 10915–10926, 2019.

[96] P. Zimmer, L. Burkhardt, A. Friedrich, J. Steube, A. Neuba, R. Schepper, P. Müller, U. Flörke, M. Huber, S. Lochbrunner, and M. Bauer, "The Connection between NHC Ligand Count and Photophysical Properties in Fe(II) Photosensitizers: An Experimental Study," *Inorganic Chemistry*, vol. 57, pp. 360–373, 1 2018.

[97] T. Duchanois, L. Liu, M. Pastore, A. Monari, C. Cebrián, Y. Trolez, M. Darari, K. Magra, A. Francés-Monerris, E. Domenichini, M. Beley, X. Assfeld, S. Haacke, and P. Gros, "NHC-Based Iron Sensitizers for DSSCs," *Inorganics*, vol. 6, no. 2, p. 63, 2018.

[98] L. A. Fredin, K. Wärnmark, V. Sundström, and P. Persson, "Molecular and Interfacial Calculations of Iron(II) Light Harvesters," *ChemSusChem*, vol. 9, pp. 667–675, 4 2016.

[99] T. C. B. Harlang, Y. Liu, O. Gordivska, L. A. Fredin, C. S. Ponseca, P. Huang, P. Chábera, K. S. Kjaer, H. Mateos, J. Uhlig, R. Lomoth, R. Wallenberg, S. Styring, P. Persson, V. Sundström, and K. Wärnmark, "Iron sensitizer converts light to electrons with 92% yield," *Nature Chemistry*, vol. 7, pp. 883–889, 11 2015.

[100] T. Duchanois, T. Etienne, C. Cebrián, L. Liu, A. Monari, M. Beley, X. Assfeld, S. Haacke, and P. C. Gros, "An Iron-Based Photosensitizer with Extended Excited-State Lifetime: Photophysical and Photovoltaic Properties," *European Journal of Inorganic Chemistry*, vol. 2015, pp. 2469–2477, 5 2015.

[101] D. P. Hagberg, J.-H. Yum, H. Lee, F. De Angelis, T. Marinado, K. M. Karlsson, R. Humphry-Baker, L. Sun, A. Hagfeldt, M. Grätzel, and M. K. Nazeeruddin, "Molecular Engineering of Organic Sensitizers for Dye-Sensitized Solar Cell Applications," *Journal of the American Chemical Society*, vol. 130, pp. 6259–6266, 5 2008.

[102] S. Aghazada and M. Nazeeruddin, "Ruthenium Complexes as Sensitizers in Dye-Sensitized Solar Cells," *Inorganics*, vol. 6, p. 52, 5 2018.

[103] W. A. Rosero, R. Guimaraes, T. Matias, and K. Araki, "Effect of Push-Pull Ruthenium Complex Adsorption Conformation on the Performance of Dye Sensitized Solar Cells," *Journal of the Brazilian Chemical Society*, vol. 31, no. 11, pp. 2250–2264, 2020.

[104] S. Lyu, Y. Farré, L. Ducasse, Y. Pellegrin, T. Toupance, C. Olivier, and F. Odobel, "Push–pull ruthenium diacetylide complexes: new dyes for p-type dye-sensitized solar cells," *RSC Advances*, vol. 6, no. 24, pp. 19928–19936, 2016.

[105] J. Lu, S. Liu, and M. Wang, "Push-Pull Zinc Porphyrins as Light-Harvesters for Efficient Dye-Sensitized Solar Cells," *Frontiers in Chemistry*, vol. 6, 11 2018.

[106] S. Mathew, A. Yella, P. Gao, R. Humphry-Baker, B. F. E. Curchod, N. Ashari-Astani, I. Tavernelli, U. Rothlisberger, M. K. Nazeeruddin, and M. Grätzel, "Dye-sensitized solar cells with 13% efficiency achieved through the molecular engineering of porphyrin sensitizers," *Nature Chemistry*, vol. 6, pp. 242–247, 3 2014.

[107] A. K. C. Mengel, C. Förster, A. Breivogel, K. Mack, J. R. Ochsmann, F. Laquai, V. Ksenofontov, and K. Heinze, "A Heteroleptic Push-Pull Substituted Iron(II) Bis(tridentate) Complex with Low-Energy Charge-Transfer States," *Chemistry - A European Journal*, vol. 21, pp. 704–714, 1 2015.

[108] M. Pastore, T. Duchanois, L. Liu, A. Monari, X. Assfeld, S. Haacke, and P. C. Gros, "Interfacial charge separation and photovoltaic efficiency in Fe(II)–carbene sensitized solar cells," *Physical Chemistry Chemical Physics*, vol. 18, no. 40, pp. 28069–28081, 2016.

[109] A. Cadranel, G. E. Pieslinger, P. Tongying, M. K. Kuno, L. M. Baraldo, and J. H. Hodak, "Spectroscopic signatures of ligand field states in {Ru II (imine)} complexes," *Dalton Transactions*, vol. 45, no. 13, pp. 5464–5475, 2016.

[110] K. S. Kjær, K. Kunnus, T. C. B. Harlang, T. B. Van Driel, K. Ledbetter, R. W. Hartsock, M. E. Reinhard, S. Koroidov, L. Li, M. G. Laursen, E. Biasin, F. B. Hansen, P. Vester, M. Christensen, K. Haldrup, M. M. Nielsen, P. Chabera, Y. Liu, H. Tatsuno, C. Timm, J. Uhlig, V. Sundstöm, Z. Németh, D. S. Szemes, E. Bajnóczi, G. Vankó, R. Alonso-Mori, J. M. Glownia, S. Nelson, M. Sikorski, D. Sokaras, H. T. Lemke, S. E. Canton, K. Wärnmark, P. Persson, A. A. Cordones, and K. J. Gaffney, "Solvent control of charge transfer excited state relaxation pathways in [Fe(2,2′-bipyridine)(CN)4]2–," *Physical Chemistry Chemical Physics*, vol. 20, no. 6, pp. 4238–4249, 2018.

[111] L. Schmid, P. Chábera, I. Rüter, A. Prescimone, F. Meyer, A. Yartsev, P. Persson, and O. S. Wenger, "Borylation in the Second Coordination Sphere of FeII Cyanido Complexes and Its Impact on Their Electronic Structures and Excited-State Dynamics," *Inorganic Chemistry*, vol. 61, pp. 15853–15863, 10 2022.

[112] Q. Sun, S. Mosquera-Vazquez, L. M. Lawson Daku, L. Guénée, H. A. Goodwin, E. Vauthey, and A. Hauser, "Experimental Evidence of Ultrafast Quenching of the 3MLCT Luminescence in Ruthenium(II) Tris-bipyridyl Complexes via a 3 dd State," *Journal of the American Chemical Society*, vol. 135, pp. 13660–13663, 9 2013.

[113] M. Darari, A. Francés-Monerris, B. Marekha, A. Doudouh, E. Wenger, A. Monari, S. Haacke, and P. C. Gros, "Towards Iron(II) Complexes with Octahedral Geometry: Synthesis, Structure and Photophysical Properties," *Molecules*, vol. 25, p. 5991, 12 2020.

[114] D. Jacquemin and D. Escudero, "The short device lifetimes of blue PhOLEDs: insights into the photostability of blue Ir(III) complexes," *Chem. Sci.*, vol. 8, no. 11, pp. 7844–7850, 2017.

[115] Y. Rojas Pérez, L. D. Slep, and R. Etchenique, "Cis – Trans Interconversion in Ruthenium(II) Bipyridine Complexes," *Inorganic Chemistry*, vol. 58, pp. 11606–11613, 9 2019.

[116] D. Escudero, "Mer-Ir(ppy)3 to Fac-Ir(ppy)3 Photoisomerization," *ChemPhotoChem*, vol. 3, pp. 697–701, 9 2019.

[117] L. Feng, Y. Wang, and J. Jia, "Triplet Ground-State-Bridged Photochemical Process: Understanding the Photoinduced Chiral Inversion at the Metal Center of [Ru(phen)2(l-ser)]+ and Its Bipy Analogues," *Inorganic Chemistry*, vol. 56, pp. 14467–14476, 12 2017.

[118] A. J. Göttle, I. M. Dixon, F. Alary, J.-L. Heully, and M. Boggio-Pasqua, "Adiabatic Versus Nonadiabatic Photoisomerization in Photochromic Ruthenium Sulfoxide Complexes: A Mechanistic Picture from Density Functional Theory Calculations.," *Journal of the American Chemical Society*, vol. 133, pp. 9172–9174, 6 2011.

[119] S. Arroliga-Rocha and D. Escudero, "Facial and Meridional Isomers of Tris(bidentate) Ir(III) Complexes: Unravelling Their Different Excited State Reactivity," *Inorganic Chemistry*, vol. 57, pp. 12106–12112, 10 2018.

[120] L. Liu, D. Agathangelou, T. Roland, O. Crégut, T. Duchanois, M. Beley, J. Léonard, P. Gros, and S. Haacke, "High sensitivity fluorescence up-

conversion spectroscopy of 3 MLCT emission of metal-organic complexes," *EPJ Web of Conferences*, vol. 205, p. 09009, 4 2019.

[121] F. Hainer, N. Alagna, A. Reddy Marri, T. J. Penfold, P. C. Gros, S. Haacke, and T. Buckup, "Vibrational Coherence Spectroscopy Identifies Ultrafast Branching in an Iron(II) Sensitizer," *The Journal of Physical Chemistry Letters*, vol. 12, pp. 8560–8565, 9 2021.

[122] K. Kunnus, M. Vacher, T. C. B. Harlang, K. S. Kjær, K. Haldrup, E. Biasin, T. B. van Driel, M. Pápai, P. Chabera, Y. Liu, H. Tatsuno, C. Timm, E. Källman, M. Delcey, R. W. Hartsock, M. E. Reinhard, S. Koroidov, M. G. Laursen, F. B. Hansen, P. Vester, M. Christensen, L. Sandberg, Z. Németh, D. S. Szemes, E. Bajnóczi, R. Alonso-Mori, J. M. Glownia, S. Nelson, M. Sikorski, D. Sokaras, H. T. Lemke, S. E. Canton, K. B. Møller, M. M. Nielsen, G. Vankó, K. Wärnmark, V. Sundström, P. Persson, M. Lundberg, J. Uhlig, and K. J. Gaffney, "Vibrational wavepacket dynamics in Fe carbene photosensitizer determined with femtosecond X-ray emission and scattering," *Nature Communications*, vol. 11, p. 634, 1 2020.

[123] P. Chábera, K. S. Kjaer, O. Prakash, A. Honarfar, Y. Liu, L. A. Fredin, T. C. B. Harlang, S. Lidin, J. Uhlig, V. Sundström, R. Lomoth, P. Persson, and K. Wärnmark, "FeII Hexa N-Heterocyclic Carbene Complex with a 528 ps Metal-to-Ligand Charge-Transfer Excited-State Lifetime," *The Journal of Physical Chemistry Letters*, vol. 9, pp. 459–463, 2 2018.

[124] P. Chábera, Y. Liu, O. Prakash, E. Thyrhaug, A. E. Nahhas, A. Honarfar, S. Essén, L. A. Fredin, T. C. B. Harlang, K. S. Kjær, K. Handrup, F. Ericson, H. Tatsuno, K. Morgan, J. Schnadt, L. Häggström, T. Ericsson, A. Sobkowiak, S. Lidin, P. Huang, S. Styring, J. Uhlig, J. Bendix, R. Lomoth, V. Sundström, P. Persson, and K. Wärnmark, "A low-spin Fe(III) complex with 100-ps ligand-to-metal charge transfer photoluminescence," *Nature*, vol. 543, pp. 695–699, 3 2017.

[125] S. J. Messersmith, K. Kirschbaum, and J. R. Kirchhoff, "Luminescent Low-Valent Rhenium Complexes with 1,2-Bis(dialkylphosphino)ethane Ligands. Synthesis and X-ray Crystallographic, Electrochemical, and Spectroscopic Characterization," *Inorganic Chemistry*, vol. 49, pp. 3857–3865, 4 2010.

[126] J. J. Adams, N. Arulsamy, B. P. Sullivan, D. M. Roddick, A. Neuberger, and R. H. Schmehl, "Homoleptic Tris-Diphosphine Re(I) and Re(II) Complexes and Re(II) Photophysics and Photochemistry," *Inorganic Chemistry*, vol. 54, pp. 11136–11149, 12 2015.

[127] P. Chábera, L. Lindh, N. W. Rosemann, O. Prakash, J. Uhlig, A. Yartsev, K. Wärnmark, V. Sundström, and P. Persson, "Photofunctionality of iron(III) N-heterocyclic carbenes and related d transition metal complexes," *Coordination Chemistry Reviews*, vol. 426, p. 213517, 1 2021.

[128] J. Steube, A. Kruse, O. S. Bokareva, T. Reuter, S. Demeshko, R. Schoch, M. A. Argüello Cordero, A. Krishna, S. Hohloch, F. Meyer, K. Heinze, O. Kühn, S. Lochbrunner, and M. Bauer, "Janus-type emission from a cyclometalated iron(III) complex," *Nature Chemistry*, vol. 15, pp. 468–474, 4 2023.

[129] O. Prakash, P. Chábera, N. W. Rosemann, P. Huang, L. Häggström, T. Ericsson, D. Strand, P. Persson, J. Bendix, R. Lomoth, and K. Wärnmark, "A Stable Homoleptic Organometallic Iron(IV) Complex," *Chemistry – A European Journal*, vol. 26, pp. 12728–12732, 10 2020.

[130] M. Abrahamsson, "Solar energy conversion using iron polypyridyl type photosensitizers – a viable route for the future?," in *Photochemistry*, vol. 44, pp. 285–295, Royal Society of Chemistry, 2017.

[131] J. Knof, F. J. Theiss, and J. Weber, "Influence of Aggregation on the Fluorescence Decay of Organic Laser Dyes," *Zeitschrift fur Naturforschung - Section A Journal of Physical Sciences*, vol. 33, no. 1, pp. 98–104, 1978.

[132] C. Förster and K. Heinze, "Bimolecular reactivity of 3d metal-centered excited states (Cr, Mn, Fe, Co)," *Chemical Physics Reviews*, vol. 3, p. 041302, 12 2022.

[133] P. S. Wagenknecht and P. C. Ford, "Metal centered ligand field excited states: Their roles in the design and performance of transition metal based photochemical molecular devices," *Coordination Chemistry Reviews*, vol. 255, pp. 591–616, 3 2011.

[134] J. D. Braun, I. B. Lozada, C. Kolodziej, C. Burda, K. M. E. Newman, J. van Lierop, R. L. Davis, and D. E. Herbert, "Iron(II) coordination complexes with panchromatic absorption and nanosecond charge-transfer excited state lifetimes," *Nature Chemistry*, vol. 11, pp. 1144–1150, 12 2019.

[135] L. H. M. de Groot, A. Ilic, J. Schwarz, and K. Wärnmark, "Iron Photoredox Catalysis–Past, Present, and Future," *Journal of the American Chemical Society*, vol. 145, pp. 9369–9388, 5 2023.

[136] R. A. Marcus, "Chemical and electrochemical electron-transfer theory," *Annu. Rev. Phys. Chem.*, vol. 15, no. 1, pp. 155–196, 1964.

[137] R. Marcus and N. Sutin, "Electron transfers in chemistry and biology," *Biochimica et Biophysica Acta (BBA) - Reviews on Bioenergetics*, vol. 811, pp. 265–322, 8 1985.

[138] J. R. Miller, L. T. Calcaterra, and G. L. Closs, "Intramolecular long-distance electron transfer in radical anions. The effects of free energy and solvent on the reaction rates," *Journal of the American Chemical Society*, vol. 106, pp. 3047–3049, 5 1984.

[139] M. N. Paddon-row, A. M. Oliver, J. M. Warman, K. J. Smit, and M. P. D. Haas, "Factors affecting charge separation and recombination in photoexcited rigid donor-insulator-acceptor compounds," *Journal of Physical Chemistry*, vol. 92, no. 24, pp. 6958–6962, 1988.

[140] V. Balzani, A. Credi, and M. Venturi, *Molecular Devices and Machines: Concepts from the Nanoworld*. Weinheim: Wiley-VCH, 2nd ed., 2008.

[141] A. Rosspeintner, G. Angulo, and E. Vauthey, "Bimolecular Photoinduced Electron Transfer Beyond the Diffusion Limit: The Rehm–Weller Experiment Revisited with Femtosecond Time Resolution," *Journal of the American Chemical Society*, vol. 136, pp. 2026–2032, 2 2014.

[142] S. Farid, J. P. Dinnocenzo, P. B. Merkel, R. H. Young, D. Shukla, and G. Guirado, "Reexamination of the Rehm–Weller Data Set Reveals Electron Transfer Quenching That Follows a Sandros–Boltzmann Dependence on Free Energy," *Journal of the American Chemical Society*, vol. 133, pp. 11580–11587, 8 2011.

[143] M. H. Gehlen, "The centenary of the Stern-Volmer equation of fluorescence quenching: From the single line plot to the SV quenching map," *Journal of Photochemistry and Photobiology C: Photochemistry Reviews*, vol. 42, p. 100338, 3 2020.

[144] N. W. Rosemann, P. Chábera, O. Prakash, S. Kaufhold, K. Wärnmark, A. Yartsev, and P. Persson, "Tracing the Full Bimolecular Photocycle of Iron(III)–Carbene Light Harvesters in Electron-Donating Solvents," *Journal of the American Chemical Society*, vol. 142, pp. 8565–8569, 5 2020.

[145] A. Aydogan, R. E. Bangle, A. Cadranel, M. D. Turlington, D. T. Conroy, E. Cauët, M. L. Singleton, G. J. Meyer, R. N. Sampaio, B. Elias, and L. Troian-Gautier, "Accessing Photoredox Transformations with an Iron(III) Photosensitizer and Green Light," *Journal of the American Chemical Society*, vol. 143, pp. 15661–15673, 9 2021.

[146] N. Kaul and R. Lomoth, "The Carbene Cannibal: Photoinduced Symmetry-Breaking Charge Separation in an Fe(III) N -Heterocyclic Carbene," *Journal of the American Chemical Society*, vol. 143, pp. 10816–10821, 7 2021.

[147] A. Aydogan, R. E. Bangle, S. De Kreijger, J. C. Dickenson, M. L. Singleton, E. Cauët, A. Cadranel, G. J. Meyer, B. Elias, R. N. Sampaio, and L. Troian-Gautier, "Mechanistic investigation of a visible light mediated dehalogenation/cyclisation reaction using iron(III), iridium(III) and ruthenium(II) photosensitizers," *Catalysis Science & Technology*, vol. 11, no. 24, pp. 8037–8051, 2021.

[148] A. Ripak, S. De Kreijger, R. N. Sampaio, C. A. Vincent, E. Cauët, I. Jabin, U. K. Tambar, B. Elias, and L. Troian-Gautier, "Photosensitized activation of diazonium derivatives for C–B bond formation," *Chem Catalysis*, vol. 3, p. 100490, 2 2023.

[149] Y. J. Jang, H. An, S. Choi, J. Hong, S. H. Lee, K.-H. Ahn, Y. You, and E. J. Kang, "Green-Light-Driven Fe(III)(btz)3 Photocatalysis in the Radical Cationic [4+2] Cycloaddition Reaction," *Organic Letters*, vol. 24, pp. 4479–4484, 6 2022.

[150] A. Ilic, J. Schwarz, C. Johnson, L. H. M. de Groot, S. Kaufhold, R. Lomoth, and K. Wärnmark, "Photoredox catalysis via consecutive 2LMCT- and 3MLCT-excitation of an Fe(III/II)–N-heterocyclic carbene complex," *Chemical Science*, vol. 13, no. 32, pp. 9165–9175, 2022.

[151] J. Schwarz, A. Ilic, C. Johnson, R. Lomoth, and K. Wärnmark, "High turnover photocatalytic hydrogen formation with an Fe(III) N-heterocyclic carbene photosensitiser," *Chemical Communications*, vol. 58, no. 35, pp. 5351–5354, 2022.

[152] S. Ferrere and B. A. Gregg, "Photosensitization of TiO2 by [FeII(2,2'-bipyridine-4,4'-dicarboxylic acid)2(CN)2]: Band Selective Electron Injection from Ultra-Short-Lived Excited States," *Journal of the American Chemical Society*, vol. 120, pp. 843–844, 2 1998.

[153] S. Ferrere, "New Photosensitizers Based upon [Fe(L)2(CN)2] and [Fe(L)3] (L = Substituted 2,2'-Bipyridine): Yields for the Photosensitization of TiO2 and Effects on the Band Selectivity," *Chemistry of Materials*, vol. 12, pp. 1083–1089, 4 2000.

[154] C. S. Ponseca, P. Chábera, J. Uhlig, P. Persson, and V. Sundström, "Ultrafast Electron Dynamics in Solar Energy Conversion," *Chemical Reviews*, vol. 117, pp. 10940–11024, 8 2017.

[155] W. R. Duncan and O. V. Prezhdo, "Theoretical Studies of Photoinduced Electron Transfer in Dye-Sensitized TiO2," *Annual Review of Physical Chemistry*, vol. 58, pp. 143–184, 5 2007.

[156] M. Yang, D. W. Thompson, and G. J. Meyer, "Charge-Transfer Studies of Iron Cyano Compounds Bound to Nanocrystalline TiO2 Surfaces," *Inorganic Chemistry*, vol. 41, pp. 1254–1262, 3 2002.

[157] N. A. Anderson and T. Lian, "Ultrafast Electron Transfer at the Molecule-Semiconductor Nanoparticle Interface," *Annual Review of Physical Chemistry*, vol. 56, pp. 491–519, 5 2005.

[158] R. A. Marcus, "On the Theory of Electron-Transfer Reactions. VI. Unified Treatment for Homogeneous and Electrode Reactions," *The Journal of Chemical Physics*, vol. 43, pp. 679–701, 7 1965.

[159] H. Gerischer, "Charge transfer processes at semiconductor-electrolyte interfaces in connection with problems of catalysis," *Surface Science*, vol. 18, pp. 97–122, 11 1969.

[160] A. Reddy-Marri, E. Marchini, V. D. Cabanes, R. Argazzi, M. Pastore, S. Caramori, and P. C. Gros, "Panchromatic light harvesting and record power conversion efficiency for carboxylic/cyanoacrylic Fe(II) NHC co-sensitized FeSSCs," *Chemical Science*, vol. 14, no. 16, pp. 4288–4301, 2023.

[161] H. Němec, J. Rochford, O. Taratula, E. Galoppini, P. Kužel, T. Polívka, A. Yartsev, and V. Sundström, "Influence of the electron-cation interaction on electron mobility in dye-sensitized ZnO and TiO2 nanocrystals: A study using ultrafast terahertz spectroscopy," *Physical Review Letters*, vol. 104, no. 19, pp. 1–4, 2010.

[162] A. Furube, R. Katoh, and K. Hara, "Electron injection dynamics in dye-sensitized semiconductor nanocrystalline films," *Surface Science Reports*, vol. 69, pp. 389–441, 12 2014.

[163] A. Furube, R. Katoh, K. Hara, S. Murata, H. Arakawa, and M. Tachiya, "Ultrafast Stepwise Electron Injection from Photoexcited Ru-Complex into Nanocrystalline ZnO Film via Intermediates at the Surface," *The Journal of Physical Chemistry B*, vol. 107, pp. 4162–4166, 5 2003.

[164] M. Karpacheva, C. E. Housecroft, and E. C. Constable, "Electrolyte tuning in dye-sensitized solar cells with N-heterocyclic carbene (NHC) iron(II) sensitizers," *Beilstein Journal of Nanotechnology*, vol. 9, pp. 3069–3078, 12 2018.

[165] M. Karpacheva, V. Wyss, C. E. Housecroft, and E. C. Constable, "There Is a Future for N-Heterocyclic Carbene Iron(II) Dyes in Dye-Sensitized Solar Cells: Improving Performance through Changes in the Electrolyte," *Materials*, vol. 12, p. 4181, 12 2019.

[166] E. Marchini, M. Darari, L. Lazzarin, R. Boaretto, R. Argazzi, C. A. Bignozzi, P. C. Gros, and S. Caramori, "Recombination and regeneration dynamics in FeNHC(II)-sensitized solar cells," *Chemical Communications*, vol. 56, no. 4, pp. 543–546, 2020.

[167] M. Becker, V. Wyss, C. E. Housecroft, and E. C. Constable, "The influence of alkyl chains on the performance of DSCs employing iron(ii) N-heterocyclic carbene sensitizers," *Dalton Transactions*, vol. 50, no. 46, pp. 16961–16969, 2021.

[168] A. R. Marri, E. Marchini, V. D. Cabanes, R. Argazzi, M. Pastore, S. Caramori, C. A. Bignozzi, and P. C. Gros, "A Series of Iron(II)-NHC Sensitizers with Remarkable Power Conversion Efficiency in Photoelectrochemical Cells," *Chemistry – A European Journal*, vol. 27, pp. 16260–16269, 11 2021.

[169] A. Reddy-Marri, E. Marchini, V. Diez Cabanes, R. Argazzi, M. Pastore, S. Caramori, and P. C. Gros, "Record Power Conversion Efficiencies for Iron(II)-NHC-Sensitized DSSCs from Rational Molecular Engineering and Electrolyte Optimization," *Journal of Materials Chemistry A*, vol. 9, no. 6, pp. 3540–3554, 2021.

[170] C. Zhang, S. Chen, L. Mo, Y. Huang, H. Tian, L. Hu, Z. Huo, S. Dai, F. Kong, and X. Pan, "Charge Recombination and Band-Edge Shift in the Dye-Sensitized Mg2+ -Doped TiO2 Solar Cells," *The Journal of Physical Chemistry C*, vol. 115, pp. 16418–16424, 8 2011.

[171] J. R. Jennings and Q. Wang, "Influence of Lithium Ion Concentration on Electron Injection, Transport, and Recombination in Dye-Sensitized Solar Cells," *The Journal of Physical Chemistry C*, vol. 114, pp. 1715–1724, 1 2010.

[172] L. Kavan, M. Grätzel, S. E. Gilbert, C. Klemenz, and H. J. Scheel, "Electrochemical and Photoelectrochemical Investigation of Single-Crystal Anatase," *Journal of the American Chemical Society*, vol. 118, pp. 6716–6723, 1 1996.

[173] N. Sinha and O. S. Wenger, "Photoactive Metal-to-Ligand Charge Transfer Excited States in 3d6 Complexes with Cr0 , MnI , FeII , and CoIII," *Journal of the American Chemical Society*, vol. 145, pp. 4903–4920, 3 2023.

[174] M. Sandroni, Y. Pellegrin, and F. Odobel, "Heteroleptic bis-diimine copper(I) complexes for applications in solar energy conversion," *Comptes Rendus Chimie*, vol. 19, pp. 79–93, 1 2016.

[175] R. Czerwieniec, M. J. Leitl, H. H. Homeier, and H. Yersin, "Cu(I) complexes – Thermally activated delayed fluorescence. Photophysical approach and material design," *Coordination Chemistry Reviews*, vol. 325, pp. 2–28, 10 2016.

[176] W. R. Kitzmann, C. Ramanan, R. Naumann, and K. Heinze, "Molecular ruby: exploring the excited state landscape," *Dalton Transactions*, vol. 51, no. 17, pp. 6519–6525, 2022.

Scientific publications